

AD-A040 668

PENNSYLVANIA STATE UNIV UNIVERSITY PARK APPLIED RESE--ETC F/G 20/1
ACOUSTIC DIFFRACTION. PART I. PLANE DIFFRACTORS AND WEDGES. (U)
MAY 73 E J SKUDRZYK, S I HAYEK, A D STUART N00017-70-C-1407

UNCLASSIFIED

TM-73-109-PT-1

NL

4 OF 2
AD
AO40668



AD A 040668

2
B.51

6
ACOUSTIC DIFFRACTION
Part I. PLANE DIFFRACTORS AND WEDGES.

E. J. Skudrzyk, S. I. Hayek, A. D. Stuart

10
Eugene J. Skudrzyk,
Sabih I. Hayek
Alan D. Stuart

11 14 May 73

12 16 pp.

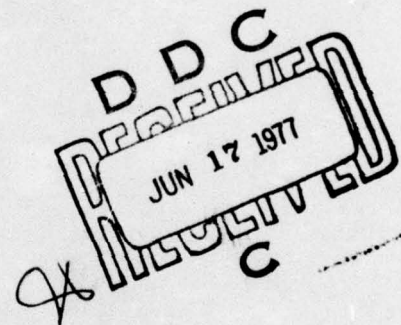
9
Technical Memorandum

14
File No. TM-73-109-PE-1

May 14, 1973

Contract No. N00017-70-C-1407

15
Copy No. 19



The Pennsylvania State University
Institute for Science and Engineering
APPLIED RESEARCH LABORATORY
University Park, Pennsylvania

NAVY DEPARTMENT

NAVAL ORDNANCE SYSTEMS COMMAND

AD No.
DDC FILE COPY

APPROVED FOR PUBLIC RELEASE
DISTRIBUTION UNLIMITED

1473
391007

LB

SECTION 201	
NTIS	Write Section <input checked="" type="checkbox"/>
DES	Burt Section <input type="checkbox"/>
UNANNOUNCED	<input type="checkbox"/>
JUSTIFICATION.....	
BY.....	
DISTRIBUTION/AVAILABILITY CODES	
Dist.	AVAIL. and/or SPECIAL
A	

Subject: Acoustic Diffraction
Part I- Plane Diffractors and Wedges

Abstract: This memorandum documents the theoretical investigations in the Acoustic Diffraction Program. This report discusses the acoustic diffraction and backscattering phenomena for plane and wedge scatterers, which are insonified by plane or point sources. The theories of diffraction used in this report are those of the approximate integral representations of Kirchoff-Rubinowicz. Those were compared with the geometrical theory of diffraction (GTD) which is developed by J. B. Keller, and is based on the ray theory. It was found that the integral representation agrees well with the GTD at high frequencies for infinite edges and long curved edges only. The agreement was worse when the scatterer size or edge length is finite. New expressions for diffraction from finite scatterers and edges were derived and the deviation of the GTD from these solutions were estimated.

TABLE OF CONTENTS

	<u>Page</u>
List of Figures	iv
1. INTRODUCTION	1
1.1 Plane Diffractors and Wedges - Part I	1
1.2 Three Dimensional Diffractors - Part II	1
1.3 The Effect of the Structure and Structural Vibrations on the Diffraction - Part III	4
2. WHAT IS DIFFRACTION?	
2.1 Classical Interpretation	4
2.2 Diffraction as a Diffusion Phenomenon	5
2.3 Diffraction as a Phenomenon Caused by the Shadow Zone	6
3. THE KIRCHOFF THEORY OF DIFFRACTION	
3.1 The exact Huyghens - Helmholtz Diffraction Integral and the Kirchhoff Theory of Diffraction	11
3.2 The Kirchhoff Solution	17
4. THE RUBINOWICZ INTEGRAL	21
5. THE GEOMETRICAL THEORY OF DIFFRACTION	28
6. CAUSTICS	36
7. THE FIELD AT AND NEAR THE SHADOW BOUNDARY AND THE PHYSICAL SIGNIFICANCE OF EDGE WAVES	41
8. THE STRAIGHT EDGE - KIRCHOFF AND SOMMERFELD	46
9. THE WEDGE	50
10. COMPARISON OF THE KIRCHOFF STRAIGHT EDGE SOLUTION WITH THE SOMERFELD STRAIGHT EDGE AND WEDGE SOLUTION	52
11. DIRECTIVITY FACTOR OF THE EDGE RADIATION	55
12. EDGES OF FINITE LENGTH	57

	<u>Page</u>
13. THE LIMITS OF GEOMETRICAL REFLECTION AND DIFFRACTION FOR FINITE FLAT REFLECTORS	61
14. DIFFRACTION FIELD FROM EDGES OF FINITE LENGTH	74
15. SUMMARY AND CONCLUSIONS	83
15.1 The Geometrical Theory of Diffraction	83
15.2 The Kirchoff-Rubinowicz Integral Representation	84
15.3 Diffraction and the Shadow Boundary	84
15.4 Diffraction and its Role in Determining Backscattering	85
15.5 Range of Validity of the Geometrical Theory of Diffraction	86
15.6 Diffraction Field from a Finite Edge	87
REFERENCES	88
APPENDIX I: Stationary Phase Method	90
APPENDIX II: Derivation of the Helmholtz-Huyghens Integral	93
APPENDIX III: Fermat's Principle	97
APPENDIX IV: Derivation of the Rubinowicz Integral	100
APPENDIX V: Frenet Formulae	103

LIST OF FIGURES

<u>Figure</u>		<u>Page</u>
1	Surfaces of Integration in the Helmholtz-Huyghens Integral	105
2	Angle Dependence of the Scattered Field from a Particle	106
3	Scattered Pressure Field on the Surface of a Rigid Disc, Leitner a. Real Part, b. Imaginary Part, K refers to Kirchhoff Solution, c. Absolute Value by Leitner, approx. by Spence, experimental Data by Weiner. I and S Refer to the Illuminated and Shadow Sides of the Disc.	107
4	Comparison of the Exact Solution of Meixner (M) with Approximation of Kirchhoff (K) and Braunbeck (B)	108
5	Diffraction Contour and the Shadow Boundary of an Aperture	109
6	Integration Surface on the Shadow Cone	110
7	Coordinate System and Angles for the Rubinowicz Integral	111
8	(a) Section through diffraction cone containing incident ray and shadow boundary. The great intensity of the diffracted amplitude near the shadow boundary is indicated by a thickening of the ellipse on the drawing. (b) Amplitude of diffracted rays as a function of angle from shadow region	112
9	Unit Vectors and Angles in the Rubinowicz Solution, Equation (32)	113
10	Cross Section of a Diffracted Bundle of Rays	114
11	A pair of neighboring rays incident on a curved edge of a flat screen, and resulting diffracted cones. The two cones of diffracted rays intersect at the caustic, which is at the distance R_α from the edge along one of the diffracted rays	115
12	The focal lines of a pencil. A portion of the axis of rotation and a surface of revolution whose meridian section is the evolute of the meridian section of the wavefront. (D. S. Jones, The Theory of Electromagnetism, Page 375.)	116

<u>Figure</u>		<u>Page</u>
13	Coordinates for the Diffraction from the Arc of a Circular Edge of Radius a	117
14	Coordinates for Computing Field Near Shadow Boundary	118
15	Shadow Boundaries of Incident and Reflected (Image Space) Waves	119
16	Coordinates used for Determining Stationary Phase Point for a Plane Wave Incident on a Straight Edge	120
17	Coordinates used for Determining Stationary Phase Point for a Spherical Wave Incident on a Straight Edge	121
18	Kirchoff Solution for the Diffraction from a Rigid Edge, for Various Angles of Incidence ϕ_0	122
19	Kirchoff Solution for the Diffraction from a Pressure Release Edge, for Various Angles of Incidence ϕ_0	123
20	Sommerfeld (Exact) Solution for Diffraction from Rigid Edge, for Various Angles of Incidence ϕ_0	124
21	Sommerfeld (Exact) Solution for the Diffraction from a Pressure Release Edge, for Various Angles of Incidence ϕ_0	125
22	Backscattered Field of Rigid Edge, Sommerfeld and Kirchoff Solutions	126
23	Backscattered Field of a Pressure Release Edge, Sommerfeld and Kirchoff Solutions	127
24	Shadow Boundaries of Incident and Reflected (Image Space) Waves for a Wedge Angle 2Ω	128
25	Diffraction from a 30° Rigid Wedge for Various Angles of Incidence ϕ_0	129
26	Diffraction from a 30° Pressure Release Wedge, for Various Angles of Incidence ϕ_0	130
27	Diffraction from a 60° Rigid Wedge for Various Angles of Incidence ϕ_0	131
28	Diffraction from a 60° Pressure Release Wedge, for Various Angles of Incidence ϕ_0	132
29	Diffraction from a 90° Rigid Wedge for Various Angles of Incidence ϕ_0	133
30	Diffraction from a 90° Pressure Release Wedge, for Various Angles of Incidence ϕ_0	134

<u>Figure</u>		<u>Page</u>
31	Diffraction from a 120° Rigid Wedge for Various Angles of Incidence ϕ_0	135
32	Diffraction from a 120° Pressure Release Wedge, for Various Angles of Incidence ϕ_0	136
33	Backscattering from Rigid Wedges, Wedge Angles $2\Omega = 30^\circ, 60^\circ, 90^\circ$ and 120°	137
34	Backscattering from Pressure Release Wedges, Wedge Angles $2\Omega = 30^\circ, 60^\circ, 90^\circ$ and 120°	138
35	Discontinuity Factor for Wedge	139
36	Comparison of the Kirchoff and Sommerfeld Solutions of the Diffraction from a Straight Edge for an Incident Wave Only	140
37	Comparison of the Kirchoff and Sommerfeld Solutions of the Diffraction from Wedges of Various Wedge-Angles 2Ω for Incident Wave Only	141
38	Cornu Spiral Curve	142
39	Limit Range and Angles of the Geometrical Theory of Diffraction from a Square Scatterer for (a) Point Source and (b) Plane Wave Incidence	143
40	Coordinate System for the Diffracted Field of Plane Scatterers	144
41	Limiting Range r for geometric optical propagation as a function of m wavelength in water (or frequency) v.s. the linear dimension of diffractor h for plane wave incidence	145
42	(a) Scattering Cone for an Infinite Edge at Oblique Incidence (b) Scattering Plane for an Infinite Edge at Normal Incidence (c) Scattering Conical Shell for a Finite Edge	146
43	Scattering by a Finite Edge of Length l of an Incident Point Source Field	147
44	Coordinate System for Curved and Straight Finite Edges	148
45	Radiation from a Finite Linear Array. The Off-Axis Radiation is Independent of the Number of Elements in the Array	149
46	Diagram for Proof of Fermat's Principle	150
47	Transformation of the Kirchoff Surface Integral to a Line (Edge) Integral	151

ACOUSTIC DIFFRACTION

1. INTRODUCTION

In dealing with acoustic diffraction it is expedient to distinguish between three groups of problems. For this reason the report will be divided into three basic parts which distinguish the types of diffractors: (I) plane diffractors and wedges, (II) three dimensional bodies, and (III) structures whose vibrations are coupled with the diffracted field.

1.1 Plane Diffractors and Wedges - Part I

The first and simplest group deals with plane screens, plane wedges and plane apertures. Considerable effort has been made in the past to deal with such diffractors. Exact solutions have been derived for the straight edge, the wedge, and for the circular and elliptical apertures and screens, with both rigid and pressure release surfaces. Recently, elastic wedges have also been investigated and exact solutions derived.

The exact methods are very complex, and while they yield numerical solutions, they provide relatively little insight into the physical phenomena causing the diffraction. Simple methods have therefore been developed ever since diffraction was first studied. The most famous method is Kirchhoff's method, where an exact surface integral for the diffracted field is solved by replacing the exact diffractor's surface boundary conditions by approximate ones. The approximation involves the assumptions that the diffractor's surface is a totally absorbant one, and that there is no acoustic field whatsoever immediately behind the diffracting surfaces. The field in front of the screen and aperture is assumed to be identical with that of the incident wave. It is found by comparison with exact solutions that this heuristic procedure does indeed lead to very useful solutions.

Because of the success of the Kirchhoff theory, solutions have been derived by refining the Kirchhoff assumptions (W. Braunbek, 1950, 1954, and 1959) or by developing a method of successive approximations that consists of pairs of steps, one satisfying the differential equation, the other satisfying the exact boundary conditions

- 2 -

(W. Franz, 1949, 1950, 1957, Schelkunoff, 1951). These refined methods lead to an improvement of the Kirchhoff solution; however, since the deviation from the exact solution is still relatively great in some angular range or the methods do not converge, it hardly seems worthwhile to use them.

Recently, a semi-empirical theory has been derived by Keller (1956) using the concept of rays. The distance variation of the solution is derived on the basis of geometrical optics, on the (implicit) assumption that the diffracting edges are large compared to the wave length, so that only the stationary phase points (see Appendix I) contribute to the diffraction field. The directivity factor then is deduced by comparison of the geometrical optics solutions with the exact solutions. This is permissible since, in the frequency range in which his method applies, diffraction is due to the contributions of the very small regions along the diffracting edge that correspond to the stationary phase points and their neighborhoods.

The geometrical and hence also the Keller theory for plane diffractors breaks down at caustics* because, in the geometric optical limit, the contributions of a very small but finite region of the diffractor are condensed at the caustic to a space of zero volume such as the space occupied by a point or a line (see pp 36).

* A caustic is a surface at which adjacent rays intersect. If this surface degenerates to a point it becomes a focus. For example, for a lens with spherical surfaces the focal length depends on the angle of incidence. The focal points then vary with the angle of incidence and if the incident wave is spherical so that the directions of the incident rays vary within a certain angular range, the focal points will lie on a surface, i.e., on the caustic surface.

- 3 -

This accounts for the far fetched assumptions needed to save this theory. The geometrical theory also breaks down whenever the edges are of finite length and the distance from the diffractor exceeds a limit that depends on the length of the edge, the wave length, and the angle of incidence. The geometrical theory also breaks down in practically all situations when the diffractor surface area is finite, where the distance from the diffractor is greater than its linear dimensions, and the angle of incidence is not exactly normal.

A theory equivalent to the geometrical theory of diffraction for plane diffractors that are free of all the limitations with respect to size of the diffractor and distance from it can be derived by exact methods on the basis of the Kirchhoff assumptions. This method has the advantage that the mathematics is rigorous in all its steps, and that the derivations are based on well defined assumptions. As a result, we obtain the correct distance variation of the solution whether the diffractor is small or large, and a directivity factor that turns out to represent a very good approximation to that of the exact solution range, provided the linear dimensions of the diffractor are greater than a wave length. We may then use Keller's method and improve the directivity factor by comparison with an exact solution. In deriving the theory it is of advantage to use the Kirchhoff solution in the form of the Rubinowicz integral, (Rubinowicz, 1917) and to take the reflected field into account independently. The results can then easily be extended to surfaces of given impedance.

It is expected that the theory derived in Part I is adequate for all practical computations of the diffracted field for plane diffractors, including the straight edge and for sharp wedges of angular openings up to at most 90 degrees. However, it is not suited to study diffraction of blunt bodies.

1.2 Three-Dimensional Diffractors - Part II

The diffraction theory for blunt bodies and for three dimensional

- 4 -

0 diffractors in general is considerably more complex than that for plane diffractors. In the small number of cases that have been investigated in conjunction with this report, the Kirchoff assumptions seemed to lead to acceptable results only when the linear dimensions of the diffractor exceeded about 50 wavelengths. It has not yet been ascertained whether the Kirchoff theory can be used as a starting point for improved types of solutions as was done for the plane diffraction solutions. Results of such attempts will be reported separately in Part II.

Keller's method of deriving the results represents a considerable shortcut compared to all other methods, and right now it seems that this method is the only practical method to arrive at useful results for the prediction of the field produced by three dimensional diffractors. As will be shown, Keller's expressions can be obtained by almost exact procedures. It will be shown in Part II that the amplitude variation normal to the direction of propagation and consequently also normally to the shadow boundary obeys a diffraction equation and that the three dimensional Keller theory can be derived by solving this equation for curved surfaces. Part II of the report will then represent a basic and critical review of the Keller method for three dimensional diffractors.

1.3 The Effect of the Structure and Structural Vibrations on the Diffraction - Part III

This part will be devoted to the effect of the structure and of structural vibrations of the diffractor on the diffraction field. Every edge, rib, or appendage on an elastic structure represents a discontinuity of the vibration field and leads to sound radiation. Because of the phase correlation of the vibration with the incident wave, the vibration and diffraction depend on each other and cannot be dealt with separately.

2. WHAT IS DIFFRACTION?

Diffraction is a very complex phenomenon that can be interpreted in a number of different ways, as will be discussed in the following sections.

2.1 Classical Interpretation

The classical interpretation of diffraction (scattering) is based on the ideas of Huyghens. The diffractor transforms the incident wave field into a wave field that originates at the diffractor (scatterer) and that propagates off into all directions.

In the classical theories, scattering and diffraction are usually described by assuming a coordinate system whose coordinate surfaces are also surfaces of the scatterer or diffractor. The solution is given by a series of wave functions that originate at the center of the scatterer. The effect of the scatterer then is usually represented by the acoustic power that is contained in the scattered field. To obtain this power, the square of the scattered pressure is computed and integrated over all space.

One of the most important parameters of the classical theory is the scattering cross section. It is defined as the ratio of the scattered power to the incident power. Thus, the area of the incident wave front that transports the same power as the power that is scattered is called the scattering cross section. The classical interpretation pretends that the scattered field is independent (uncorrelated) with the incident field and can thus be considered as an independent entity so that it makes sense to talk about a diffracted (scattered) field and a diffracted (scattered) energy. But the fact is that the diffracted (scattered) field is not uncorrelated everywhere with the incident field. The definition of the scattering cross section, therefore, is somewhat problematic.

Incident and scattered fields are strongly correlated in the direction of propagation of the incident wave, and it is no longer possible to consider the diffracted energy as an independent entity. For instance, at the geometrical shadow boundary, the diffracted field is always equal to half the incident field and is in phase with it as we move into the shadow space and in antiphase as we

- 6 -

move into the illuminated space. The scattered field then is nothing more than the field (the mathematical function) that we have to superimpose on the incident field to make the transition from the shadow region to the illuminated region continuous. The quantity that the classical theory defines as the scattered energy is not related to any energy at all, but represents the square of the deviation of the total acoustic field at some point from the incident field, at that same point as if the scatterer were absent. However, it turns out that as we move far away from the scatterer, the angular range near the geometrical shadow boundary over which incident and scattered field are correlated is small and decreases to zero as r increases to infinity (for the wedge, this range is proportional to $1/\sqrt{r}$; see Fig. 24.13 with $\rho = 1$, and $\theta = x/r$ in Skudrzyk, 1971). If we integrate over a surface of very large radius, the contribution of the coherence range can be neglected and the scattering cross section represents a meaningful and useful parameter that describes diffraction and scattering.

2.2 Diffraction as a Diffusion Phenomenon

If the diffractor is ideally absorbant, and is a plane screen, diffraction is a simple phenomenon that is basically connected with the formation of a shadow boundary. But if the diffractor is not ideally absorbant, a reflected field is generated. The reflected field can be assumed to be generated by an image source, and the resultant field consists of the incident waves the reflected waves, and their respective diffraction fields. The exact solutions for the straight edge (semi-infinite plane) and for the wedge are made up of two such fields.

That such a decomposition is also possible for the exact solution of the wedge is due to the fact that for a wedge multiple reflections and diffractions do not occur. But such

- 7 -

a decomposition of the solution is no longer possible for three dimensional curved bodies. For instance, a sound wave that travels down a horn is intensified by multiple reflections, besides the fact that the field that is generated by diffraction at its neck is also considerably modified by multiple reflections and the diffraction fields connected with each of the reflection fields. Thus, reflection and diffraction can no longer be separated.

That one aspect of diffraction is due to the diffusion of particle motion into the shadow spaces follows directly from the consideration of the scattering cross section. At very high frequencies, all the power that impinges on the scattering object is reflected. One would thus expect, at very high frequencies, that the scattering cross section is equal to the projection of the cross section of the scatterer on the wave front of the incident wave. But the computation shows that, at very high frequencies, the scattering cross section is twice as large (J. Y. Bowmann, T. B. Senior, P.L. Uslenghi, 1969). This means that rays that have passed many wave lengths beyond the scatterer are still being scattered. Still, in the geometric optical limit, we know that acoustic or optical coupling takes place over distances of millions of wavelengths. The explanation of what happens is a relatively simple one. The scatterer also generates a shadow zone. The boundary of this shadow zone is a region of discontinuity and consequently acts like a distribution of sound sources. These sound sources emit radiation in all directions. At distances sufficiently far away behind the scatterer, the shadow region is filled in and the intensity is again the same everywhere as in the incident wave. Thus the incident wave has to supply not only the reflected energy but also the energy that is needed to fill in the shadow region behind the scatterer. At very high frequencies, both phenomena require the same amount of energy and the scattering cross

- 8 -

section increases with the radius of the cylinder over which we compute the square of the diffracted field and becomes infinite as this radius becomes infinite. Since the shadow space behind the edge is infinitely extended, an infinite amount of energy is required to fill the shadow space and consequently the scattering cross sections become infinite.

The diffraction of energy into the shadow space is thus a consequence of the diffusion of momentum in a direction transverse to the direction of propagation. The wave amplitudes vary drastically transverse to the direction of propagation in directions parallel to the wave fronts. To satisfy the wave equation this variation must satisfy differential equations of the diffusion type. The sound field diffuses into the shadow space. If this aspect of diffraction is carried on for three-dimensional diffractors, we arrive at solutions similar to the Keller solution for the sound propagation along curved surfaces.

2.3 Diffraction as a Phenomenon Caused by the Shadow Boundary

The contribution of the shadow boundary to the diffraction phenomenon is of particular interest. The shadow boundary represents a surface of discontinuity, - at least in the geometric optical limit - and consequently, according to Huyghens principle or in the Kirchhoff approximation, acts like a continuous distribution of dipole sources whose axes are normal to the shadow boundary. For a plane incident wave, the wave amplitude of the incident wave is constant. In the geometric optical limit, the acoustic field near the shadow boundary is therefore the same everywhere.

If we look at a homogeneous plane shadow boundary and apply the Helmholtz Huyghens integral to it (see Appendix II), we find that the field amplitude decreases exponentially with the distance perpendicular from it. In the case of a plane incident

- 9 -

0 wave, the diffracted wave field is generated solely near the edge that defines the shadow boundary. The shadow boundary itself does not radiate. If the incident wave is cylindrical or spherical, radiation can also be generated by the shadow boundary. So both, the region near the edge, and the whole shadow boundary may radiate.

To investigate the question whether edge waves are real, we look at the diffraction of a Dirac pulse. Let the pulse travel first as a plane wave pulse, and let it be diffracted at a straight edge. The computation then shows (F. Oberhettinger, 1958) that this pulsed wave continues along the illuminated region up to the shadow boundary. The shadow boundary then does not radiate because it is homogeneous in directions parallel to the wave front. An edge wave does not exist except for points extremely close to the edge or the shadow boundary. But if the incident Dirac pulse has a cylindrical wave front, the incident wave amplitude near the shadow boundary is no longer constant but decreases inversely proportionally to the square root of the distance from the edge. The first scattered contribution then arrives at a time that corresponds to the shortest distance from the source to the edge and from there to the field point. But instead of a Dirac pulse at only the shadow boundary, we observe through the entire shadow space a significant diffraction pulse whose amplitude decreases as

$1/\sqrt{c^2 t^2 - \text{const.}}$, i.e. inversely proportional to the distance from a point that travels with sound velocity in the direction of the incident radiation along the shadow boundary. The original pulse now is drawn out because all points from the shadow boundary radiate. That the amplitude decreases not as $1/\sqrt{ct}$ but as $1/ct$ could have been expected. The shadow boundary for a Dirac pulse can be interpreted as a sequence of line elements of width dx and of infinite length (more correctly as semi circular rings). But such a strip of ring (because

- 10 -

its radius of curvature is very great) acts like a very long

line array. Its directivity function is $\left[\frac{2 \sin [(k\ell \sin \theta)/2]}{k\ell \sin \theta} \right]_{k\ell \gg 1}$

and radiates as if all the field were coming from a single point at its center, the point opposite the field point (E. J. Skudrzyk, 1971, page 599). The pressure decreases as $1/ct$ where ct is the distance of this energized strip element dx along the shadow boundary from the field point.

The solution seems very different for a train of sinusoidal oscillations. The combined effect of edge and shadow boundary then becomes equivalent to a wave train that originates at the stationary phase point (see Appendix I). The effect of the shadow boundary no longer dominates (see page) in the solution. We end up with Fermat's principle (see Appendix III) which is more of a mathematical than a physical nature. The diffracted field originates at and near a point of the edge such that the sum of the distances from the source to the edge point and from this edge point to the field point is a minimum (see page 24 and Appendix IV). The incident wave field acts like a continuous sequence of Dirac pulses of varying amplitudes. For the first few pulses the shadow boundary may be expected to play a decisive role, but the pulses interfere and after a very short time the diffracted field seems to originate from the stationary phase points. The diffracted pulse arrives with a time equal to the distance from the edge, if the incident wave is plane, but, if the incident wave is spherical the pulse arrives on time, as if it had travelled along the shadow boundary to a point nearly perpendicular to the field point and from there to the field point. This means that for sinusoidally modulated pulses, the greater the curvature of the wave front the greater will be the distortion of the shape of incident pulses by edge diffraction. These conclusions can be easily drawn by computing the group velocity delay from the solution for the straight edge.

- 11 -

3. THE KIRCHOFF THEORY OF DIFFRACTION

The exact treatment of diffraction is relatively complicated because it must include multiple reflections as well as multiple diffractions and the reflection of diffracted waves. For plane diffractors, the diffracted field decomposes naturally into that of the incident wave and that of the reflected wave. But for three-dimensional diffractors, such a decomposition is, in general, not possible. Kirchhoff simplified the treatment of diffraction considerably by assuming all diffractors to be ideally absorber. Primary reflections and multiple reflections do not occur and all that needs to be considered is the incident wave and its diffraction field. This field can be easily approximated and further improved by computation. If the diffractor is plane, the reflected field solution can be determined by an image method. As a consequence of neglecting multiple diffraction and reflection and the reflection of diffracted waves, the Kirchhoff solution depends only on the shadow boundary and computations are very simple.

It is understandable that the Kirchhoff method will lead to good approximations for plane screens. In fact, it leads to excellent approximations. But the Kirchhoff approximation may fail grossly for three-dimensional diffractors. Multiple reflection and diffraction can then no longer be neglected. In the Kirchhoff solution, a horn shaped diffractor is absorber on its inside, and the amplitude of the wave that reaches the neck is assumed to be the same as that of the undisturbed incident wave. That this assumption is grossly wrong is apparent.

3.1 The Exact Huyghens-Helmholtz Diffraction Integral and the Kirchhoff Theory of Diffraction

Probably the deepest insight into the theory of diffraction is obtained with the aid of the (exact) Helmholtz-Huyghens

- 12 -

integral (see Appendix II) for the sound pressure p :

$$p = \frac{-1}{4\pi} \int_{\sigma} \left[p \frac{\partial g}{\partial n} - \frac{\partial p}{\partial n} g \right] d\sigma \quad (1)$$

where g is the infinite free-space Green's function

$$g = g(r) = \frac{1}{r} e^{-jkr} \quad (2)$$

and where it's derivative in the n -direction is

$$\frac{\partial g(r)}{\partial n} = \frac{-jk}{r} e^{-jkr} \cos(\vec{r}, \vec{n}) + \text{a term proportional to } 1/r^2 \quad (3)$$

Integration is performed over a closed surface $\sigma = S + A$ that separates the field point P from the source point L , \vec{n} is its outward normal; the source $g(\rho) = e^{-jk\rho}/\rho$ is thus outside this surface, and ρ is the distance from the source. The surfaces denoted by A and S represent the aperture and the screens respectively (see Figure 1). In the above integral, the first term describes the contribution of the pressure in terms of a layer of dipole sources, because $\frac{\partial g}{\partial n} = \frac{\partial g}{\partial r} \cos(\vec{r}, \vec{n})$ is proportional to $\cos \theta = \cos(\vec{r}, \vec{n})$. The second term is equivalent to a distribution of simple sources over the boundary surfaces.

Let us first investigate the field behind the screen in the space τ opposite the point source. If one represents the solution in the space that is insonified directly as

$$p = e^{-jk\rho}/\rho + \Delta p = g(\rho) + \Delta p \quad (4)$$

where $g(\rho) = e^{-jk\rho}/\rho$ represents the incident amplitude in the light space and is zero in the shadow space and Δp is the correction to the geometric optical intensity by the diffraction phenomenon.

Kirchoff assumes that $p = g(\rho)$, i.e. that the pressure is the

- 13 -

same as that in the incident wave, and thus neglects any reflections and the effect of diffraction on the field values near the diffracting object. Kirchhoff also assumes $p(\rho) = 0$ and $\frac{\partial p(\rho)}{\partial n} = 0$ at all shaded surfaces. The terms containing Δp will thus represent the deviation of the Kirchhoff solution from the exact solution. Let the integrating surface now be a closed surface just behind the screens and the aperture, so that $g(\rho)$ and $\frac{\partial g(\rho)}{\partial n}$ are zero everywhere on S . The above integral then becomes

$$\begin{aligned}
 4\pi p &= - \int_{S+A} \left\{ g(r) \frac{\partial}{\partial n} [g(\rho) + \Delta p] - [g(\rho) + \Delta p] \frac{\partial g(r)}{\partial n} \right\} d\sigma \\
 &= \int_A - [g(r) \frac{\partial}{\partial n} g(\rho) - g(\rho) \frac{\partial g(r)}{\partial n}] d\sigma \\
 &\quad - \int_{S+A} \left\{ g(r) \frac{\partial}{\partial n} (\Delta p) - (\Delta p) \frac{\partial g(r)}{\partial n} \right\} d\sigma \\
 &= 4\pi p_{\text{Kirch}} + 4\pi \delta p \tag{5}
 \end{aligned}$$

where

$$p_{\text{Kirch}} = - \frac{1}{4\pi} \int_A [g(r) \frac{\partial}{\partial n} g(\rho) - g(\rho) \frac{\partial g(r)}{\partial n}] d\rho \tag{6a}$$

- 14 -

is the Kirchhoff solution, and δp is the deviation of the Kirchhoff solution from the exact solution:

$$4\pi\delta p = \int_{S+A} - \left\{ g(r) \frac{\partial}{\partial n} (\Delta p) - \Delta p \frac{\partial g(r)}{\partial n} \right\} d\sigma \quad (6b)$$

For plane rigid diffractors as the study of special cases shows, the deviation δp is usually represented by fluctuations of the pressure and velocity field near the diffracting edges. For instance, for an infinite straight edge, the distance x between successive maxima in the plane of the straight edge is practically equal to the sound wave length. The space spectrum of these ripples is similar to that of a sinusoidal pulse of finite width. It centers at the carrier wave length which corresponds to the coincidence wave length for sound radiation. The sound components whose wavelength is slightly longer, radiate in a direction at or close to grazing to the plane of the aperture and thus affect the sound radiation in directions normal to the shadow boundary whereas the long wave number components radiate in the forward and backward direction (see Theory of Sound Vibration from Infinite Plate, for instance, E. J. Skudrzyk, 1971, page 319).

The Kirchhoff diffraction solution, which assumes ideally absorbent screens and consequently neglects the diffraction due to the reflected field, vanishes for observation points which are located in the direction opposite to the direction of propagation of the incident rays (as for an infinite plane wave, see page 46). This conclusion follows from the Rubinowicz ingegral, page 22 (because $\cos(\vec{\rho}, \vec{n}) = 0$). Since there is no Kirchhoff error, δp is responsible for all the radiation in this direction.

If the screen or diffractor is of the pressure release type, an additional source field will be generated near the edges of the

- 15 -

diffraction, because of periodic compression of the material by the sound wave. The pressure scattered by a small particle is given by Rayleigh, Theory of Sound, Volume II or Skudrzyk 1971, pages 416, 504:

$$\frac{\tilde{p}_{sc}}{\tilde{p}_i} = - \frac{k^2 e^{-jkr}}{r} \tau \left[\frac{\lambda_k - \lambda_{k0}}{\lambda_k} + \frac{\rho - \rho_0}{\rho} \cos \theta \right] \quad (7)$$

τ = volume of scatter

λ_k = bulk modulus

ρ = density

where θ is the angle between the direction of propagation and the vector from the scatterer to the field (see Figure 2). Letters with no subscripts refer to the undistributed medium, letters with subscripts zero refer to the scatter. Backscattering occurs for $\theta = \pi$. If $\lambda_{k0} = \rho_0 = 0$, i.e. pressure release, we have

$$\frac{\tilde{p}_{sc}}{\tilde{p}_i} = - \frac{k^2 e^{-jkr}}{r} \tau [1 + \cos \theta] \quad (8)$$

A similar expression is obtained for a rigid scatterer except that the expression in the bracket is replaced by $[-1 + \cos \theta]$. Thus for a pressure release scatterer there is practically no scattering in the direction back to the source, and considerable scattering in the forward direction where exactly the opposite is true for a pressure release scatterer. We can expect that the Kirchhoff solution for scattering along the axis of a pressure release screen (at low frequencies) deviates more from that of the exact solution than it does for a rigid screen. Both the rigid and pressure release Kirchhoff solutions will be less

- 16 -

accurate for scattered rays that are incident at or near grazing to the screen.

Figure 3 shows a comparison between the exact solution and the Kirchhoff solution for the diffraction of a rigid disk for normally incident sound. Agreement is very good for large values of ka up to angles close to the first zero in the Kirchhoff solution. In the exact solution the zeroes of the Kirchhoff solution are filled in, and scattering for grazing incident rays is greater. However, over quite a wide angular range, i.e. over the range where scattering or diffraction is significant, the Kirchhoff solution gives a very good description of the phenomenon, see Leitner 1949.

We may expect that at high frequencies, the velocity over the aperture is very nearly that in the incident wave and deviations from it will only occur near the edge of the aperture. If also the ratio of the radius of curvature to the wave length is great, then the field in the proximity of the edge will be similar to that near the edge of a straight edge. We can then use this field to correct the Kirchhoff solution. W. Braunbeck, in a series of papers from 1950 onwards, developed this method using the exact Sommerfeld solution for the correction field. It happens that this relatively complex solution when substituted in the Kirchhoff formula leads to a known integral. The Braunbeck-Kirchhoff solution then leads to a solution for the disc or aperture that agrees fairly closely with the exact results of Meixner 1949 even at relatively low frequencies as is illustrated by Figure 4.

We thus arrive at the conclusion that the Kirchhoff theory is a good approximation for the phenomena of diffraction by plane diffractors. It has the great advantage of being based on assumptions that are clearly specified and is exact in the derivations that are derived from these assumptions.

The Kirchhoff theory does not include the field that is generated by the reflected wave nor by multiply reflected waves. For plane diffractors, the field of the reflected wave can

- 17 -

easily be supplied as the field generated by the image source. But multiple reflections as it occurs with three-dimensional diffractors is not in the reach of the Kirchhoff theory (see the case of the open horn discussed above), because all the diffracting surfaces are assumed to be ideally absorbent. For the reflected, as well as for the diffracted waves, the diffractor is ideally transparent and multiply reflected waves are excluded by the definition of the Kirchhoff diffractor. From the point of the diffracted wave, the diffractor seems to have no volume and the diffracted waves always propagate into the full angular space 4π . In contrast, the exact solution describes a diffracted field that is confined to the space outside the diffractor. Thus for a blunt wedge, the free space around the edge extends over an angle of only a little more than π radians, whereas for the Kirchhoff space this angle is always 2π radians. A ray that has been diffracted once is immune to further interaction with the diffractor. It traverses it as if the diffractor is transparent. Because of this assumption, the shape of the diffractor has no effect on the field near to it. Therefore, we can not expect the Kirchhoff theory to yield approximations for the diffraction field produced by three-dimensional diffractors.

3.2 The Kirchhoff Solution

The Kirchhoff Solution leads to excellent agreement with the exact solution whenever the direction of the diffracted rays do not differ greatly from that of the incident beam, and it is a relatively easy task to derive this solution. It leads to fair agreement also for other angles of diffraction. It gives insight into the physics of diffraction like no other method or type of solution does.

Because the Kirchhoff solution agrees closely with the exact solution in certain angular ranges, it is a theory that is well suited to derive the distance dependence of the diffracted

- 18 -

field. It is very suited as nucleus for an improved solution, for instance, by applying the Keller method to the Kirchhoff solution as a starting point rather than to the geometric optical divergence relations. This procedure will safeguard us from committing any serious error because the results are exact conclusions derived from well defined and very reasonable assumptions.

The Helmholtz Huyghens integral (Appendix II) expresses the field ϕ at a point at an origin $P(\vec{r} = 0)$ inside a closed surface in terms of the values of ϕ and $\frac{\partial \phi}{\partial n}$ at that surface:

$$\phi(0) = \frac{1}{4\pi} \int_{\sigma} \left(g \frac{\partial \phi}{\partial n} - \phi \frac{\partial g}{\partial n} \right) d\sigma \quad (9)$$

where n is the outward normal to the surface σ and

$$g(r) = e^{-jkr}/r \quad (10)$$

is the full space Green's function and r is the distance from the field point to the surface. The sources are outside the surface σ , so that σ separates the sources from the field point.

If the field point and the sources are on the same side of the surface (either outside or inside) then the above integral is zero

$$0 = \frac{1}{4\pi} \int_{\sigma} \left(g \frac{\partial \phi}{\partial n} - \phi \frac{\partial g}{\partial n} \right) d\sigma \quad (11)$$

where

$$g = e^{-jkr}/r \quad (12)$$

and r is the distance from any fixed field point on the source side to the surface of integration.

It is convenient to separate the geometric optical field from the diffraction field. This is done by considering the

- 19 -

volume outside the volume taken up by the screen as integration volume (see Fig. 5) and both sides of the screens as the surface of integration. The source now is contained in the space of integration and must be excluded by a little sphere in the same manner, as was excluded the immediate vicinity of the field point previously from the space of integration. Source and field points thus are surrounded by little spheres and (except for the sign) contribute in the same manner.

The integral over the source sphere then is equal to the volume flow of the source (unity here) taken with a sign opposite to that of the surface integral around the field point and the source term thus appears on the right hand side of ϕ_K with positive sign, n is the normal pointing into the screen. If the screens are thin, we can combine the contribution of the illuminated and the shadow side of the screens and integrate only over the surface of the screen.

If we do this with the Helmholtz Huyghens integral, Equation (8), we obtain the result

$$\phi = \frac{e^{-jkR}}{4\pi R} + \frac{1}{4\pi} \int_{\substack{\text{screen} \\ \text{illum. side}}} \left(g \frac{\partial \phi}{\partial n} - \phi \frac{\partial g}{\partial n} \right) d\sigma \quad (13)$$

The normal now points into the illuminated space. Here we have an exact result, and ϕ and $\frac{\partial \phi}{\partial n}$ represent the discontinuities in the pressure and pressure gradient (velocity) across the screen surfaces.

The Kirchhoff integral is obtained by replacing ϕ and $\frac{\partial \phi}{\partial n}$ by their values in the incident wave as if the screens were perfectly absorbent, and assuming $\phi = 0$, $\frac{\partial \phi}{\partial n} = 0$ on the shadow side of the screens.

The last assumption means that ϕ is identically zero everywhere;

this amounts to neglecting the diffracted field adjacent to the screen in the boundary conditions for the shadow region.

The incident wave can be represented by an exactly similar integral over a closed surface (screen + aperture). The normal \vec{n} then is positive from the shadow space to the light space (towards the source). In the above integral, \vec{n}' is chosen positive in the opposite direction ($\vec{n}' = -\vec{n}$). By changing \vec{n}' into $-\vec{n}$, and replacing the incident wave by the surface integral, the parts over the screen have opposite signs and we are left with

$$\begin{aligned}\Phi &= \Phi_K = \frac{1}{4\pi} \int_{\substack{\text{illum. screen} \\ + \text{ aperture}}} \left\{ g(r) \frac{\partial g(\rho)}{\partial n} - g(\rho) \frac{\partial}{\partial n} g(r) \right\} d\sigma \\ &= \frac{1}{4\pi} \int_{\text{illum. screen}} \left\{ g(r) \frac{\partial g(\rho)}{\partial n} - g(\rho) \frac{\partial g(r)}{\partial n} \right\} d\sigma \\ &\quad + \frac{1}{4\pi} \int_{\text{aperture}} \left\{ g(r) \frac{\partial g(\rho)}{\partial n} - g(\rho) \frac{\partial}{\partial n} g(r) \right\} d\sigma \quad (14)\end{aligned}$$

The last formula represents the deviation of the Kirchhoff formula from the exact solution.

Next we introduce the integral over the aperture A and the truncated shadow (i.e. the shadow) K, (see Fig. 6). This integral obviously represents the incident wave $g(R) = e^{-jkR}/4\pi R$

$$\Phi_g = g(R) = \frac{1}{4\pi} \int_{A + K} \left\{ g(r) \frac{\partial}{\partial n} g(\rho) - g(\rho) \frac{\partial}{\partial n} g(r) \right\} d\sigma \quad (15)$$

Φ_g represents the illumination of the aperture if diffraction is

- 21 -

neglected. The integral we are interested in (Eq. 14) is exactly as the one above (Eq. 15) except that it is taken only over the surface A. Thus

$$\phi_K = \phi_g - \phi_{\text{cone}}$$

This integral represents the resultant field, i.e. the sum of the incident field ϕ_g and the diffraction field. Hence

$$\phi_K = \phi_g - \phi_{\text{cone}} = \phi_g + \phi_d \quad (16)$$

The last form of the right hand side defines the diffracted field ϕ_d .

$$\phi_d = - \phi_{\text{cone}}. \quad (17)$$

We have thus transformed the Kirchhoff integral into an integral over the shadow boundary K (K = shadow cone surface:)

$$\phi_d = - \frac{1}{4\pi} \int_K \left\{ g(r) \frac{\partial}{\partial n} g(\rho) - g(\rho) \frac{\partial}{\partial n} g(r) \right\} d\sigma \quad (18)$$

This integral now describes the diffraction as the exclusive effect of the shadow boundary. In the Kirchhoff approximation the diffractors that cast the same geometrical shadow generate the same diffraction field.

4. THE RUBINOWICZ INTEGRAL

The Kirchhoff integral (Eq. 18) over the shadow boundary can be transformed with a line integral over the diffracting edge. The surface $\rho = \text{constant}$ (ρ is the distance along light ray from source point) intersects with the surface K at right angles.

- 22 -

Hence at K we must have:

$$v_n = - \left. \frac{\partial}{\partial n} g(\rho) \right|_K = 0 \quad (19)$$

Therefore, the diffracted field becomes

$$\Phi_d = \frac{1}{4\pi} \int_K g(\rho) \frac{\partial}{\partial n} g(r) d\sigma = \frac{-jk}{4\pi} \int_K \frac{e^{-jk(\rho+r)}}{\rho r} \left(1 + \frac{1}{jkr}\right) \cos(\vec{n}, \vec{r}) d\sigma \quad (20)$$

where, as before, ρ is the distance from the source and r that from the field point to the element $d\sigma$ of the surface of integration. Thus, every element of the shadow boundary acts like a dipole source, whose amplitude is proportional to that of the incident wave, and whose axis is normal to the shadow boundary, where the normal vector points into the shadow region. It is possible to transform this surface integral into a line integral over the diffracting edge by performing a somewhat tricky partial integration (see Appendix IV). The result is

$$\Phi = \alpha \Phi_g - \frac{1}{4\pi} \int_{\text{edge}} \left\{ \frac{e^{-jk\rho}}{\rho} \sin(\vec{\rho}, d\vec{s}) ds \right\} \frac{\cos(\vec{r}, \vec{n})}{1 + \cos(\vec{r}, \vec{\rho})} \frac{e^{-jkr}}{r} \quad (21)$$

Note that \vec{r} and $\vec{\rho}$ are vectors that point to the edge element $d\vec{s}$, and that $\angle \vec{r}, \vec{\rho}$ is the angle subtended between the positive direction of these end vectors (see Fig. 7). The factor α is equal to unity if the incident wave reaches the field point unobstructed and zero otherwise. The terms in the bracket describe the field that is incident on the element ds , $\sin(\vec{\rho}, d\vec{s})$ being the length of the projection of $d\vec{s}$ onto the incident ray. The second group

of factors represents the elementary, but fictitious wave that is emitted by the edge element ds . This fictitious wave has the directivity factor $\cos \theta = \cos (\vec{r}, \vec{n})$ as if it came from a dipole with the axis normal to the shadow boundary; but its amplitude depends in a complex manner on the distance. As far as its amplitude is concerned, it seems to come from a point at a distance r' from the field point where

$$r' = r[1 + \cos (\vec{r}, \vec{\rho})]. \quad (22)$$

It is not possible to interpret the whole function $\cos (\vec{n}, \vec{r}) / [1 + \cos (\vec{r}, \vec{\rho})]$ as a directivity factor of a wave, since this function becomes infinite at the shadow boundary ($\vec{r}, \vec{\rho} = \pi$). If interpreted as a directivity function, it would have to be represented by a kind of delta function. For a plane incident wave, $\rho \rightarrow \infty$, and

$$\phi = \alpha \phi_g - \frac{1}{4\pi} \int_{\text{edge}} e^{-jkx} \frac{e^{-jkr}}{r} \frac{\cos (\vec{n}, \vec{r})}{1 + \cos (\vec{r}, \vec{\rho})} \sin (\vec{x}, \vec{ds}) ds \quad (23)$$

where the x axis has been assumed parallel to the direction of the incident rays, and x is the x coordinate of the edge element ds .

Every point of the diffracting edge can then be identified with a sound source and the resultant diffraction field is given by an integral of the form

$$\phi_d = \int_{\text{edge}} \frac{e^{-jk\rho_s}}{\rho_s} \frac{e^{-jkr_s}}{r_s} A(\vec{\rho}_s, \vec{r}_s, \vec{ds}) ds \quad (24)$$

where ρ_s is the distance from the source from the diffracting element, r_s that of the field point to the edge element ds and $A(\vec{\rho}_s, \vec{r}_s, \vec{ds}) ds$ represents the amplitude of the edge wave that is generated at the element ds . Unless the edge has sharp corners, the function A will be a slowly varying function of s , and if we assume that the wavelength $2\pi/k$ is sufficiently large compared to

- 24 -

the length of the edge, the integral can be evaluated by the stationary phase method. The stationary phase point is given by the zero of the derivative of the exponent (see Appendix I)

$$\frac{d}{ds}[k(\rho_s + r_s)] = 0$$

or

$$\frac{d}{ds}(\rho_s + r_s) = 0. \quad (25)$$

This means that the path of the diffracted ray from the source to the field point is stationary (i.e. is a maximum, a minimum, or represents a point of inflection when plotted as a function of s). Relation (25) is identical with Fermat's principle which is derived by assuming geometric optical conditions.

The law of edge refraction shows that Fermat's geometric optical principle applies to the stationary phase points of the diffraction integral whenever it is possible to decompose the resultant field into a geometric optical field and a diffraction field, i.e. whenever Huyghens principle, the Kirchoff theory, or the Rayleigh diffraction integral, or a similar approximation applies.

The edge law can also be written in the following form

$$\frac{dr_s}{ds} + \frac{d\rho_s}{ds} = 0 = \cos(\vec{r}_s, \vec{ds}) + \cos(\vec{\rho}_s, \vec{ds}), \quad (26)$$

which implies that the stationary phase contribution arises from the geometrical relation

$$\cos(\vec{r}_s, \vec{ds}) = -\cos(\vec{\rho}_s, \vec{ds}) \quad (27)$$

The condition that radiation is emitted to the field point is that

$$\angle(\vec{\rho}_s, \vec{ds}) = \pi - \angle(\vec{r}_s, \vec{ds}) \quad (28)$$

- 25 -

The incident ray hits the edge under the same (grazing) angle as the diffracted ray leaves it (see Figure 8). The basic diffraction law is thus very similar to the reflection law of a mirror

Angle of incidence (with respect to the edge) = Angle of Reflection

The only difference is that because of the one-dimensionality of the edge diffractor the incident and reflected rays lie not in a single plane as they do for a flat mirror; the reflected ray lies on the surface of a cone whose semi-apex angle is equal to the angle of reflection (Fig. 8a). We shall show below that the amplitude of the diffracted field is a maximum in the direction of the incident ray, i.e., at the shadow boundary, for which it is equal to one half the incident amplitude, and that it is approximately inversely proportional to the angular distance from the shadow boundary (Fig. 8b). This means that the diffracted field concentrates on the surface of a cone, whose angle at the apex with $d\vec{s}$ is the same as that of the incident ray. Thus incident and diffracted rays lie at opposite sides of the diffracting edge element ds . If we are interested in back scattering only, the diffracted and incident ray must be coincident. For backscattering $\beta = 90^\circ$, i.e. the radiation must impinge normally to the scattering edge.

The locations of the stationary phase points can easily be determined by the edge law of diffraction, (Eq. 25). Their contribution to the diffracted field then is given by the standard formula

$$\phi_d = \int_{\text{edge}} S(s) e^{ug(s)} ds = \sum_v \frac{S(s_v) e^{ug(s_v)} \sqrt{2\pi}}{(u g''(s_v))^{1/2}} \quad (29)$$

and in terms of the variables of diffraction, writing $ug(s) = -jk\zeta = -jk(\rho + r)$, we have for each stationary phase point the

- 26 -

following contribution to the diffracted field

$$(\phi_d)_v = \frac{1}{2\sqrt{2\pi k}} \frac{1}{\sqrt{\rho_v r_v}} \frac{1}{\sqrt{\zeta_v''}} e^{-j[k(\rho_v + r_v) \pm \pi/4]} \frac{\cos(\vec{n}, \vec{r}_v)}{1 + \cos(\vec{r}_v, \vec{\rho}_v)} \sin(\vec{\rho}_v, \vec{ds}_v)$$

where ds_v represents an element of the edge for which

$$\frac{d}{ds}(\zeta) = \frac{d}{ds}(\rho_s + r_s) = 0.$$

The derivative of r_s and ρ_s with respect to s are computed with the aid of the well known Frenet formulae. We find (see Appendix V)

$$\zeta'' = \frac{\partial^2}{\partial s^2}(\rho_s + r_s) = \sin^2(\vec{\rho}_s, \vec{ds}) \left(\frac{1}{\rho_s} + \frac{1}{r_s} \right) + \frac{1}{R_K} [\cos(\vec{\rho}_s, \vec{h}) + \cos(\vec{r}_s, \vec{h})]$$

If this is substituted above, we obtain the exact Kirchhoff contribution of a stationary phase point on an edge of arbitrary radius of curvature R_K , see Figure (9):

$$\phi_d = \frac{1}{2\sqrt{2\pi k}} \frac{1}{\rho r} \frac{e^{-jk(\rho + r) \pm j\pi/4}}{\sqrt{\frac{1}{\rho} + \frac{1}{r} + \frac{1}{R_K} \left\{ \frac{\cos(\vec{\rho}, \vec{h}) + \cos(\vec{r}, \vec{h})}{\sin^2(\vec{\rho}, \vec{ds})} \right\}}} \left[\frac{\cos(\vec{n}, \vec{r})}{1 + \cos(\vec{r}, \vec{\rho})} \right] \quad (32)$$

Where r and ρ denote the distances to the stationary phase point s_v as determined by Eq. 25, and \vec{h} is the unit vector along the main normal of the edge curve, and R_K is the radius of curvature of the edge. R_K is basically positive and points towards the center of curvature. Note that \vec{r} points from the field point and $\vec{\rho}$ from the source point to the edge (see Fig. 7). The effect of the curvature R_K of the edge curve is interesting, as can be exhibited from the following example: Consider a disk of radius a , such that a polar coord system (r, θ, ϕ) is centered at its center with its axis normal to the plane of the disc. Let the source be located at $(\ell, \theta, 0)$ and the receiver be located at $(\ell, \frac{\pi}{2}, \pi)$. Thus, the diffracted field has two stationary phase points, s_1 at $(a, \frac{\pi}{2}, 0)$

- 27 -

(minimum) and s_2 at $(a, \frac{\pi}{2} \cdot \pi)$ (maximum). The contribution of the first point s_1 to the diffracted field can be computed from (32) as follows if $\ell \gg a$:

$$\oint \vec{\rho}_1, \vec{h}_1 \doteq \frac{\pi}{2} - \theta, \oint \vec{r}_1, \vec{h}_1 = \pi, \oint \vec{\rho}_1, d\vec{s} = \frac{\pi}{2}$$

$$\oint \vec{n}, \vec{r}_1 \doteq \pi - \theta, \oint \vec{r}_1, \vec{\rho}_1 \doteq \frac{\pi}{2} + \theta, r = \ell + a, \rho = \ell - a, R_K = a$$

Thus

$$(\Phi_d)_1 \doteq \frac{1}{2\sqrt{2\pi k \ell}} \frac{e^{-jk[2\ell + a(1 - \sin\theta)] + j\pi/4}}{\ell \sqrt{\frac{\ell}{a}(1 - \sin\theta)}} \frac{\cos\theta}{1 - \sin\theta}$$

The contribution of the second stationary phase $s_2 = a, \frac{\pi}{2}, \pi$ is the same except that \vec{h} and \vec{n} must be replaced by $-\vec{h}$ and $-\vec{n}$ and the angles relative to \vec{h} and \vec{n} by angles that are measured by $\pm\pi$.

The contribution of the second stationary phase point is then given by

$$\Phi_{d2} = + \frac{1}{2\sqrt{2\pi k \ell}} \frac{e^{-jk[2\ell - a(1 - \sin\theta)] - j\pi/4}}{\ell \sqrt{\frac{\ell}{a}(1 - \sin\theta)}} \frac{\cos\theta}{1 - \sin\theta}$$

The factor $1/\sqrt{\ell/a} = \sqrt{R_K/\ell}$ describes the strong divergence of the diffracted field due to the curvature of the edge. In performing the computation, we have implicitly assumed the existence of a shadow boundary. For $\theta = \frac{\pi}{2}$, a shadow boundary would only be formed if the disc was infinitely large. If $\theta = \frac{\pi}{2}$ and the disc was finite, waves would pass over both its surfaces undisturbed, and consequently no diffraction would be observed.

The stationary phase evaluation makes sense only if the diffracting edge is sufficiently long relative to the wave length so that the limits of integration along the edge can be replaced by minus and plus infinity. This requirement is usually not

- 28 -

fulfilled for finite edges if the incident wave is oblique or if the edges are short. Thus, a stationary phase point is either beyond the edge and consequently integration does not extend to this point, or the integrand may vary so little during the integration that the effects of phase cancellation are negligible, and that every element ds along the whole range contributes about the same amount to the resultant field. The stationary phase method leads to the same variation of the solution with the distance from the diffractor of Fermat's principle or the geometrical theory of diffraction. This result shows that the geometrical theory of diffraction is applicable to real finite diffractors only in very special instances. More about the solution in the distance, angle and frequency range where the geometrical theory fails will follow in sections 10, 11 and 12.

5. THE GEOMETRICAL THEORY OF DIFFRACTION

The geometrical theory of diffraction as it is understood today is a theory that is based on the laws of geometrical optics. The missing details are impressed on this theory by comparison with exact solutions. The diffraction field obtained from the geometrical theory of diffraction has the same amplitude distance dependence as does the high frequency limit of the Kirchhoff-Rubinowicz theory when diffraction reduces to the energy emitted by a single or a finite number of stationary phase points. However, the geometric optical theory gives no indication of the amplitude of the diffracted field and its variation with angle. Keller supplied the two missing items by replacing his constants by angle functions that make the geometrical solution agree with the exact solution. In the high frequency limit, all plane diffractors are equivalent to semi-infinite planes. Furthermore, since the diffraction fields are generated by only the edge elements near and at the stationary phase points, and since the divergence of the diffracted field is only a function of the curvature of the edge, it is thus understandable why Keller's method of geometrical diffraction is very successful.

Let us now turn to the derivation of the basic relations that lead to the geometrical theory of diffraction.

Let us first consider the wave front of a bundle of diffracted rays. The rays are the normal trajectories of the wave front. Let us then consider a tube of diverging rays, whose cross-section is rectangular, with dimensions ds_1 and ds_2 and consider a wave front in the plane in which its radii of curvature are R_α and R_β . The height and breadth of the cross section of the tube (Fig.10) then are $ds_1 = R_\alpha d\theta_1$ and $ds_2 = R_\beta d\theta_2$
 $d\sigma_1 = ds_1 ds_2 = R_\alpha R_\beta d\theta_1 d\theta_2$

Let the cross-sectional surfaces of the tube of rays represent surfaces of principle curvatures. Consider an edge element ds_1 and let R_α be a principle radius of curvature of the wave front in the plane of ds_1 and let ds'_1 be the height of the cross section at $R_\alpha + \ell$. We then have

$$\frac{ds'_1}{ds_1} = \frac{(\ell + R_\alpha) d\theta_1}{R_\alpha d\theta_1} = \frac{(\ell + R_\alpha)}{R_\alpha} \quad (34)$$

A similar relation applies for the width of the tube

$$\frac{ds'_2}{ds_2} = \frac{\ell + R_\beta}{R_\beta} \quad (35)$$

The change in cross-sectional area of the tube over the distance ℓ is thus given by

$$\frac{ds'_1 ds'_2}{ds_1 ds_2} = \frac{d\sigma_2}{d\sigma_1} = \frac{(\ell + R_\alpha)(\ell + R_\beta)}{R_\alpha R_\beta} \quad (36)$$

We assume that the power dN transmitted through an area $d\sigma$ by a wave incident in the direction of its normal is proportional to the area of $d\sigma$ and to the square of the amplitude A of the wave. Since the same power passes through $d\sigma_1$ and $d\sigma_2$, then

$$dN = d\sigma_1 A_1^2 = d\sigma_2 A_2^2, \quad (37)$$

- 30 -

and the wave amplitudes are related as follows:

$$A_2^2 = A_1^2 \frac{d\sigma_1}{d\sigma_2} = A_1^2 \frac{R_\alpha R_\beta}{(R_\alpha + \ell)(R_\beta + \ell)} \quad (38)$$

If (ds) is the elementary length of the scatterer, waves will propagate outward from (ds) in all directions. This means that one principal radius of curvature will be the distance from the edge (ds) regardless of the second principal radius of curvature of the incident wave front. Hence we set $R_\beta \ll \ell$.

The preceding equation then reduces to

$$A_2^2 = \frac{[A_1^2 R_\beta] R_\alpha}{(R_\alpha + \ell) \ell} \quad (39)$$

The quantity

$$2\pi R_\beta A_1^2 = 2\pi \text{const.} = 2\pi B_0^2 \quad (40)$$

is the energy that is emitted per unit length of the edge, where B_0^2 is a constant that represents the energy that crosses the surface of a cylinder of a very small radius R_β per unit length. Introducing B_0 into Eq. (39) then leads to

$$A_2^2 = \frac{B_0^2 R_\alpha}{(R_\alpha + \ell) \ell}$$

and

$$A_2 = B_0 \sqrt{\frac{R_\alpha}{(R_\alpha + \ell) \ell}} = B_0 \sqrt{\frac{1}{(1 + \ell/R_\alpha) \ell}} \quad (41)$$

If A_2 is an amplitude, B_0 is an amplitude multiplied by the square root of a length. The radius of curvature R_α of an elementary area $d\sigma$ normal to the diffracted rays (i.e. the divergence of the elementary rays) is determined by the intersection of the diffraction cones that correspond to two points

- 31 -

on the edge, a small distance (ds) apart (see Figs. 10 and 11). The scattering cones intersect. Let $\vec{x}(s)$ be the vector from an arbitrary origin to the scattering element $d\vec{s}$ where (s) is the distance along the curved edge. First, let us derive the equation of a single scattering cone with the apex on the edge at $\vec{x}(s)$ and the half angle $\beta(s) = \angle(\vec{\rho}, d\vec{s})$ where $\vec{\rho}$ is vector from the source to the edge. The direction of the cone axis is the same as that of the edge element $d\vec{s}$. A variable point \vec{y} on a cone surface whose apex is at $\vec{x}(s)$ satisfies the equation

$$\frac{[\vec{y} - \vec{x}(s)] \cdot \dot{\vec{x}}(s)}{|\vec{y} - \vec{x}(s)|} = \cos\beta(s), \quad \dot{\vec{x}}(s) = \frac{\partial \vec{x}(s)}{\partial s} = \frac{d\vec{s}}{ds},$$

$$|\dot{\vec{x}}(s)| = 1. \quad (42)$$

A second cone is obtained by increasing s by ds. The curve of intersection of two cones with the apexes at $\vec{x}(s)$ and $\vec{x}(s + ds)$ is given by eliminating s from the two equations. This is best done by retaining Eq. (42) and, instead of writing out the equation with the apex at $\vec{x}(s + ds)$, and forming the difference between the two equations, one can differentiate Eq. 42 with respect to s,

$$[\vec{y} - \vec{x}(s)] \cdot \ddot{\vec{x}}(s) - \dot{\vec{x}}(s) \cdot \dot{\vec{x}}(s) = -|\vec{y} - \vec{x}(s)| \sin\beta(s) \frac{\partial \beta(s)}{\partial s}$$

$$- \frac{[\vec{y} - \vec{x}(s)] \cdot \dot{\vec{x}}(s)}{|\vec{y} - \vec{x}(s)|} \cos\beta(s) \quad (43)$$

Because of Eq. (42), the last term on the right reduces to $-\cos^2 \beta(s)$. If the square root in the first term on the right is represented by Eq. (42) and with the aid of the relations: $\dot{\vec{x}} \cdot \dot{\vec{x}} = |\dot{\vec{x}}|^2 = 1$, $\ddot{\vec{x}}(s) = \vec{h}/R_K$, $\dot{\vec{x}}(s) = \vec{t}(s)$, we obtain

- 32 -

$$[\vec{y} - \vec{x}(s)] \cdot [\vec{h}(s) - \vec{t}(s) R_K \frac{\partial \log(\cos \beta)}{\partial s}] = R_K \sin^2 \beta.$$

Here R_K is the radius of curvature of the diffracting edge, $\vec{h}(s)$ the unit normal vector at the edge, and $\vec{t}(s)$ the unit tangent vector to the edge. Equation (42) can be written in the form:

$$[\vec{y} - \vec{x}(s)] \cdot \vec{t}(s) = |\vec{y} - \vec{x}(s)| \cos \beta(s). \quad (44)$$

The angle δ between the diffracted ray and \vec{h} is given by

$$\cos \delta = \frac{[\vec{y} - \vec{x}(s)] \cdot \vec{h}}{|\vec{y} - \vec{x}(s)|} \quad (45)$$

The radius of curvature of the diffracted ray R_α has been defined above as the distance $|\vec{y} - \vec{x}|$ from the edge to the caustic where two adjacent diffraction cones intersect. This distance is obtained by substituting Eqs. (44) and (45) into Eq. (43):

$$R_\alpha [\cos \delta + R_K \dot{\beta} \sin \beta] = R_K \sin^2 \beta. \quad (46)$$

The result [Eq. (46)] of the computation for the radius of curvature (the divergence of the elementary rays), can be written in the following form:

$$R_\alpha = \frac{(\pm) R_K \sin^2 \beta}{\cos \delta + R_K \dot{\beta} \sin \beta}, \quad (47)$$

where again $R_K(s)$ is the radius of curvature of the edge, $\beta(s)$ the angle between the incident ray \vec{p} and the (positive) tangent $\vec{t}(s)$ to the edge (i.e., the semi-angle of the diffraction cone) and $\dot{\beta} = \partial \beta / \partial s$ the angle rate between the diffracted ray and the edge. The unit vector \vec{h} then is the normal pointing from the edge point towards the center of curvature of the edge in the plane of the screen. The direction in which the arc length increases is of no consequence, since both $\dot{\beta}$ and $\sin \beta$ change

- 33 -

sign when this direction is reversed.

The sign of the radius of curvature R_α has still to be determined. It is standard practice to consider R_K as a basically positive quantity. If the edge is curved away from the source point, one would expect diffraction to lead to a caustic focus whose position is away from the edge in the direction of the diffracted rays. The wave should, therefore, appear to diverge from $(\vec{r} - \vec{R}_\alpha)$ and we have to use the negative sign in the above formula. That this sign is indeed the right one to use is borne out by the results. The wrong sign would lead to absurd results. We next evaluate the inverse $1/R_\alpha$, from Eq. (47)

$$\frac{1}{R_\alpha} = - \frac{(\cos \delta + R_K \dot{\beta} \sin \beta)}{R_K \sin^2 \beta} \quad (48)$$

We still have to compute $\dot{\beta}$. We have, from the vector diagram,

$$\cos \beta = \frac{d\rho}{ds} = \cos(\vec{\rho}, \vec{ds}) \quad (49)$$

differentiating this with respect to s yields

$$-\dot{\beta} \sin \beta = \frac{d^2 \rho}{ds^2} \quad (50)$$

The derivative $\frac{d^2 \rho}{ds^2}$ is computed with the aid of the well known Fresnet formula (see any text book on differential geometry). If \vec{t} is the unit tangent vector along ds , $|\vec{t}| = 1$,

$$\frac{d\vec{\rho}}{ds} = \vec{t}, \quad \frac{d\rho}{ds} = \cos(\vec{\rho}, \vec{ds}) = \cos \beta = \frac{\vec{\rho}}{\rho} \cdot \vec{t},$$

and

$$\frac{d\vec{t}}{ds} = \frac{\vec{h}}{R_K}$$

- 34 -

We thus have:

$$\begin{aligned}
 - \dot{\beta} \sin \beta &= \frac{d^2 \rho}{ds^2} = \frac{d}{ds} \left[\frac{\vec{\rho} \cdot \vec{t}}{\rho} \right] = - \frac{1}{\rho^2} (\vec{\rho} \cdot \vec{t}) \frac{d\rho}{ds} + \\
 + \frac{1}{\rho} \left[\frac{d\vec{\rho}}{ds} \cdot \vec{t} \right] + \frac{1}{\rho} \left[\vec{\rho} \cdot \frac{d\vec{t}}{ds} \right] &= \frac{1}{\rho} \sin^2 \beta + \frac{1}{R_K} \cos(\vec{\rho}, \vec{h}) . \quad (51)
 \end{aligned}$$

If Eqs. (49) and (51) are substituted in Eq. (48), the following expression results for the principal radius of curvature R_α

$$\frac{1}{R_\alpha} = - \frac{\cos \delta}{R_K \sin^2 \beta} + \frac{1}{\rho} + \frac{1}{R_K} \frac{\cos(\vec{\rho}, \vec{h})}{\sin^2 \beta} = \frac{1}{\rho} + \frac{1}{R_K \sin^2 \beta} [- \cos \delta + \cos(\vec{\rho}, \vec{h})] \quad (52)$$

In the Rubinowicz notation, $\delta = \pi - \angle(\vec{r}, \vec{h})$ (\vec{r} points from the observation point to edge element). Hence we have

$$\frac{1}{R_\alpha} = \frac{1}{\rho} + \frac{1}{R_K \sin^2 \beta} [\cos(\vec{r}, \vec{h}) + \cos(\vec{\rho}, \vec{h})] \quad (53)$$

The radius of curvature R_α represents the curvature of the diffracted wave front in a plane that contains the edge element. The last result shows that diffraction increases the curvature of the incident wave by an amount that is proportional to the curvature of the diffracting edge. The second principal curvature of the wave front then is simply given by the inverse of the distance from the diffracting edge.

If we enter this result in Eq. (41), writing r (distance from stationary phase edge point) for ℓ , and recalling that A_0/ρ is equal to B_0 and $\sin \beta = \sin(\vec{\rho}, d\vec{s})$ we obtain

- 35 -

$$A_2 = \frac{A_0}{\rho \sqrt{r} \sqrt{\frac{1}{r} + \frac{1}{\rho} + \frac{1}{R_K}} \left[\frac{\cos(\vec{r}, \vec{h}) + \cos(\vec{\rho}, \vec{h})}{\sin^2(\vec{\rho}, \vec{ds})} \right]} \quad (54)$$

The Keller result is thus identical with the Rubinowicz-Kirchoff distance variation for a stationary phase point. This result is quite suprising. Even the curvature of the incident wave front has no other effect than those described by geometrical optics and Fermats' principle. The Rubinowicz-Kirchoff does furnish the directivity factor

$$\sin(\vec{\rho}, \vec{ds}) \frac{\cos(\vec{r}, \vec{h})}{1 + \cos(\vec{\rho}, \vec{r})} \quad (55)$$

for the incident wave, and a similar factor for its mirror image, i.e. for the reflected wave. Since the sum of the two factors does not reduce to a simple expression, it is expedient to stop at this point and to consider the fields generated by the incident and the reflected waves separately.

Thus, we have obtained the correct distance dependence for the diffraction field in the high frequency limit from geometric optical principles. But the method gives no indication of the angular variation of the diffraction field. Keller determines the directivity factor by replacing the constant A_0 with whatever is needed to make his solution agree with the exact solution for the straight edge and using the resulting formula for all other curved edges. In contrast to Keller's methods, the Rubinowicz-Kirchoff integral can be applied to all but the very low frequencies, i.e. whenever the linear dimensions of the diffractor exceed one wave length. Likewise the Rubinowicz integrals furnishes the directivity function, or at least a very good approximation to it. It seems, however, that the Rubinowicz-Kirchoff method in present form fails for blunt three-dimensional diffractors, which can be handled very

well by Keller's method.

6. CAUSTICS

Rays diffracted by adjacent elements of a curved edge, generate diffraction cones which intersect along a second order curve common to both cones, as seen in Figure (11). Since the wave length of the incident field has been assumed as being infinitely small and since all the contribution from the edge element pass through this curve which is a space of zero volume, the energy density there becomes infinitely great. This curve acts as if it were a line focus. As we move smoothly along the edge, these focal lines form a surface of particular concentration of the diffracted energy, which we called a caustic surface. The diffracted rays appear to originate from this caustic surface.

As an example, we will consider the focusing properties of a pencil of rays. All the rays in a homogeneous medium are straight lines and are orthogonal to the wavefronts. Consider now the small pencil of rays which intersects a wavefront in the small rectangle PQRS (Fig. 12) bounded by lines of curvature. The normals at P, Q intersect at X and those at R, S intersect at Y. Similarly the normals at P, S intersect at Z and those at Q, R intersect at W. All the rays through the rectangle, to the first order of approximation, pass through the lines XY and ZW which are called the "focal lines" of the pencil. This concentration of rays is easily observed with a lens held obliquely in the sun. A small fan-like pencil cutting the surface along PS at Z. A small fan-like pencil in any other direction is not brought into focus at all. The planes PXY and PZW are perpendicular but XY is not in general perpendicular to PX nor ZW to PZ.

Only in the special case when the wavefront is spherical do all the rays of the pencil intersect in a common point; the

- 37 -

pencil is then said to be homocentric point source but the pencil does not remain homocentric in general after reflection and refraction. Instead, the radiation becomes concentrated in focal lines.

If we carry out the preceding construction for all pencils of a wavefront the points Z will generate a surface and so will the points X . These two surfaces are known as the focal surfaces or caustics. Every normal to a wavefront is tangent to both the caustics. The caustics are the loci of the two principal centers of curvature. Therefore, for a wavefront which is a surface of revolution, the caustics consist of a portion of the axis of rotation and a surface of revolution whose meridian section is the evolute of the meridian section of the wavefront.

The caustic surface can be defined by $R_\alpha = r$, so that $1/r - 1/R_\alpha = 0$ where R_α is the distance of the caustic along the diffracted ray from the edge element. For a field point at a caustic surface, $\phi'' = 0$, the standard stationary phase solution therefore becomes infinite. The reason is obvious. The Taylor development in the exponent is the integrand and has been broken off with the square terms. Because $\phi'' = 0$, recalling that also $\phi' = 0$ for a stationary phase point, the exponent is constant and extending the limits to $+\infty$ and $-\infty$ makes the integrand infinite. For a simple caustic surface, $\phi'' = 0$ but $\phi''' \neq 0$; in fact, we may consider this relation as the definition of a simple caustic. Near this caustic ϕ'' will be small, and the Taylor development of the exponent about the stationary phase integrand must be carried up to third order terms:

$$\phi = \phi_0 + (s - s_0) \phi'(s_0) + \frac{(s - s_0)^2}{2!} \phi'' + \frac{(s - s_0)^3}{3!} \phi''' \quad (56)$$

Here, $\phi'(s_0) = 0$, because by definition, the stationary phase

- 38 -

point is at s_0 . But because $(s - s_0)^3$ is negative for $s < s_0$, there is another point for which the above development vanished. This point is given by

$$\phi'(s_1) = 0 = (s_1 - s_0)\phi'' + \frac{1}{2}(s_1 - s_0)^2\phi''' \quad (57)$$

or $s_1 - s_0 = -2\phi''/\phi'''$

provided ϕ''/ϕ''' is small (say compared to π), the above series assumes large values for $(s - s_0) \gg \pi$ and the limits of integration can again be replaced by $\pm\infty$. The above condition means that the field point should not be very far away from the caustic surface. The stationary phase integral can then be evaluated (see Foundations of Acoustics, page 64). The result is

$$\begin{aligned} \phi &= \int_{-\infty}^{\infty} S(s) e^{-jk\phi(s)} ds = \\ &= 2 S(s_v) \sqrt{\frac{3\pi}{k\phi'''(s_v)}} e^{jk\left[\phi(s_v) + \phi''(s_v)^3/3\phi'''(s_v)^2\right]} \\ &\cdot \int_0^{\infty} \cos \left[\frac{\pi(v^3 - mv)}{2} \right] dv \end{aligned} \quad (58)$$

where

$$m = \sqrt{\frac{3k^2}{\pi^2}} \frac{\phi''^2}{(\phi''')^{4/3}} \quad (59)$$

The integral is the Airy integral (see loc. cit). To obtain ϕ''' , we start out with the expression

$$\frac{d\rho}{ds} = \cos(\vec{\rho}, d\vec{s}) = \frac{1}{\rho} (\vec{\rho} \cdot \vec{t}) \quad (60)$$

Hence we obtain

$$\frac{d^2 \rho}{ds^2} = -\frac{1}{\rho^2} (\vec{\rho} \cdot \vec{t}) \cos(\vec{\rho}, d\vec{s}) + \frac{1}{\rho} + \frac{1}{\rho} \left(\vec{\rho} \cdot \frac{d\vec{t}}{ds} \right) \quad (61)$$

and differentiate again with respect to s , making use of the following relations.

$$\frac{d\vec{t}}{ds} = \vec{\tau}, \quad \vec{t} \cdot \vec{t} = \vec{t}^2 = 1, \quad \vec{t} \cdot \frac{d\vec{t}}{ds} = 0 \quad (62)$$

$$\frac{d\rho}{ds} = \cos(\vec{\rho}, d\vec{s}) = \frac{\vec{\rho}}{\rho} \cdot \vec{t}, \quad \frac{d\vec{t}}{ds} = \frac{\vec{h}}{R_K} \quad (\vec{h} \text{ unit vector along main normal})$$

and

$$\frac{d\vec{h}}{ds} = \frac{\vec{B}}{T} \quad (63)$$

where \vec{B} is the unit vector along the binormal and T the torsion. Also $\cos(\vec{r}, d\vec{s}) = -\cos(\vec{\rho}, d\vec{s})$ and $\sin(\vec{r}, d\vec{s}) = \sin(\vec{\rho}, d\vec{s})$

(Eq. 27). A similar expression is obtained for $\frac{d^3 \vec{r}}{ds^3}$. Hence

$$\begin{aligned} \phi''' = & 3 \sin^2 \beta \cos \beta \left[\frac{1}{r^2} - \frac{1}{\rho^2} \right] + \frac{3 \cos \beta}{R_K} \left[\frac{\cos(\vec{r}, \vec{h})}{r} - \frac{\cos(\vec{\rho}, \vec{h})}{\rho} \right] \\ & + \frac{1}{TR_K} [\cos(\vec{r}, \vec{B}) + \cos(\vec{\rho}, \vec{B})] - \frac{1}{R_K^2} \frac{dR_K}{ds} [\cos(\vec{r}, \vec{h}) + \cos(\vec{\rho}, \vec{h})] \end{aligned} \quad (64)$$

In deriving Eq. (64), we have used the stationary phase condition that $\cos \beta = \cos(\vec{\rho}, d\vec{s}) = -\cos(\vec{r}, d\vec{s})$.

If the incident wave is plane and if part of the edge is an arc of the circle of radius a whose plane is normal to the incident radiation, then ϕ'' and all higher derivatives of ϕ are zero. The exponent then is constant for the caustic point and the integral is equal to integral of $S(s)$ over the arc of the circle. Since $S(s)$ is a slowly varying function of s , it can also be considered to be constant over the range Δs and

- 40 -

$$|\phi_d| = S(s) \Delta s \quad (65)$$

where $\Delta s = a(\phi_2 - \phi_1)$ and $\phi_2 - \phi_1$ is the angle the circular arc subtends with its center of curvature. The quantity is the distance on the field point from the arc. For points near the caustic (near the center of curvature) which, by rotating the diffractor, we assume to lie on the x-axis, the projection of the vector from the field point to the edge element on to the plane of the diffractor is given by (see Fig. 13)

$$\begin{aligned} r'^2 &= (a - x \cos \phi)^2 + x^2 \sin^2 \phi = a^2 + x^2 - 2ax \cos \phi \\ &= a^2 \left(1 - \frac{2x}{a} \cos \phi\right) \\ r' &= a \left(1 - \frac{x}{a} \cos \phi\right) + \dots \end{aligned} \quad (66)$$

where x is the distance of the projection of the field point from the center of the circular arc on the plane of the circular arc, and ϕ the angular coordinate of the edge element (see Fig. 13). The distance of the field point from the edge element is then given by

$$\begin{aligned} r &= \sqrt{z^2 + (a - x \cos \phi)^2} = \sqrt{z^2 + a^2 - 2ax \cos \phi + \dots} \\ &= r_0 \sqrt{1 - \frac{2ax \cos \phi}{r_0^2}} = r_0 \left(1 - \frac{ax \cos \phi}{r_0^2} + \dots\right) \end{aligned} \quad (67)$$

where

$$r_0^2 = z^2 + a^2$$

because $x \ll r_0$. The diffraction integral now simplifies to

- 41 -

$$\begin{aligned}\phi &= \int_{\phi_1}^{\phi_2} S(s) \exp[-jkr_o (1 - ax \cos \phi / r_o^2)] ds, \\ &= S(\phi) e^{-jkr_o} \int_{\phi_1}^{\phi_2} e^{j(k ax \cos \phi) / r_o} a d\phi\end{aligned}\quad (68)$$

If the curve is a complete circle, $\phi_1 = 0$, $\phi_2 = 2\pi$ and

$$\phi = S(\phi) e^{-jkr_o} 2\pi a J_0 \left(\frac{kxa}{r_o} \right) \quad (69)$$

If $\phi_2 - \phi_1 \ll \pi$, then $\cos \phi \doteq 1$, and

$$\phi = S(\phi) \cdot e^{-jkr_o} \Delta s \quad (70)$$

where Δs is the length of the arc, whose curvature is constant and whose plane is normal to that of the incident radiation.

Keller's method of taking account of the caustic can only be applied to the case when the diffractor is a circular piston. He multiplies his stationary phase solution for the circular aperture by a factor that is good for the circular aperture, and, hence his account for the caustic is only good for this aperture.

7. THE FIELD AT AND NEAR THE SHADOW BOUNDARY AND THE PHYSICAL SIGNIFICANCE OF EDGE WAVES

In the Kirchhoff-Rubinovicz theory, the diffracted field is expressed as the cumulation of waves that originate at every edge element and is given by Eq. (21),

- 42 -

$$\phi_d = \int_{\text{edge}} \left[-\frac{1}{4\pi} \frac{1}{\rho r} \frac{\cos(\vec{n}, \vec{r})}{1 + \cos(\vec{r}, \vec{\rho})} \sin(\vec{\rho}, d\vec{s}) \right] e^{-jk(\rho + r)} ds \quad (74)$$

The factor $\sin(\vec{\rho}, d\vec{s})ds$ measures the incident intensity, i.e. width of light beam normal to direction of propagation that impinges on ds . At the shadow boundary, $\angle(\vec{n}, \vec{r}) = \pi/2, \angle(\vec{r}, \vec{\rho}) = \pi$, so that $\cos(\vec{n}, \vec{r}) = 0$ and $1 + \cos(\vec{r}, \vec{\rho}) = 0$ and the limiting value for $\cos(\vec{n}, \vec{r})/(1 + \cos(\vec{r}, \vec{\rho}))$ turns out to be infinite. Physically, amplitudes cannot become infinite, and therefore one suspects that the Rubinowicz edge wave is only a mathematical fiction without physical reality. To see what happens near the shadow boundary, let us analyze the factor (see Fig.14).

$$\frac{\cos(\vec{n}, \vec{r})}{1 + \cos(\vec{r}, \vec{\rho})} = \frac{r \cos(\vec{n}, \vec{r})}{r + r \cos(\vec{r}, \vec{\rho})} \quad (75)$$

Let z be the distance between the projection of the field point P' on the edge and the diffracting edge element ds , y be the distance between P and its projection P'' on the shadow boundary, and ℓ the perpendicular distance of P'' to the edge (see Fig. 14). We then have

$$\begin{aligned} r^2 &= \ell^2 + y^2 + z^2 \\ \cos(\vec{r}, \vec{\rho}) &= -\frac{\ell}{r} \\ \cos(\vec{n}, \vec{r}) &= \frac{y}{r} \end{aligned} \quad (76)$$

Hence the factor becomes,

$$\frac{r \cos(\vec{n}, \vec{r})}{r + r \cos(\vec{r}, \vec{\rho})} = \frac{y}{r - \ell}$$

Its main contribution thus originates near $r = \ell$, or y and $z \ll \ell$.

- 43 -

If y and z are small, we have

$$\frac{y}{r - \ell} = \frac{y}{\sqrt{y^2 + z^2 + \ell^2} - \ell} = \frac{y}{\frac{1}{2} \frac{y^2 + z^2}{\ell} + \dots} \quad (77)$$

We have developed the square root into a Taylor series and retained only the lowest order terms. For $z = 0$, and $y = 0$ the result diverges. It is important to note that the edge does not consist of points but of infinitely small elements $ds = dz > 0$ that have a length greater than zero. If we integrate the edge wave for a very small edge element Δz , we obtain

$$\begin{aligned} \Phi_d &= - \frac{1}{4\pi} \frac{1}{\rho r} \sin(\vec{\rho}, d\vec{s}) \, 2\ell y \int_{-\Delta z/2}^{\Delta z/2} \frac{dz}{y^2 + z^2} e^{-jk(r + \rho)} \\ &= - \frac{1}{4\pi} \frac{1}{\rho \ell} \sin(\vec{\rho}, d\vec{s}) \, 2\ell \left[\tan^{-1} \frac{z}{y} \right]_{-\Delta z/2}^{\Delta z/2} e^{-jk(r + \rho)} \\ &= - \frac{1}{2\rho} \sin(\vec{\rho}, d\vec{s}) e^{-jk(r + \rho)} = - \frac{1}{2\rho} e^{-jk(r + \rho)} \sin(\rho, ds) \quad (78) \end{aligned}$$

because $y \rightarrow 0$ at the shadow boundary, and Δz is very small but finite and also z has been assumed to be small. Also, because the integration interval Δz is very small, the exponent can be assumed to be constant during the integration.

The main contribution to the field at the shadow boundary is thus generated by the edge element that casts its shadow to the field point at the shadow boundary. The integrand becomes infinite for their midpoint of this element, but the average of it (like the integral over a delta function) is finite. The contribution of this element then is equal to

- 44 -

half the amplitude of the incident wave at the edge point. If we had applied the stationary phase method in a form that is valid when the integrand has a pole near the stationary field point, we would have integrated over an edge length of many wavelengths, so that phase cancellations would occur, and would have obtained the same result for the stationary phase contribution except that the distance factor $\frac{1}{\rho}$ would have been replaced by $\frac{1}{r + \rho}$, so that the diffracted amplitude is exactly half the amplitude that is incident at the field point and not half of the amplitude that is incident at the edge, (see E. J. Skudrzyk, 1971, page 528). Thus, approaching the shadow boundary from the insonified zone leads to an edge-generated wave whose value is exactly equal to half the incident amplitude and opposite in sign to it.

The factor of the integrand

$$\frac{1}{r [1 + \cos (\vec{r}, \vec{\rho})]} = \frac{1}{r + r \cos (\vec{r}, \vec{\rho})} = \frac{1}{r'} \quad (79)$$

is the distance from the edge to the field point minus the projection of this distance on the shadow boundary. One is tempted to interpret r' as the effective distance the edge generated wave has travelled. For a point at the shadow boundary, ($\vec{r}, \vec{\rho} = \pi$), $r' = 0$, for points away from the shadow boundary in the space opposite the sound source $r' < r$, and for points in the insonified side of the screen $r' > r$. However r' is not the distance from any particular point on the shadow boundary. Also, the location for the "source point" at $r' = 0$ turns out to be a function of the field point, r , even if we move along a line passing through this "source point" and the diffracting edge.

Thus it is not possible, therefore, to interpret the diffracted field ϕ_d as resulting from elementary waves that originate at the edge. The phase of the diffracted field

- 45 -

does agree with that for an edge-generated wave, but the amplitude of the diffracted field varies in a strange manner with the distance from the edge. The elementary edge waves in the Rubinowicz integrand thus represent only a mathematical formalism with no physical significance. The elements of a diffracting edge do not generate real waves that propagate from the edge points as spherical waves to the field point like the waves in Huyghens' principle. However, the Rubinowicz integral proves that each element contributes to the diffracted field observed at the field point, and that the phase of this field is the same as that of a wave that travels from the source to the diffracting edge element, and from there to the field point. However, if we add up the contributions of all the edge elements, real waves result that originate at the stationary phase.

According to the transformed Kirchoff integral, the shadow boundary is the exact set of the sources that give rise to the scattered field. The contribution of the shadow surface can then be transformed into that of a source distribution around the edges of the diffractor. However, these sources are of a non-physical nature and have properties that cannot be realized by real sources. For example, there are no known sources nor any simple multiple sources whose contribution varies with the distance as the integrand varies in the Rubinowicz integral.

This result explains why the theory of diffraction based on equivalent elementary edge sources has not been more successful in general, and why it had not been possible to represent most of the exact solution in a similar form. The edge sources are only a formalism equivalent to the Kirchoff theory, and equivalent to the exact solution for straight edges and wedges.

8. THE STRAIGHT EDGE - KIRCHOFF AND SOMMERFELD

For a plane wave incident at an angle ϕ_0 with the plane that contains the edge whose wave fronts are parallel to the edge, the stationary phase point, (see Fig. 15), the field point and incident ray are in the same plane, $R_K = \infty$ and

$$\angle (\vec{r}, \vec{\rho}) = 360^\circ - (\phi - \phi_0), \quad (80)$$

$$\angle (\vec{n}, \vec{r}) = \phi - \phi_0 - 90^\circ, \quad (81)$$

$$\sin (\vec{\rho}, d\vec{s}) = 1 \quad (82)$$

The angle factor thus reduces to

$$\frac{\cos (\vec{n}, \vec{r}) \sin (\vec{\rho}, d\vec{s})}{1 + \cos (\vec{r}, \vec{\rho})} = \frac{\sin (\phi - \phi_0)}{1 + \cos (\phi - \phi_0)} = \tan \left(\frac{\phi - \phi_0}{2} \right). \quad (83)$$

and the complete solution is

$$\phi_d = - \left[\frac{e^{-j(kr + \pi/4)}}{2\sqrt{2\pi kr}} \right] \left[\tan \frac{\phi - \phi_0}{2} \right]. \quad (84)$$

Here $(\phi - \phi_0)$ represents the angle of the rays from the edge to the field point relative to the rays that delineate the shadow boundary of the incident wave. The exact Sommerfeld solution leads to the same first factor, but the second factor is

$1/\cos[(\phi - \phi_0)/2]$. A similar result then is obtained for the diffraction generated by the reflected wave. It is represented by a similar solution except that the angular distance from the shadow boundary $\phi - \phi_0$ now is replaced by that for the reflected wave $\phi + \phi_0 - 2\pi$ (see Fig. 15). The angle $(\phi + \phi_0 - 2\pi)$ then represents the angle of the field point relative to the shadow boundary (the angular limit) of the reflected wave.

The Kirchhoff formula gives the same distance dependance as

- 47 -

the exact theory, but the directivity function is in error by the factor $\sin [(\phi - \phi_0)/2]$. This error is less than 30 percent if the angle between field point and shadow boundary is less than 90° . Since the diffraction at greater angles is dominated by that of the reflected waves which is well approximated by the Kirchhoff solution in this angular range, the Kirchhoff theory may be considered as a very good approximation to the exact theory of diffraction. However, it is necessary to include the reflected wave field and its diffraction separately.

If the incident wave front is not parallel to the edge, so that the incident rays make an angle $\beta = \angle(\vec{\rho}, \vec{ds})$ with the edge, then the stationary phase point is no longer the point on the edge that is closest to the field point, but is displaced from this point towards the direction of the source. To find this point, we begin by drawing the line from field point that perpendicularly intersects with the edge. This point P will be designated as the origin of s (see Fig. 16).

The incident ray that corresponds to this origin, $s = 0$, is called ρ_0 . The distance from the source to the edge plus that from the edge to field point is a function of s and can be written as

$$\rho(s) + r(s) = \rho_0 - s \cos \beta + \sqrt{d^2 + s^2} \quad (85)$$

To find the specific location of point $(s)_{s.p.}$ for which the phase is stationary, we set

$$\frac{\partial (\rho + r)}{\partial s} = 0 = -\cos \beta + \frac{s}{\sqrt{d^2 + s^2}} = 0 \quad (86)$$

Hence

$$\cos^2 \beta (d^2 + s^2) = s^2 ,$$

- 48 -

$$d \cos \beta = (+) s \sin \beta ,$$

or

$$\tan \beta = d/(s)_{s.p.} , (s)_{s.p.} = \frac{d \cos \beta}{\sin \beta} , \quad (87)$$

as would have followed directly from the edge law. The quantity $(s)_{s.p.}$ represents the distance of the stationary phase point from the point on the edge that is closest to the field point. Note that the stationary phase point is very far away from the point at the edge that is closest to the field point unless the incident rays are normal to the edge. For instance, if the incident rays form an angle of 45° with the edge, the stationary phase point is as far away from the point on the edge that is closest to the field point as the field point is from the edge. Hence, for the stationary phase point

$$\begin{aligned} (\rho + r)_{s.p.} &= \rho_0 - \frac{d \cos^2 \beta}{\sin \beta} + d \left(1 + \frac{\cos^2 \beta}{\sin^2 \beta} \right)^{1/2} \\ &= \rho_0 + \frac{d}{\sin \beta} (1 - \cos^2 \beta) = \rho_0 + d \sin \beta \end{aligned} \quad (88)$$

The right hand side represents the exact distance from the source (very far away) to the stationary phase point and from there to the field point. Thus we obtain the result:

$$\phi_d = - \frac{\sin \beta}{2\sqrt{2\pi kr}} e^{-jk(\rho_0 + d/\sin \beta) + j\pi/4} \tan \left(\frac{\phi - \phi_0}{2} \right) \quad (89)$$

where $r = d/\sin \beta$, and d is the perpendicular distance of the field point from the edge. ρ_0 represents the phase of the incident wave at the origin $s = 0$, which is the point on the edge defined by the projection of the field point on the edge.

If the incident wave is a spherical wave, if s_0 is the s coordinate of the normal projection of the source point on

- 49 -

the edge, and ρ_0 is the distance from the source to the projection point or the edge, then the s coordinate of the stationary phase point satisfies the relation (see Fig. 17)

$$\tan \beta = \frac{d}{s} = \frac{\rho_0}{s_0 - s},$$

$$(s)_{s.p.} = \frac{d s_0}{\rho_0 + d},$$

and

$$(\rho + r)_{s.p.} = \frac{s_0 - s}{\cos \beta} + \frac{s}{\cos \beta} = \frac{s_0}{\cos \beta} =$$

$$\left[(\rho_0 + d)^2 + s_0^2 \right]^{1/2} = R \quad (90)$$

where R is an abbreviation for the sum $[\rho + r]_{s.p.}$.

We now have

$$\phi_d = - \frac{e^{-j(kR + \pi/4)}}{2\sqrt{2\pi k} \rho r R} \sin \beta \tan \frac{\phi - \phi_0}{2} \quad (91a)$$

where $\vec{\rho}, \vec{r}$ represent the distance vectors to the stationary phase point, and ρ, r the corresponding distances. Thus, the total Kirchhoff solution for the diffracted field by the incident and reflected fields give:

$$\phi_d = - \frac{e^{-j(kR + \pi/4)}}{2\sqrt{2\pi k} \rho r R} \sin \beta \left[\tan \frac{\phi - \phi_0}{2} \pm \tan \frac{\phi + \phi_0}{2} \right] \quad (91b)$$

The directivity factors of the diffracted field in the Kirchhoff solution, equation (91b) for rigid (+) and pressure release (-) edges, are shown in Figures (18) and (19) respectively for a few

- 50 -

incidence angles. The corresponding total, exact (Sommerfeld) solution for the diffracted field, see Bowman, Senior and Uslenghi, 1969, can be written as:

$$\phi_d = - \frac{e^{-j(kR + \pi/4)}}{2\sqrt{2\pi k} \rho r R} \sin \beta \left[\frac{1}{\cos \frac{\phi - \phi_0}{2}} \pm \frac{1}{\cos \frac{\phi + \phi_0}{2}} \right], \quad (91c)$$

The directivity factors of the diffracted field in the Sommerfeld solution, equation (91c) for rigid (+) and pressure source release (-) edges, are shown in Figures (20) and (21) respectively.

The backscattered field when $\beta = \pi/2$, $r = \rho = d = \rho_0$, $s_0 = 0$, $R = 2\rho$, and $\phi = \phi_0$ becomes

$$\phi_{bs} = - \frac{e^{-j(2k\rho + \pi/4)}}{4\rho\sqrt{\pi k\rho}} \cdot \begin{cases} \pm \tan \phi_0 & (\text{Kirchoff}) \\ 1 \pm \frac{1}{\cos \phi_0} & (\text{Sommerfeld}) \end{cases} \quad (91d)$$

The directivity factors of the backscattered field for the Kirchoff and Sommerfeld solutions are shown in Figure (22) for rigid edges and in Figure (23) for pressure release edges.

9. THE WEDGE

Since the Kirchoff solution depends only on the shadow boundary, it is the same for both a wedge and a straight edge. For a plane incident wave, the diffracted field of a wedge becomes:

$$\phi_{\text{Kirchoff}} = - \frac{\phi_0 e^{-j(kr + \pi/4)}}{2\sqrt{2\pi kr}} \left\{ \frac{\sin \left[\frac{\phi - \phi_0}{2} \right]}{\cos \frac{\phi - \phi_0}{2}} \right\} \quad (92)$$

In the exact solution, the factor in the braces is replaced by unity.

A wedge is characterized by the apex angle 2Ω of the wedge, and the angle $v\pi$ that supplements it to 2π is:

$$v\pi = 2\pi - 2\Omega \quad ,$$

$v\pi$ being the number of radians exterior to the wedge.

For a straight edge, $\Omega = 0$ and $v = 2$.

For a wedge of angle 90° , $\Omega = \pi/4$ and $v\pi = 2\pi - \pi/2 = \frac{3\pi}{2}$, $v = \frac{3}{2}$,

likewise for wedge of 180° , $\Omega = \pi/2$, $v\pi = 2\pi - \pi = \pi$, and $v = 1$ (93)

For a wedge, the exact solution for the diffraction field of an incident plane wave is given as (J. J. Bowman, I.B.A. Senior and P.L.E. Uslenghi, 1969):

$$\begin{aligned} \phi_d &= \frac{\phi_0 e^{-j(kr + \pi/4)}}{2\sqrt{2\pi kr}} \left(\frac{2}{v} \sin \frac{\pi}{v} \right) \left\{ \frac{1}{\cos \frac{\pi}{v} - \cos \frac{\phi - \phi_0}{v}} \pm \frac{1}{\cos \frac{\pi}{v} + \cos \left[\frac{2\pi - (\phi + \phi_0)}{v} \right]} \right\} \\ &= w(\Psi_{\text{inc}}) \pm w(\Psi_{\text{ref}}) \end{aligned} \quad (94)$$

where $\Psi_{\text{inc}} = \phi - \phi_0$ is the angle the observer makes with the shadow boundary of the incident wave and $\Psi_{\text{ref}} = \phi + \phi_0 - 2\Omega$ is the angle the observer makes with the shadow boundary of the image wave, see Figure (24).

The directivity function of the diffracted field from a wedge, given in the bracketed terms of equation (94), is plotted for wedge angles $2\Omega = 30^\circ, 60^\circ, 90^\circ$, and 120° for rigid (+) in Figures (25, 27, 29 and 31), and for pressure release (-) in Figures (26, 28, 30, and 32), respectively.

The backscattered field of these wedges, when $\phi = \phi_0$, were plotted in Figures (33) and (34) for rigid (+) and pressure release (-) respectively. It should be noted that the diffracted field represented

by equation (94) becomes unbounded at the following angles:

$$\left. \begin{aligned} \Psi &= \phi - \phi_0 = \pi \\ \Psi &= \phi - \phi_0 = 3\pi - 4\Omega \\ \Psi_+ &= \phi + \phi_0 = 3\pi - 2\Omega \\ \Psi_+ &= \phi + \phi_0 = \pi + 2\Omega \end{aligned} \right\} \text{ for } 2\Omega \leq \pi \left\{ \begin{array}{l} \text{provided that} \\ \Omega \leq \phi \leq 360^\circ - \Omega \end{array} \right.$$

The factor $\frac{2}{v} \sin \frac{\pi}{v}$, shown in Figure (35), can be interpreted as the discontinuity factor for a wedge. For a blunt wedge (straight edge), the factor is unity. The factor for an almost flat wedge, whose angle is $2\Omega = \pi - \epsilon$, or whose angle v is:

$$v = \frac{2\pi - 2\Omega}{\pi} = 1 + \frac{\epsilon}{\pi}$$

become for small ϵ ,

$$\frac{2}{v} \sin \frac{\pi}{v} = 2(1 - \frac{\epsilon}{\pi} + \dots) \sin (\pi + \epsilon) \doteq 2\epsilon \dots \quad (95)$$

it is proportional to the change of the slope multiplied by two.

10. COMPARISON OF THE KIRCHOFF STRAIGHT EDGE SOLUTION WITH THE SOMMERFELD STRAIGHT EDGE AND WEDGE SOLUTION

The solution for the straight edge consists of the linear combination of two identical terms with different arguments:

$$\phi_d = w \left[\frac{\phi - \phi_0}{2} \right] \pm w \left[\frac{\phi + \phi_0}{2} \right] = w \left[\frac{\Psi_{inc.}}{2} \right] \pm w \left[\frac{\Psi_{refl.}}{2} \right] \quad (96)$$

where Ψ_{inc} represents the angular distance from the shadow boundary of the incident wave and $\Psi_{refl} - 2\pi$ that from the shadow boundary of the reflected (the image) wave (see Fig. 18 & 24). The plus sign applies for a rigid straight edge, the minus sign for a pressure release straight edge. The two terms are identical except for a difference in the origin of the angle count. It is therefore sufficient to consider only one term alone. The distance factors $f(r)$ are the same in the Kirchoff solution and in the Sommerfeld solution. The only difference

- 53 -

is in the angle functions. The angle function for the Kirchhoff solution is $\tan \Psi/2$, and that for the Sommerfeld solution is $1/(\cos \Psi/2)$. Fig. 36 shows a comparison of these two functions. In the regions where scattering is significant, i.e. near the shadow boundary, the two solutions are practically identical. The two functions differ for scattering in directions normal to the shadow boundary by the factor $\sin 45^\circ = 0.707$ or 30%. Thus for diffraction into the half space that extends in the direction of propagation, the Kirchhoff error is practically negligible. The Sommerfeld value then is 1.4, the Kirchhoff value is 1. For the backscattered amplitude, $\Psi=0$ and the Kirchhoff backscattered amplitude is zero, while the Sommerfeld backscattered amplitude is unity. Backscattering is predominantly determined by the diffraction field of the reflected wave. We can thus conclude that the Kirchhoff error for plane diffractors is negligible under all practical situations provided the radius of curvature is large compared to the wave length.

The Kirchhoff-Rubinowicz solution for the straight edge leads to the angle factor $\tan [(\phi - \phi_0)/2]$, where the exact Sommerfeld solutions differ from that of the Kirchhoff solution practically only in the range $(\phi - \phi_0)/2 > \pi/4$, or $\phi - \phi_0 > \pi/2$, i.e. in the range in which scattering is extremely small. In this range the diffracted field is practically exclusively that of the reflected wave. We may attempt to improve the solution using Keller's method, and simply drop the factor $\sin (\phi - \phi_0)/2$ in the Kirchhoff solution in all cases of edge diffraction.

In the Kirchhoff-Rubinowicz theory, the diffraction phenomenon is represented by an integral over the shadow boundary. The resulting integral then is transformed into a line integral over the edge that generates the shadow boundary. The solution reproduces the correct distance dependence of the diffraction field at high frequencies, and is dimensionally correct. As has been proven in the literature that for plane diffractors,

the Kirchhoff solution represents a very good approximation in the angular range near the direction of incidence, provided the linear dimensions of the diffractor exceed one to two wave lengths, (see Figs. 3 and 4). We can therefore assume that the Kirchhoff-Rubinowicz solution also represents a very good approximation to the distance dependence of the exact solution of Sommerfeld.

The Sommerfeld computation does not include the terms that contain the curvature R_K of the edge. It would be very difficult to derive an exact solution for a curved edge at low frequencies when the edge is not very long compared to the wave length. We may expect that the Kirchhoff solution without the factor $\sin [(\phi - \phi_0)/2]$ will give a very good approximation to the exact solution for edges with slight curvature.

It will be recalled that the Kirchhoff theory yield a similar formula except for an additional directivity factor $\sin[(\phi - \phi_0)/2]$ for the diffracted field. A similar angular factor relative to the shadow boundary is associated with the reflected wave, but the Kirchhoff theory does not contain the factor $\frac{2}{v} \sin \frac{\pi}{v}$ of the exact Sommerfeld result. In the exact theory, the angle space outside the edge $2\pi - 2\Omega$ is dilated to 2π by dividing

$$\phi \text{ by } v \text{ where } 2\pi - 2\Omega = v\pi, \left[\frac{2\pi - 2\Omega}{\frac{1}{2}v} = 2\pi \right] \text{ so that the argument } \frac{\psi_{inc}}{v} \text{ in terms } \cos \left(\frac{\psi_{inc}}{v} \right) \text{ and that of } \left(\frac{2\pi - \psi_{refl}}{v} \right) \text{ in the term } \cos \frac{2\pi - \psi_{refl}}{v} \text{ always varies from 0 to } 2\pi. \quad (9')$$

For wedge angle of 90° , we see that:

$$2\Omega = \frac{\pi}{2}, \quad v = \frac{3}{2}, \quad \frac{2}{v} \sin \frac{\pi}{v} = \frac{4}{3} \quad \sin \frac{2\pi}{3} = 1.17.$$

- 55 -

Similarly, for wedge angle 135° , we have:

$$2\Omega = \frac{3\pi}{4}, \quad \nu = \frac{5}{4}, \quad \frac{2}{\nu} \sin \frac{\pi}{\nu} = \frac{8}{5} \sin \frac{4}{5} = \frac{8}{5} \sin 36^\circ = 0.94.$$

The deviation between Kirchhoff and exact theory become serious when the wedge angle 2Ω exceeds $\frac{\pi}{2}$.

11. DIRECTIVITY FACTOR OF THE EDGE RADIATION

The diffracted field establishes the mathematical continuity from the illuminated to the shadow zone (see Sec. 6). The peak of the diffracted field propagates in the same direction as the incident wave and is half as great as this wave.

Thus the diffracted field near the shadow zone becomes (see Eq. 32)

$$\Phi_d = \frac{1}{2\sqrt{2\pi k}} \frac{e^{jk(r + \rho)} \sin \beta}{r\rho \sqrt{\frac{1}{r} + \frac{1}{\rho} + \frac{\gamma}{R_K}}} f(\phi) \quad (98)$$

where

$$\gamma = \frac{\cos(\vec{\rho}, \vec{h}) + \cos(\vec{r}, \vec{h})}{\sin^2(\vec{\rho}, d\vec{s})}$$

and for the Sommerfeld solution, the angular factor:

$$f(\phi) = \frac{1}{\cos \frac{\phi - \phi_0}{2}} = \frac{-1}{\cos \frac{\epsilon + \pi}{2}} = \frac{1}{\sin(\epsilon/2)} \quad (99)$$

where in the vicinity of the shadow boundary

$$\phi - \phi_0 = \pi + \epsilon \quad (100)$$

Here ϵ is the angle or lateral space deviation from the shadow

- 56 -

boundary. The above expression for $f(\Psi)$ applies everywhere with the exception of the immediate vicinity of the shadow boundary. At the shadow boundary, its value is given by the amplitude of the diffracted field which is equal to half that of the incident field (see Sec. 6). Hence

$$\phi_d = \frac{1}{2\sqrt{2\pi k}} \frac{e^{jk(r+\rho)} \sin \beta}{r\rho \sqrt{\frac{1}{r} + \frac{1}{\rho} + \frac{\gamma}{R_K}}} f(\phi) = \frac{e^{jkr}}{2R} \quad (101)$$

where R is the distance between source and receiver and is equal to $r + \rho$ and ρ and r the distances of the stationary phase point from source and receiver. Thus,

$$f(\phi) = \frac{\sqrt{2\pi k} r\rho \sqrt{\frac{1}{r} + \frac{1}{\rho} + \frac{\gamma}{R_K}}}{R} = \frac{1}{\sin \epsilon/2} \leq \frac{2}{\epsilon_0} \quad (102)$$

where $\epsilon = \epsilon_0$ is the smallest value of ϵ , we are allowed to use in Eq. (102). For this value of ϵ , the diffracted amplitude is equal to half the amplitude of the incident wave. The amplitude then stays at this value and as ϵ passes through the shadow boundary to $-\epsilon_0$ then decreases again proportionally to $1/\epsilon$. We thus have $\epsilon > \epsilon_0$.

To simplify the computation, let the incident wave be very nearly a plane wave ($\rho \rightarrow \infty$) and let it be normally incident on the edge. Let $R_K = \infty$. The stationary phase point then is coincident with the projection of the field point onto the edge. To fix the amplitude of the incident wave, let $\rho = r$. We then have

- 57 -

$$f(\phi) = \frac{\sqrt{2r^3 \cdot 2\pi k}}{2r} = \frac{2}{\epsilon_0} \quad (103)$$

$$\epsilon_0 = \frac{2}{\sqrt{\pi k r}}$$

For values of ϵ greater than ϵ_0 , $f(\phi) = 1/\sin(\epsilon/2) \doteq 2/\epsilon$ up to crudely $\epsilon/2 = \pi$, $\epsilon = 2\pi$, i.e. for the complete angular range. For $\rho \doteq r$, we thus have

$$|\phi_d|_{\epsilon > \epsilon_0} \cong \frac{P_0 \epsilon_0}{2\rho \epsilon} = \frac{P_0}{\rho \sqrt{\pi k r} \epsilon} = P_{\text{incident}} \frac{1}{\sqrt{\pi k r} \epsilon} \quad (104)$$

Thus the scattered pressure decreases inversely proportional to the perpendicular distance ϵ from the shadow boundary.

12. EDGES OF FINITE LENGTH

The theory of geometrical diffraction is based on Fermat's principle, see Appendix III, which is equivalent to the presence of a stationary phase point well within the length of the diffracting edge. The diffraction field is then considered to arise primarily from the contributions of the edge elements at and near the stationary phase point. If the edge is not long enough, or is so situated relative to the field point that no stationary phase point is located within the length of the edge, then no diffracted field will reach the field point.

For the case when the stationary phase point is within the length of the edge, the exponent function in the diffraction integral

$$I = \int_{\text{edge}} S(s, r) e^{-jk(r + \rho)} ds, \quad (105)$$

- 58 -

can be developed into a Taylor series.

The stationary phase point satisfies the condition

$\frac{\partial}{\partial s} (\rho + r) = 0$, which will be considered as the origin

for the s -coordinate along the edge. The series expansion of the exponent about the stationary phase point $s = 0$, where $r = r_0$ and $\rho = \rho_0$ becomes:

$$(\rho + r) = (\rho_0 + r_0) + \frac{s^2}{2} \left. \frac{\partial^2 (\rho + r)}{\partial s^2} \right|_{\rho_0, r_0} + \dots \quad (106)$$

If the sound impinges normally to a straight edge

$$\begin{aligned} \rho^2 &= \rho_0^2 + s^2, & \rho &= \rho_0 + \frac{1}{2} s^2 / \rho_0 + \dots, \\ r^2 &= r_0^2 + s^2, & r &= r_0 + \frac{1}{2} s^2 / r_0 + \dots, \end{aligned} \quad (107)$$

$$\left. \frac{\partial^2 (\rho + r)}{\partial s^2} \right|_{\rho_0, r_0} = \frac{1}{r_0} + \frac{1}{\rho_0} + \dots, \quad (108)$$

and the exponent in the integrand in Equation (105) above reduces to the following Taylor's series:

$$-jk \left[(r_0 + \rho_0) + \frac{s^2}{2} \left(\frac{1}{r_0} + \frac{1}{\rho_0} \right) + \dots \right]. \quad (109)$$

Since the amplitude factor $S(s, r)$ of the integrand is assumed as slowly varying function of s , the integral is basically

Fresnel integral of the variable $v^2 = k \frac{s^2}{2} \left(\frac{1}{r_o} + \frac{1}{\rho_o} \right)$ (see E. Skudrzyk, 1972, page 122). The value of the integral in Equation (105) is given by twice the distance from the origin of the Cornu spiral to the point $v^2 = k \frac{s_{\max}^2}{2} \left(\frac{1}{r_o} + \frac{1}{\rho_o} \right)$, that represents the upper limit of integration of Equation (105). Except for insignificant fluctuations due to s being located on the spiral near its upper end, see Figure 38, the integral assumes its final value $1 - j = 2 e^{-j\pi/4}$ if $v \geq \sqrt{\pi}/2$.

If the projector and receiver are in the central plane of symmetry, the solution for a finite edge of length h ($s_{\max} = h/2$), therefore is the same as for the infinite edge only if we satisfy by the following limits,

$$\frac{1}{2} k \left(\frac{1}{r_o} + \frac{1}{\rho_o} \right) \frac{h^2}{4} \geq \frac{\pi}{4} \quad (110)$$

so that the finite limits of the integral (105) can be replaced by infinite limits of the length of the edge.

For backscattering, $\rho_o = r_o$, the maximum limit range r'_m for the geometrical theory of diffraction to be valid is reached when

$$\frac{2h^2}{r'_m \lambda} = 1$$

or

$$\frac{r'_m}{\lambda} = 2 \left(\frac{h}{\lambda} \right)^2 \quad (111)$$

where (h/λ) and (r'_m/λ) are the dimensionless length of edge and range normalized to the acoustic wavelength. For

- 60 -

example, in water at 30 kHz, $\lambda = \frac{1}{20}$ m, and we obtain the following table:

r'_m (m.)	$\frac{r'_m}{\lambda}$	$\frac{h}{\lambda}$	h
40	800	20	1.0
1.0×10^3	2×10^4	100	5.0
4.0×10^3	8×10^4	200	10.0
1.6×10^4	3.2×10^5	400	20.0

As the size of the target is reduced, the values of h become smaller and the exponential is practically equal to unity. The integral in (105) then is no longer a stationary phase integral but becomes proportional to s .

If the angular range that contributes to the intensity at the field point P is 2θ , (see Fig. 39) then we have

$$\tan \theta = \frac{h}{2r'_m} = \frac{\lambda}{4h}$$

$$\theta \doteq \tan \theta \doteq \sin \theta = \frac{\lambda}{4h} \quad (112)$$

The result is similar to the diffraction formula for a slot or an aperture, except for a slightly different numerical constraint. We may conclude that either all diffracted beams open up to an angle θ , or else there will not be any elementary beam contributing at the field point if the distance r_0 is greater than that given by the above formula, Equation (110).

- 61 -

It is interesting to note that physically, a diffraction field from finite edge acts similar to the radiation field from a line array of finite length; both generate a beam pattern whose angular opening is described by the above formula.

For a plane incident wave, let $\rho_0 \rightarrow \infty$ in Equation (110), and the limit range r_m of the geometrical theory of diffraction is given by

$$\frac{h^2}{r_m \lambda} = 1$$

or

$$\frac{r_m}{\lambda} = \left(\frac{h}{\lambda} \right)^2 \quad (113)$$

Similarly, the angle range that contributes to the intensity at the field point P is θ , see Figure (39), now given by

$$\tan \theta = \frac{h}{2r_0} = \frac{\lambda}{2h}$$

$$\theta \doteq \tan \theta \doteq \sin \theta = \frac{\lambda}{2h} \quad (114)$$

13. THE LIMITS OF GEOMETRICAL REFLECTION AND DIFFRACTION FOR FINITE FLAT REFLECTORS

It is well known that a plane rigid reflector is equivalent to a planar piston projector. Every point on the rigid surface of a reflector can be considered to have a particle velocity that is 180° out of phase with the incident wave. Thus, if $P_i(x,y)$ is the amplitude of an incident pressure wave at the surface of a plane reflector, then the reflected far-field pressure amplitude $P(r,\theta,\phi)$ at a field point (r,θ,ϕ) is given by the Huygens-Rayleigh integral:

- 62 -

$$P(r, \theta, \phi) = \frac{jk}{2} \iint_{\sigma} \frac{P_i(x, y) e^{-jkr}}{r} dx dy \quad (115)$$

where (x, y) are the coordinates of a point in the plane reflector, $(dx dy)$ is an elemental area of the plane reflector, and r is the distance of the field point to the point (x, y) on the surface, σ , of the reflector, see Figure (40).

If the origin of the coordinate system (x, y) is located on the reflector, whose distance from the field point r_0 is given by

$$r_0^2 = x_0^2 + y_0^2 + z_0^2,$$

then the distance r from the field point to any point (x, y) on the reflector becomes, see Figure (40),

$$\begin{aligned} r^2 &= (x-x_0)^2 + (y-y_0)^2 + z_0^2 \\ &= \rho^2 + r_0^2 - 2xx_0 - 2yy_0 = r_0^2 \left[\frac{\rho^2}{r_0^2} + 1 - \frac{2xx_0}{r_0^2} - \frac{2yy_0}{r_0^2} \right] \end{aligned}$$

where ρ is the distance of the point (x, y) to the origin:

$$\rho^2 = x^2 + y^2.$$

The direction cosines of the line connecting the center of the radiator with the field point are

$$x_0/r_0 = \cos(r_0, x) = \cos \theta, \quad y_0/r_0 = \cos(r_0, y) = \cos \phi$$

and

$$r = r_0 \sqrt{1 + \rho^2/r_0^2 - \frac{2x}{r_0} \cos \theta - \frac{2y}{r_0} \cos \phi}. \quad (116)$$

- 63 -

If the linear dimensions of the reflector are small compared to the distance from the field point, $\rho^2/r_o^2 \ll 1$, the square root can be developed into a power series

$$r = r_o \left\{ 1 + \frac{1}{2} (\rho/r_o)^2 - [(x/r_o) \cos \theta + (y/r_o) \cos \phi] + \right. \\ \left. - \frac{1}{2} \left(\frac{x \cos \theta + y \cos \phi}{r_o} \right)^2 + \dots \right\} \quad (117)$$

Thus, retaining terms up to the second power in the exponent of the integral in equation (115), one obtains:

$$P(r_o, \theta, \phi) = \frac{jke^{-jkr_o}}{2\pi r_o} \iint_{\sigma} P_i(x, y) \exp jk \\ \left[x \cos \theta + y \cos \phi + \frac{[x \cos \theta + y \cos \phi]^2}{2r_o} - \frac{\rho^2}{2r_o} \right] dx dy, \quad (118)$$

where $r \doteq r_o$ over the surface of the reflector.

Let an incident plane pressure wave, whose amplitude at the surface of the reflector is a constant P_o , insonify a rectangular plane reflector. If the coordinates of the reflector extends over $-a < x < a$ and $-b < y < b$, then the reflected pressure amplitude at a field point, to a first order (Fraunhofer) approximation, is given by the integral

$$P(r, \theta, \phi) = \frac{jk P_o e^{-jkr_o}}{2\pi r_o} \int_{-a}^{+a} \int_{-b}^b e^{jk[x \cos \theta + y \cos \phi]} dx dy \\ = \frac{jk P_o (4ab) e^{-jkr_o}}{2\pi r_o} D(\theta, \phi), \quad (119)$$

- 64 -

where directivity factor $D(\theta, \phi)$ is given by

$$D(\theta, \phi) = \frac{\sin (ka \cos \theta)}{ka \cos \theta} \frac{\sin (kb \cos \phi)}{kb \cos \phi} \quad (120)$$

It is obvious that maximum reflection is attained at a field point in a direction normal to the plane reflector at the origin, i.e. as θ and $\phi \rightarrow \frac{\pi}{2}$, where the directivity factor $D(\theta, \phi)$ approaches unity. The reflected pressure at a far field point, where $r_o \gg a$ and $r_o \gg b$, decreases as $1/r_o$, just like spherical spreading of a point source. Thus, for such large distances, the laws of geometrical optics, whose pressure amplitude decreases as $1/\sqrt{r_o}$, are no longer applicable.

The preceeding computations, see Section 12, do not apply for ranges $r < r_m$, where r_m is the limit range of the geometric theory as defined in Equation (113). Thus, one needs to get a better approximation by retaining more terms in the eikonal expression of Equation (118). For a field point, whose projection on the plane reflector falls within its boundaries, let the origin of (x, y) coordinates be that projected point. Thus, $\theta = 0$, $\phi = 0$ and the integral for the reflected pressure, given in equation (118), reduces to the following second order (Fresnel) approximation:

$$\begin{aligned} P(r_o) &= \frac{jk P_o e^{-jkr_o}}{2\pi r_o} \int_{x_1}^{x_2} \int_{y_1}^{y_2} e^{-jk\rho^2/2r_o} dx dy \\ &= \frac{jk P_o e^{-jkr_o}}{2\pi r_o} \left[\int_{x_1}^{x_2} e^{-jk x^2/2r_o} dx \right] \left[\int_{y_1}^{y_2} e^{-jky^2/2r_o} dy \right] \end{aligned} \quad (121)$$

Substituting $u^2 = \frac{kx^2}{\pi r_o}$, $v^2 = \frac{ky^2}{\pi r_o}$,

the integrals in Equation (121) become the Cornu spirals (see E. Skudrzyk, pp 629, Equation 156):

$$P(r_0) = j P_0 e^{-jkr_0} \left[\frac{1}{\sqrt{2}} \int_{u_1}^{u_2} e^{-j\pi u^2/2} du \right] \left[\frac{1}{\sqrt{2}} \int_{v_1}^{v_2} e^{-j\pi v^2/2} dv \right] \quad (122)$$

where $u_{1,2} = x_{1,2} \sqrt{\frac{2}{\lambda r_0}}$ and $v_{1,2} = y_{1,2} \sqrt{\frac{2}{\lambda r_0}}$.

Each of the Cornu spirals, see Figure (38), have an asymptotic value of $(1-j)$ if the limits of the integral are equal to or exceed $\pm \frac{1}{\sqrt{2}}$.

Thus, in the limit of a large sized reflector, the reflected pressure in Equation (122) approaches the value

$$P(r_0) \rightarrow - P_0 e^{-jkr_0},$$

as one would expect for reflection of a plane wave from an infinite plane rigid reflector

If the field point projection falls on the center of the rectangular reflector, then $x_{1,2} = \pm a$ and $y_{1,2} = \pm b$. The limiting case of large plane reflector is reached when the limits u , or v , exceed $\frac{1}{\sqrt{2}}$, i.e. when

$$a \sqrt{\frac{2}{\lambda r_0}} \geq \frac{1}{\sqrt{2}} \quad \text{and} \quad b \sqrt{\frac{2}{\lambda r_0}} \geq \frac{1}{\sqrt{2}}$$

or

- 66 -

$$\frac{(2a)}{\lambda} > \sqrt{\frac{r_o}{\lambda}},$$

and

$$\frac{(2b)}{\lambda} > \sqrt{\frac{r_o}{\lambda}}.$$

(123)

Equation (123) shows that the linear dimensions of the reflector, normalized to the acoustic wavelength, must be larger than the square root of the normalized range r_o/λ . For a square planar, $2a = 2b = h$, the maximum range r_m where the geometrical optic theory applies is given by

$$\frac{2a}{\lambda} = \frac{2b}{\lambda} = \frac{h}{\lambda} = \sqrt{\frac{r_m}{\lambda}} \quad (124)$$

The limit range r_m is shown in Figure (41) in terms of the frequency and the linear dimension of a square reflector h .

It is instructive to obtain exact values of the integrals in Equation (122) for various values of the normalized dimensions of the reflector. If $2a = 2b = h$, and if the field point projection is located at the center of the square reflector, then the amplitude of the normalized pressure $|P(r_o)/P_o|$ is given by:

$$\left| \frac{P(r_o)}{P_o} \right| = 2 \left| \int_0^u e^{-j\pi v^2/2} dv \right|^2, \quad u = \sqrt{\frac{r_m}{2r_o}} \quad (125a)$$

The exact value of the normalized reflected pressure for a square reflector ($h \times h$) is shown in the following table for various locations of the field point r_o/r_m :

- 67 -

u	r_o/r_m	$ P(r_o)/P_o $ - Fresnel, Equation (125a)	$ P(r_o)/P_o $ - Fraunhofer, Equation (125b)
0.10	50.00	0.02	.02
0.30	5.50	0.18	0.18
0.50	2.00	0.47	0.50
0.71	*1.00*	*1.00* (Limit)	*1.00* (Limit)
1.00	0.50	1.22	2.00
1.20	0.35	1.74	3.30
1.50	0.20	1.39	5.00
2.00	0.10	0.71	10.00
3.00	0.05	1.28	20.00

Thus, in the range $r_o < r_m$, the laws of geometrical optics apply, and the reflected pressure is equal to the incident pressure, i.e. the reflected pressure is the same as if the wave was geometrically reflected at the flat surface of the reflector, see above table. The condition in equation (124) is exactly the same formula as the one given in equation (113) as the requirement for the existence of a stationary phase point, i.e. that $r < r_m = h^2/\lambda$.

For distances $r_o > r_m$, the Fresnel integral should reduce to the Fraunhofer approximation. For a field point on the normal axis, $x, y \ll r_o$ and the exponentials can be replaced by unity, then the Fresnel integral, Eq. (122), reduced to the expression given in Equation (120) with $D(\theta, \phi) = 1$:

$$P = \frac{jk P_o(4ab)}{2\pi r_o} e^{-jkr_o} = \frac{j P_o(4ab)}{\lambda r_o} \cdot e^{-jkr_o} = j P_o e^{-jkr_o} \left[\frac{r_m}{r_o} \right] \quad (125b)$$

which has the spherical $(1/r_o)$ falloff. Equation (125b) predicts the reflected amplitude accurately up to $r_o = r_m$, see above table.

- 68 -

This result is equivalent to assuming that the radiation is geometrically reflected provided the radiation makes an angle 2θ with the field point that is at least equal to θ_{\min} , which, for a square reflector, see Figure (39),

$$\sin \theta_{\min} \approx \theta_{\min} = h/2r_m = \lambda/2h, \quad (126)$$

which is also given in Equation (114).

If the incident field is produced by a point source located at field point, then the backscattered field can be computed by the use of Equation (118). Let the acoustic field of the point source be described by

$$P_i(x,y) = P_o \frac{e^{-jkr}}{r}, \quad (127)$$

where r is given by Equation (117). Using Equation (127) in the expression for the reflected pressure in Equation (118), one obtains, with $r \approx r_o$,

$$P(r_o, \theta, \phi) = \frac{jke^{-2jkr_o}}{2\pi r_o^2} P_o \int_{-a}^{+a} \int_{-b}^b \exp 2jk \left[x \cos \theta + y \cos \phi + \frac{[x \cos \theta + y \cos \phi]^2}{2r_o} - \frac{r_o^2}{2r_o} \right] dx dy. \quad (128)$$

If $\frac{a}{r_o} \ll 1$ and $\frac{b}{r_o} \ll 1$, and if the field-source points are not at normal incidence, then the integral can be simplified, to a first order (Fraunhofer) approximation, as follows:

- 69 -

$$P(r, \theta, \phi) = \frac{jk e^{-2jkr_o} P_o}{2\pi r_o^2} \int_{-a}^a \int_{-b}^b e^{2jk[x \cos \theta + y \cos \phi]} dx dy$$

$$= \frac{jk e^{-2jkr_o} P_o}{2\pi r_o^2} D(\theta, \phi) \quad (129)$$

where the directivity factor D is given by:

$$D(\theta, \phi) = \frac{\sin(2ka \cos \theta)}{(2ka \cos \theta)} \frac{\sin(2kb \cos \phi)}{(2kb \cos \phi)} =$$

$$= \frac{\sin(ka \cos \theta) \cos(ka \cos \theta)}{(ka \cos \theta)} \cdot \frac{\sin(kb \cos \phi) \cos(kb \cos \phi)}{(kb \cos \phi)} \quad (130)$$

Maximum backscattering is attained when the field-source points are at normal incidence, i.e. when $\theta = \phi = \frac{\pi}{2}$, where $D \rightarrow 1.0$. The backscattered pressure, at large distances where $r_o \gg a, b$, decreases as $1/r_o^2$. This form of backscattering is equivalent to spherical spreading from source to reflector and again from the reflector to the field point. The phase change of $(2kr_o)$ reinforces this fact. For such large distances, the laws of geometrical optics do not apply.

The preceeding computations are not valid for distances closer than r'_m , as defined in Equation (111). For normal incidence, $\theta = \phi = \pi/2$ and one must retain more terms in the eikonal expression in Equation (128). Thus, the backscattered field becomes,

$$P(r_o) = \frac{jk e^{-2jkr_o} P_o}{2\pi r_o^2} \left[\int_{x_1}^{x_2} e^{-jkx^2/r_o} dx \right] \left[\int_{y_1}^{y_2} e^{-jky^2/r_o} dy \right]$$

- 70 -

$$= \frac{j P_o e^{-jkr_o}}{2r_o} \left[\frac{1}{\sqrt{2}} \int_{u_1}^{u_2} e^{-j\frac{\pi}{2} u^2} du \right] \left[\frac{1}{\sqrt{2}} \int_{v_1}^{v_2} e^{-j\frac{\pi}{2} v^2} dv \right] \quad (131)$$

$$\text{where } u^2 = \frac{2k x^2}{\pi r_o}, \quad v^2 = \frac{2k y^2}{\pi r_o},$$

$$u_{1,2} = \frac{2 x_{1,2}}{\sqrt{\lambda} r_o}, \quad v_{1,2} = \frac{2 y_{1,2}}{\sqrt{\lambda} r_o}$$

The Cornu spiral integrals, see Figure (38), have an asymptotic value of $(1-j)$ if the limits are equal or exceed $\pm \frac{1}{\sqrt{2}}$.

In the limit of a large rigid reflector, $a, b \gg \sqrt{\lambda} r_o$ or $u_{1,2} \gg 1$,

$$P(r_o) \longrightarrow \frac{P_o e^{-2jkr_o}}{2r_o}, \quad (132)$$

which represents the reflected field of a point source by an infinite rigid reflector. If the field-source points projection on the plane falls at the center of the reflector, then $x_{1,2} = \pm b$ and the limiting case of large reflector is reached when $u_{1,2}$ and $v_{1,2}$ exceed $\pm 1/\sqrt{2}$, i.e. when

$$\frac{2a}{\sqrt{\lambda} r_o} > \frac{1}{\sqrt{2}} \quad \text{and} \quad \frac{2b}{\sqrt{\lambda} r_o} > \frac{1}{\sqrt{2}},$$

or

$$\frac{(2a)}{\lambda} > \sqrt{\frac{r_o}{2\lambda}},$$

and

$$\frac{(2b)}{\lambda} > \sqrt{\frac{r_o}{2\lambda}}$$

(133)

- 71 -

Equation (133) shows that the wavelength-normalized linear dimensions of the reflector must be larger than the square root of half of the wavelength-normalized range. For a square reflector, let $2a = 2b = h$, then the maximum range r'_m , where the geometrical optic theory applies, is given by

$$\frac{2a}{\lambda} = \frac{2b}{\lambda} = \frac{h}{\lambda} = \sqrt{\frac{r'_m}{2\lambda}} \quad (134)$$

The limit range r'_m is the same one predicted by the requirement for the existence of the stationary phase point, see Equation (111). If the field point is not on the axis of the rigid reflector, we may assume the reflector to consist of one of infinite size with two (or four) pressure release reflectors adjacent to it. The resultant effect then will be that of the finite reflector.

The above computations have been performed as if the reflector was in a baffle. This assumption is always made in computing transducer arrays. It leads to results that agree well with tests on arrays for all angles of incidence, except those close to grazing.

It is not possible, however, to deduce the results for a semi-infinite strip from the preceding reflection formulae because the strip can no longer be approximated by a reflector in a baffle. For an infinite cylinder, the reflector model will represent a reasonably good approximation. The exactly computed reflection curve for an infinite cylinder of radius R shows that for a plane wave that impinges normally to its axis, the reflection factor of a rigid cylinder, when $kR \geq 1$, is approximately equal to $\frac{1}{\sqrt{2}}$, (see E. Skudrzyk, 1971, page 448). Thus the amplitude that is scattered at a rigid infinite cylinder is:

$$|P(r_o)| = P_o \sqrt{\frac{R}{2r_o}} \quad (135)$$

- 72 -

A finite cylinder of length h one would expect that the cylindrical spreading ($1/\sqrt{r_0}$) shown in equation (135), would be valid only if $r_0 < r_m$, as defined in equation (124). In the far-field, $r_0 > r_m$, the effect of the finite dimension of the cylinder (h) must be superimposed on the curvature effect given in equation (135). One can obtain a good approximation for the far-field correction by multiplying the expression in Equation (135) by the reflection from two finite edges of length h . This correction factor can be obtained from equation (122) by neglecting the second integral, resulting in a factor $h \sqrt{\frac{2}{\lambda r_0}}$. Thus, the total reflected field from an insonified finite cylinder becomes:

$$|P(r_0)| = P_0 \sqrt{\frac{R}{2r_0}} h \sqrt{\frac{2}{\lambda r_0}} = P_0 \sqrt{\frac{R}{\lambda}} \frac{h}{r_0}, \quad r_0 > r_m \quad (136)$$

where r_m is given by equation (124). The expression for the reflected field from a finite cylinder shows the spherical falloff with the field point distance r_0 .

Similar conclusions can also be drawn by considering the Fresnel solution for a circular reflector or by analyzing the exponent in the diffraction integral near a stationary phase point. The corresponding integrand always contributes fully if $u^2 \geq 1/2$ (i.e. if $r_0 < r_m$); where u is the same variable as in the Fresnel integrals see Equation (122). This condition then represents the limiting range of the reflection or diffraction field that is satisfied by the geometric diffraction theory in which the field amplitude decreases as $1/\sqrt{r_0}$ (see proceeding section). If $u^2 < 1/2$ (i.e. if $r_0 > r_m$), the exponential can be replaced by 1, and the reflection or diffraction field decreases with the distance as $1/r_0$, as if the reflector was a point source.

- 73 -

Proper accounting must be made for the distance dependence when bodies of finite size are being investigated. Since all finite bodies, in the far-field, have a $1/r_o$ distance dependence, the one-dimensional solution (infinite edge, which has a $1/\sqrt{r_o}$ dependence) when applied to finite edges and wedges, should have its amplitude multiplied by the factor $\sqrt{r_m/r_o}$. Thus, while the amplitude of the field from an infinite edge falls off at a rate of 3 dB per doubling of distance, that of the finite edge falls off at a rate of 6 dB per doubling of distance. The error introduced by the use of the edge diffraction model, at distance $r_o > r_m$, compared to the finite diffractor is illustrated in the table below for doubling of distance relative to r_m

r_o/r_m	Error ($P_{\text{edge}}/P_{\text{finite}}$) dB
1	0.0
2	3.0
4	6.0
8	9.0

14. DIFFRACTION FIELD FROM EDGES OF FINITE LENGTH

Edge diffraction is a highly directive phenomenon. It has been shown by Fermat's principle, see Appendix III. that the radiation scattered by each edge element ds lies on a cone whose semi-apex angle is the same as the angle of the incident ray with the element. Thus, the scattering phenomenon associated with edge diffraction is somewhat similar to that of reflection - the angle of scattering at an element ds is equal to the angle of incidence. However, because the scattering element is not a surface but a line element, scattering occurs symmetrically around that line element, i.e. the scattered rays lie on the surface of a cone. For example, a plane wave that is incident at an angle β with the edge has a scattering cone angle β , see Figure (42a). For a plane wave normally incident on an edge, i.e. for $\beta = \pi/2$, the scattered rays lie in a plane that is perpendicular to the edge element, see Fig. (42b).

For a finite edge of length l , the scattered radiation is confined in the volume between two cones, whose apexes are at each end of edge, see Figure (42c). Geometrically for a plane wave incident at an angle β , the scattered field can only be received in a region corresponding to the volume of a conical shell of thickness equal to the projection of the edge length on wave front. If the receiver is in this conical shell region, then the apex of the scattering cone originates from a point on the edge. Mathematically, this point corresponds to the stationary phase point for the receiver position. The edge must be long enough so that a stationary phase point can be formed on it. If there is no stationary phase point on the finite edge, then there is no scattered or diffracted field in the sense of the geometrical theory.

Next let us assume a spherical incident wave on a finite edge of length l , see Figure (43). The condition for the stationary phase point is satisfied by, see Figure (17),

- 75 -

$$\tan \beta = \frac{d}{s} = \frac{\rho_0}{(s - s_0)} \quad (137)$$

Next, let us examine the scattered field in the plane containing the source L and the scattering edge. The opening of the scattered field then is

$$\epsilon = \frac{\lambda \sin \beta}{\rho}, \quad (138)$$

where ρ is the distance from the source L to the projection point P, see Figure (43). If the distance $\rho \gg \lambda$, the scattering opening angle ϵ is very small. According to the geometrical theory of diffraction, the scattered field at receiver points located approximately as far from the edge as the source would be confined to a conical shell not very much thicker than the twice the projection of the edge on a wave front. This means that the field that is scattered by an edge of a length of 15 feet can only be observed over a cross section of not much more than 30 feet.

This means that the geometrical theory of diffraction cannot be applied to edges of finite length. In this case, the geometrical theory gives expressions for the scattered sound field that are both correct dimensionally and in absolute value, provided it is used in the range in which it is applicable, $r_0 < r_m$, Equations (111) or (113). In the far field [$r_0 > r_m$, Equations (111) or (113)], the exact diffraction formula for a finite sized scatterer are very similar to the radiation formula of finite baffled array. However, an even more accurate solution for the diffraction field from a finite edge can be obtained using the Rubinowicz-Kirchoff integral given by Equation (21):

$$\phi_d = \frac{A}{4\pi} \int_{\text{edge}} \frac{e^{-jk(\rho+r)}}{r\rho} \cdot \frac{\cos(\vec{n}, \vec{r})}{1 + (\cos \vec{r}, \vec{\rho})} \sin(\vec{\rho}, d\vec{s}) ds \quad (139)$$

- 76 -

where the factor $\frac{A e^{-jk\rho}}{\rho}$ represents the incident spherical wave, ρ and r are the distances of the source and receiver to the edge element ds .

Consider a finite curved edge of length λ , which is small compared to ρ and r , such that one may substitute for the term $1/\rho$ in the amplitude factor by $1/r_0 \rho_0$, where r_0 and ρ_0 are the distances r and ρ to origin $s = 0$, located at the center of the edge. Retaining only r_0 and ρ_0 in the amplitude factor $1/\rho$, the integral equation (139), simplifies to:

$$\Phi_d = \frac{A}{4\pi r_0 \rho_0} \int_{\text{edge}} e^{-jk(\rho+r)} \cdot \frac{\cos(\vec{n}, \vec{r}) \sin \beta ds}{1 + \cos(\vec{r}, \vec{\rho})} \quad (140)$$

where $\beta(s) = \angle(\vec{\rho}, d\vec{s})$ is the angle the radius vector $\vec{\rho}$ of the source point makes with the edge element $d\vec{s}$. For a straight edge, the shadow boundary is plane, and consequently $\vec{n} = \text{constant}$. The influence of the curvature of the edge is contained in the functional relations of $\vec{r}(s)$, $\vec{\rho}(s)$, $\beta(s)$ and $\gamma(s)$, where $\gamma(s) = \angle(\vec{r}, d\vec{s})$ is the angle between the radius vector \vec{r} of the field point and the edge element $d\vec{s}$. The sum of the radii r and ρ can be expanded in a Taylors' series on the distance along the curved edge s , see Appendix IV, the leading term of the exponential being $\rho_0 + r_0$.

For a fixed position of the source and field points, it is convenient to establish a cartesian coordinate system centered at the diffracting element (ds), see Figure (44). Let the positive z -direction be directed in the direction of the incident ray, the x -axis in the plane of $d\vec{s}$ and \vec{u}_z , (i.e. in the plane of the shadow boundary) where $\vec{u}_{x,y,z}$ are unit vectors of the cartesian coordinate system. The direction vectors of the field and source points are:

$$\vec{\rho} = \rho \vec{u}_z \quad (141)$$

$$-\vec{r} = x \vec{u}_x + y \vec{u}_y + z \vec{u}_z \quad (142)$$

- 77 -

The unit tangent vector of the edge is given by:

$$\vec{t}(s) = \frac{d\vec{s}}{ds} = \frac{\partial \vec{r}}{\partial s} = -(\dot{x} \vec{u}_x + \dot{y} \vec{u}_y + \dot{z} \vec{u}_z) \quad (143)$$

The unit normal vector of the shadow boundary, pointing into the shadow zone, is then given by:

$$\vec{n}(s) = \vec{u}_z \times \vec{t}(s) = \dot{y} \vec{u}_x - \dot{x} \vec{u}_y \quad (144)$$

The various angular functions of the integrand in Equation (140) can now be evaluated in terms of the new coordinate system. Thus,

$$\cos(\vec{n}, \vec{r}) = \vec{n} \cdot \frac{\vec{r}}{r} = \frac{y\dot{x} - x\dot{y}}{r} \quad (145)$$

$$\cos(\vec{r}, \vec{\rho}) = \frac{\vec{r}}{r} \cdot \frac{\vec{\rho}}{\rho} = \frac{\vec{r}}{r} \cdot \vec{u}_z = -\frac{z}{r} \quad (146)$$

$$\cos \beta = \cos(\vec{\rho}, d\vec{s}) = \cos(\vec{\rho}, \vec{t}) = -\dot{z} \quad (147)$$

$$\cos \gamma = \cos(\vec{r}, d\vec{s}) = \frac{\vec{r}}{r} \cdot \vec{t} = \frac{x\dot{x} + y\dot{y} + z\dot{z}}{r} \quad (148)$$

Combining these expressions for the angular function, one obtains:

$$\frac{\cos(\vec{n}, \vec{r})}{1 + \cos(\vec{r}, \vec{\rho})} = \frac{y\dot{x} - x\dot{y}}{r - z} = \frac{\frac{y}{r} \dot{x} - \frac{x}{r} \dot{y}}{1 - \frac{z_0}{r} - \left[\frac{z}{r} - \frac{z_0}{r} \right]} \quad (149)$$

For large distance, $r \gg \lambda$, the coordinates of the numerator can be replaced by their values at the center of the diffracting edge (x_0, y_0, z_0) . Thus, the directivity factor, Equation (149), reduces to:

$$\frac{\cos(\vec{n}, \vec{r})}{1 + \cos(\vec{r}, \vec{\rho})} \approx \frac{\frac{y}{r_0} \dot{x} - \frac{x}{r_0} \dot{y}}{1 - \frac{z_0}{r_0}}, \quad (150)$$

- 78 -

where the term $z/r - z/r_0$ has been neglected when compared to the other terms. It must be noted, however, that such an approximation to the denominator of Equation (149) is not valid if the field point falls on the shadow boundary, because $\cos(\vec{r}, \vec{\rho}) = -1$. Thus, near the shadow boundary the denominator of Equation (150) must be left as it is given in Equation (149).

Introducing a polar coordinate system at $(d\vec{s})$, whose z-axis coincides with z-axis of the cartesian system, i.e.

$$\begin{aligned} z &= r \cos \theta \\ y &= r \sin \theta \sin \phi \\ x &= r \sin \theta \cos \phi . \end{aligned} \quad (151)$$

The angular factor, Equation (150), thereby reduces to:

$$\frac{\sin \theta \sin \phi \dot{x} - \sin \theta \cos \phi \dot{y}}{1 - \cos \theta} = \quad (152)$$

$$\cot \left(\frac{\theta}{2} \right) [\dot{x} \sin \phi - \dot{y} \cos \phi] .$$

The diffraction integral for a finite curved edge in Equation (140) becomes

$$\begin{aligned} \phi_d &= \frac{A}{4\pi r_0 \rho_0} \int_{-\ell/2}^{\ell/2} e^{-jk(\rho+r)} \sin \beta \cot \left(\frac{\theta}{2} \right) \\ &\quad [\dot{x} \sin \phi - \dot{y} \cos \phi] ds , \end{aligned} \quad (153)$$

where the exponential term $(\rho+r)$ can be written in terms of the edge variable (s) as shown in Appendix IV. In the special case of a straight edge the distance from the source and field points to the edge may be approximated by

$$\begin{aligned} \rho &\doteq \rho_0 - s \cos \beta \\ r &\doteq r_0 - s \cos \beta \end{aligned}$$

and the diffraction integral, Equations (153), can be written as

$$\phi_d = \frac{A e^{-jk(\rho_o + r_o)}}{4\pi r_o \rho_o} \int_{-\ell/2}^{\ell/2} e^{jks(\cos \beta + \cos \gamma)} \sin \beta \cot \left(\frac{\theta}{2}\right) [\dot{x} \sin \phi - \dot{y} \cos \phi] ds \quad (154)$$

It will be recalled that in the Kirchoff theory of diffraction, the orientation of the plane of the diffractor is unimportant and that it is only the discontinuity introduced by the edge that is of interest. Therefore, if the edge lies in the y-z plane and is inclined by an angle $\alpha = \pi/2 - \beta$ to the x-axis; we obtain the results that $y = \dot{y} = 0$ and $\dot{x} = \cos \alpha = \sin \beta$ respectively. In addition, the angular functions $\beta(s)$ and $\gamma(s)$ becomes:

$$\begin{aligned} \cos \beta &= \dot{z} = \text{constant} \\ \cos \gamma &= \dot{x}_o \sin \beta - \frac{z_o}{r_o} \cos \beta \\ &= \sin \theta \sin \beta \cos \phi - \cos \theta \cos \beta \end{aligned} \quad (155)$$

thus, defining the sum of these cosines as

$$B = \cos \beta + \cos \gamma = \sin \theta \sin \beta \cos \theta + \cos \beta(1 - \cos \theta) \quad (156)$$

the integral for a finite straight edge in Equation (154) can be approximated by:

$$\phi_d = - \frac{A e^{-jk(\rho_o + r_o)}}{4\pi r_o \rho_o} \sin^2 \beta \cot \left(\frac{\theta}{2}\right) \sin \phi \int_{-\ell/2}^{\ell/2} e^{+jk B s} ds \quad (157)$$

where all the angles were assumed to be constant along the path of integration, since $\ell \ll r, \rho$. The final result of the integration can be shown to result:

- 80 -

$$\Phi_d = \frac{A}{4\pi} \frac{\ell}{2r_o} \frac{e^{-jk(r_o + \rho_o)}}{\rho_o} \left| \frac{\sin(kB\ell/2)}{(kB\ell/2)} \right| \cot\left(\frac{\theta}{2}\right) \sin^2\beta \sin\phi \quad (158)$$

or

$$\Phi_d = \frac{C}{4\pi} \frac{\ell}{2r_o} \left\{ \frac{\sin(kB\ell/2)}{(kB\ell/2)} \sin\phi \right\} \tan\frac{\theta'}{2} \quad (159)$$

where

$$C = \frac{A}{\rho_o} e^{-jk\rho_o} \sin^2\beta$$

which is the measure of the acoustic energy incident on the edge and $\theta' = \theta + \pi/2$ is the polar angle as measured in the theory of straight edge. The factor in the paranthesis represents the directivity of a dipole line array of length ℓ , and the $\tan\frac{\theta'}{2}$ term is the directivity factor of the Kirchhoff straight edge. Equation (159) shows that the spreading is spherical (the amplitude being proportional to $\ell/2r_o$) and that the directivity pattern is that of a linear dipole array combined with that of an infinite straight edge. Except for the effect of the angle functions, the diffracted wave is the same as if the incident wave were reflected at a sphere of the same diameter as the length of the diffracting edge. However, the last formula is valid only for $\theta > 0$ (i.e. not at the shadow boundary) because it is based on Equation (150) which neglects the factor $(z-z_o)/r_o$ in the denominator of the integrand as given by Equation (149). It is possible to derive a solution that is valid very near the shadow boundary in a similar manner as this has been done for integral in Equation (153). However, we are not really interested in this solution since it describes basically only the diffusion of the sound field across the the boundary of the geometric shadow. Slightly away from shadow boundary, Equation (158) is sufficiently accurate.

Equation (158) consists of two groups of terms. The terms

- 81 -

not in the brackets are the familiar diffraction terms, the cotangent appearing in the formula because $\theta = 0$ counts the derivation in angle from the forward direction. The bracketed factor is of the form $\sin x/x$ and is the same as the directivity function of a linear transducer array. For field points not coincident with the shadow boundary, this factor leads to maxima and minima that are similar to those generated by a linear array of the same length. The amplitude of the maxima decreases proportionally to

$$\left| \frac{1}{2\sqrt{2\pi kr_0}} \right| \left| \sqrt{\frac{2}{\pi}} \frac{1}{\sqrt{kr_0}} \right| = A_{\text{diff}} \frac{1}{\sqrt{2\pi kr_0} B} \quad (160)$$

where B is the angle factor, Equation (156), that on the average is not very different from unity and A_{diff} is the amplitude of the diffracted field due to an infinite edge. Thus, Equation (160) shows that for a finite edge when the field point is far away, the edge is not long enough to generate a stationary phase point and the amplitude decreases from the diffracting edge at a rate greater (by $1/\sqrt{kr_0}$) than for an infinitely long edge.

It should be noted that the amplitude of the maxima further away from the direction of the main beam is independent of the length of the edge. This conclusion may seem very strange at first, but a similar relationship can be obtained by considering linear transducer array with, for instance, a finite number n of elements. The magnitude of the maxima then is given by (see E. Skudrzyk, 1971, page 598):

$$A_{\text{max}} = nD_v = \frac{1}{\sin \Delta} = \frac{1}{\sin [(2v + 1)\pi/2n]} \quad (161)$$

where D_v is the directivity function for the maxima, and $\Delta = (2v + 1)\pi/2n$, $v = 1, 2 \dots n$ is the phase difference between successive transducer elements in the direction of the maxima. The envelope of the maxima is obtained by varying v/n continuously in the last expression from 0 to $\pi/2$. The amplitude

- 82 -

of the main maximum is therefore proportional to the number of transducer elements in the linear array.

If n is great, then there is correspondingly a great number of side maxima near the main maximum and the beam is highly directive. As a result, little of the array's total energy is radiated at angles away from the main beam. If the number of elements is small, then the main maximum is small too and much of the energy is radiated side-ways. For the same transducer element spacing, the field radiated off axis is independent of the number of elements of the transducer array, see Figure (45). However, there is one essential difference; the field of the small array decreases as $1/kr$ while that of the large array decreases as $1/\sqrt{kr}$ for a much greater distance from the array.

15. SUMMARY AND CONCLUSIONS

The acoustic diffraction and backscattering fields generated by plane diffractors and wedges have been investigated using both the geometrical theory of diffraction (GTD) developed by Keller and the more mathematically formal theory based on the Kirchhoff-Rubinowicz integral representation. Comparisons were made of the results obtained using the two methods. A summary of these results and their physical interpretations are given below.

15.1 The Geometrical Theory of Diffraction

The geometrical theory of diffraction (GTD) is based on the high frequency assumption that the energy of a wave can be confined to tube-like bundles, and propagated along ray curves. These curves are straight lines for a homogenous, isotropic acoustic media. Since it is assumed that the energy is equal at any cross-section of a bundle of the rays, the geometrical diffraction field is obtained by determining the variation in cross-sectional area from point to point along the ray. Curvature effects of a diffracting edge are shown in Section (5) to be obtained directly by this method.

Although, the GTD gives the correct distance dependence (within its range of validity for the size of the diffractor), it gives no indication of the angular variation of the diffracted field. Keller determines the correct directivity factor by forcing his solution to agree with the exact (Sommerfeld) solution for the straight edge and then proceeds to use this relation for all other curved edges. (The Kirchhoff-Rubinowicz integral representation directly furnishes the proper directivity functions, or at least a very good approximation to it.)

15.2 The Kirchhoff-Rubinowicz Integral Representation

The Kirchhoff-Rubinowicz theory of diffraction is based on the solving the Helmholtz-Huyghen integral with the assumption that the diffractor is ideally absorbent and therefore no reflected waves occur. This allows the diffracted field to be investigated independently. (Reflections may be accounted for separately by introducing the method of images, see Section 8). The solution of the resulting Kirchhoff diffraction field is expressed as a surface integral over the shadow boundary. Rubinowicz reduces this surface integration into a line integration about the periphery edge of the diffractor.

The resulting edge integral can then be evaluated in various kr ranges (k acoustic wave number, r is the distance from the edge). It is interesting to note, that the high frequency limit of the Kirchhoff-Rubinowicz diffraction field is the same as that obtained by the GTD; i.e. the stationary phase contribution of the Kirchhoff-Rubinowicz integral is the same as the direct ray contribution of the GTD.

The Kirchhoff-Rubinowicz integral representation has the advantage of being mathematically exact, with the degree of approximation of the solution (i.e. the diffracted field) always known. This method provides both the correct distance dependences and angular directivity, and is therefore more useful than the GTD for curved and finite edges.

15.3 Diffraction and the Shadow Boundary

For steady state phenomena and plane diffractors, it generally appears that the diffraction field can be attributed to the discontinuity of the incident wave field at and near the entire shadow boundary. The shadow boundary acts basically like a surface layer of dipole sources. The effect of the shadow boundary is then to generate both a wattless near-field and a wave which propagates

- 85 -

from the region near the edge of the diffractor. (This is similar to the radiation field of a finite plate vibrating below coincidence; where only the region near the boundary radiates due to the uncanceled volume flow between adjacent quarter wavelength regions of the plate.)

The near field contribution arises physically from the diffusion of momentum from the incident wave into the shadow region. This near field is correlated with the incident field and therefore cannot be described by an independent energy function. In contrast, the field generated by the edge area, except for the region in the immediate vicinity of the shadow boundary, is uncorrelated with the incident field and therefore can be represented by a separated energy function i.e. the diffracted field. These two fields establish the continuous transition of the pressure field from the insonified to the shadow regions.

For a transient incident acoustic pulse, such as a Dirac pulse, the origination of the diffracted field at the shadow boundary can be demonstrated directly.

15.4 Diffraction and its Role in Determining Backscattering

Backscattering from a rigid or pressure release plane surface is made up primarily of two phenomena:

- (1) Spectral reflections, where the angle of the incident wave is equal but opposite to the reflected wave, and
- (2) a diffraction field that arises at the edge of the surface.

A concern of this report was to evaluate what effect the diffraction field has on the backscattered field

Two diffraction fields are generated as a result of an edge; one is caused by the discontinuity of the incident field (i.e. the familiar shadow boundary), the second by the discontinuity in the reflected field due to the termination of the reflecting surface.

- 86 -

The diffraction fields in both cases are highly directive with their major contribution occurring along the lines of the discontinuity, in the direction of their respective propagation. Very little energy is propagated in the opposite directions. What this means therefore, is that the major contributions to the backscattered field comes from the lobe of the diffracted field associated with the reflected wave. Thus the application of anechoic coatings to a plane reflector will reduce the amplitude of the reflected wave and in turn the backscattering caused by the lobes of the diffracted field associated with the reflected wave.

Mathematically, reflections from any locally reacting surface may be included in the Kirchhoff formulation by introducing the method of images as is explained in Section (8).

15.5 Range of Validity of the Geometrical Theory of Diffraction

The GTD has been shown in Section (5) to be based on Fermat's principle, which is equivalent to the necessity of having a Kirchhoff stationary phase point located well within the length of the diffracting edge. The diffracted field is then considered to arise from the edge element at and near the stationary phase point. For edges of finite length, h , the range, r_m , for a stationary phase point to be generated (and therefore the range of validity of the backscattering obtained by the GTD) is given by $r_m < N h^2 / \lambda$ where λ is the acoustic wave length and N is 1 for a plane incident wave and 2 for spherical incident wave. The GTD, therefore, applies only within a limited distance range from the diffractor. Because of the failure of the GTD for greater distances than r_m , the Kirchhoff-Rubinowicz integral representation was investigated in detail. This representation leads to solutions of the diffracted field that

- 87 -

reliable in practically the whole range of interest and lead to the correct distance dependence regardless of both the size of the diffractor and the frequency (wavelength) of interest (Provided that the diffractor is at least 3 wavelengths long).

15.6 Diffraction Field from a Finite Edge

Physically, the diffraction field from a finite edge acts similar to the radiated field from a line array of finite length. Based on Kirchhoff-Rubinowicz theory of diffraction, the diffracted field for a finite edge was shown, Equation (159), to be given by the product of the incident acoustic pressure, the directivity factor of a dipole line array, and the directivity factor of the Kirchhoff straight edge. This relation is valid everywhere except near the shadow boundary, and is equivalent to the product of the reflection from a sphere of the same diameter as the length of the edge and some combined directivity factor.

REFERENCES

- Born, M., Wolf, E.: Principles of Optics, Electromagnetic Theory of Propagation, Interference and Diffraction of Light. London - New York - Paris - Paris - Los Angeles: Pergamon Press. 1959.
- Bowman, Senior, Uslenghi: Electromagnetic and Acoustic Scattering by Simple Shapes. New York - Amsterdam: Wiley Interscience Division, John Wiley and Sons Inc.. 1969.
- Braunbek, W.: Neue Naherungsmethode für die Beugung am ebenen Schirm. Z. Physik 127 (1950) 381-390; Zur Beugung an der Kreisscheibe. Z. Physik 127 (1950) 405-415; Zur Darstellung von Wellenfeldern. Z. Naturforsch. 6a (1951) 12-15; Zur Beugung an der kreisförmigen Öffnung. Z. Physik 138 (1954) 80-88; Zur Beugung an Öffnungen in nichtebenen Schirmen. Z. Physik 156 (1959) 66-77.
- Franz, W.: Zur theorie der Beugung. Z. Physik 125 (1949) 563-596; On the theory of diffraction. Proc. Physic. Soc. London A 63 (1950) 925-939; Zur Formulierung des Huygensschen Prinzips. Z. Naturforsch. 3a (1948) 500-506; Zur Theorie der Beugung am Schirm. Z. Physik 128 (1950) 432-441.
- Fraunhofer, J. von: Neue Modifikation des Lichtes durch gegenseitige Einwirkung und Beugung der Strahlen, und Gesetze derselben. Denkschr. Münchner Akad. 8 (1822) 1; Schumachers astr. Abhandl. Bd. 2, 1823; Gilberts Ann. 74 (1823) 337; auch Gesammelte Schriften, herausg. von E. Lommel, S. 51. München: Verl. Bayer. Akad. Wiss. 1888.
- Jones, D. S.: Note on diffraction by an edge. Quart. J. Mech. Appl. Math. 3 (1950) 420-434; Removal of an inconsistency in the theory of diffraction. Proc. Cambridge Phil. Soc. 48 (1952) 733-741; Diffraction by a thick semi-infinite plate. Proc. Roy. Soc. London 217 A (1953) 153-175; A new method of calculating scattering, with particular reference to the circular disc. Comm. pure appl. Math. 9 (1956) 713-746; Theory of Electromagnetism. Pergamon Press, Oxford-London-New York-Paris. 1964.
- Keller, J. B.: Diffraction by a convex cylinder. I.R.E. Trans. 4 (1956) 312-321; Diffraction by an aperture. J. Appl. Physics 28 (1957) 426-444; A geometrical theory of diffraction. Calculus of Variations and its Applications. New York, Toronto, London: McGraw-Hill. 1958; How dark is the shadow of a round-ended screen? J. Appl Physics 30 (1959) 1452-1454. Geometrical theory of diffraction. J. Opt. Soc. Am. 52 (1962) 116-130; Diffraction by polygonal cylinders. Electromagnetic Waves. Madison: The Univ. of Wisconsin Press. 1962.

- Leitner, A.: Diffraction of sound by a circular disc. J.A.S.A. 21 (1949) 331-334; Notes on diffraction by a circular disk. Mathematics Research Group. New York University, Washington Square College 1949. Report No. EM-12 Appl. Mech. Rev. 3 (1950) 2526.
- Meixner, J., Fritze, V.: Das Schallfeld in der Nähe einer frei schwingenden Kolbenmembran. Z. angew. Physik 1 (1949) 535-542.
- Oberheitinger, F.: On asymptotic series for functions occurring in the theory of diffraction of waves by wedges. J. Math. Phys. 34 (1956) 245-255; On the diffraction and reflection of waves and pulses by wedges and corners. J. Res. Nat. Bur. Stand. 61 (1958) 343-365.
- Rubinowicz, A.: Die Beugungswelle in der Kirchhoffschen Theorie der Beugungserscheinungen. Ann. Physik (4) 53 (1917) 257-278; Zur Kirchhoffschen Beugungstheorie. Ann. Physik (4) 73 (1924) 339-364; Eine einfache Ableitung des Ausdrucks für die Kirchhoffsche Beugungswelle. Acta Phys. Polon. 12 (1953) 225-229; Die Beugungswelle in der Kirchhoffschen Theorie der Beugung. Springer-Verlag, Berlin-New York-Warsaw. 1966.
- Schelkunoff, S. A.: Field equivalence theorems. Commun. Pure Appl. Math. 4 (1951) 43-59.
- Skudrzyk, E. J.: The Foundations of Acoustics. Springer Verlag, Berlin-New York, 1971.
- Spence, R. D.: Diffraction of sound by circular discs and apertures. A note on Kirchhoff approximation in diffraction theory. J.A.S.A. 20 (1948) 380-386; 21 (1949) 98-100; A note on the Kirchhoff approximation in diffraction theory. J.A.S.A. 21 (1949) 98-100.
- Wiener, F. M.: Diffraction of sound by rigid discs and rigid square plates. J.A.S.A. 21 (1949) 334-347; Notes on sound diffraction by rigid circular cones. J.A.S.A. 20 (1948) 367-369; On the relation between the sound fields radiated and diffracted by plane obstacles. J.A.S.A. 23 (1951) 697-700.

AD-A040 668

PENNSYLVANIA STATE UNIV UNIVERSITY PARK APPLIED RESE--ETC F/G 20/1
ACOUSTIC DIFFRACTION. PART I. PLANE DIFFRACTORS AND WEDGES.(U)

MAY 73 E J SKUDRZYK, S I HAYEK, A D STUART

N00017-70-C-1407

UNCLASSIFIED

TM-73-109-PT-1

NL

2 OF 2
AD
A040668



END

DATE
FILMED

74-77

APPENDIX I

Stationary Phase Method

In diffraction work it is frequently necessary to evaluate integrals of the form

$$I = \int S(s) e^{jkr f(s)} ds = \int_{-\infty}^{\infty} S(s) e^{j\epsilon(s)} ds \quad (I-1)$$

where $\epsilon(s) = (kr) f(s)$, k is the wave number and r the range. If the function $S(s)$ is a slowly varying function of s in the range of integration and the argument of the exponential function is large, i.e. $kr \gg 1$, the integral may be evaluated asymptotically by the method of stationary phase. Thus, as s varies because of the factor kr , $\epsilon(s)$ will vary drastically unless it passes through a maximum, a minimum or a point of inflexion where $\frac{\partial \epsilon(s)}{\partial s} = 0$. Since $\epsilon(s)$ represents the phase of the integrand, the points s_v where $\frac{\partial \epsilon(s)}{\partial s}$ vanishes are called stationary phase points. Because of the rapid fluctuations of the exponential factor in the integrand everywhere except near stationary phase points, the integrand reduces to contributions in the neighborhoods of the stationary phase points. For example, if $s_v = s_0$ is a stationary phase point, we have

$$\frac{\partial \epsilon(s_0)}{\partial s_0} = 0 \quad (I-2)$$

Solving this equation gives s_0 , and if there are more stationary phase points, it gives the roots $s_0, s_1 \dots s_n$ for all the stationary phase points. The exponential $\epsilon(s)$ may then be expanded into a Taylor series near this stationary phase point:

- 91 -

$$\begin{aligned}\epsilon(s) &= \epsilon(s_0) + (s-s_0) \frac{\partial \epsilon(s_0)}{\partial s_0} + \frac{(s-s_0)^2}{2} \frac{\partial^2 \epsilon(s_0)}{\partial s_0^2} + \dots \\ &= \epsilon(s_0) + \frac{(s-s_0)^2}{2} \epsilon''(s_0) + \dots\end{aligned}\quad (I-3)$$

Higher terms need not be considered (unless $\epsilon''(s_0) = 0$) since only the region of the integration in the vicinity of the stationary phase point, $(s-s_0 \rightarrow 0)$, contributes to the integral. Substituting Equation (I-3) into (I-1) and assuming the integrand takes on the value at the stationary phase point, one obtains the following asymptotic value for the integral:

$$I = S(s_0) e^{j\epsilon(s_0)} \int_{-\infty}^{\infty} e^{j(s-s_0)^2 \epsilon''(s_0)/2} ds \quad (I-4)$$

Making the change of variable

$$u = (s-s_0) \sqrt{\epsilon''(s_0)/2} \quad ,$$

the integral may then be written in the form

$$I = \frac{S(s_0) e^{j\epsilon(s_0)}}{\sqrt{\frac{\epsilon''(s_0)}{2}}} \int_{-\infty}^{\infty} e^{ju^2} du \quad (I-5)$$

The integral can be shown to equal $\sqrt{\pi} e^{j\pi/4}$. Thus, value of the complete integral is thus determined by a single value of the functions that appear in the integrand, and is given by

$$I = \sqrt{\frac{2\pi}{\epsilon''(s_0)}} S(s_0) e^{j[\epsilon(s_0) + \pi/4]} \quad (I-6)$$

0 The square root of $\epsilon''(s_0)/2$ has been taken with the positive sign because we have assumed that ds and du have the same sign so that the new lower and upper limits of integration is again $-\infty$ and $+\infty$, respectively.

At a caustic $S(s_0)$ has a pole. The stationary phase method then must be generalized also for this integral by separating $S(s_0)$ into its pole contribution, and into its regular part. (The theory for this situation is represented with great clarity in D. S. Jones, 1964, page 689).

APPENDIX II

Derivation of the Helmholtz-Huyghens Integral

We start with the Green's formula relating a volume integral to a surface integral

$$\iint_{\sigma} \left(\varphi \frac{\partial \Psi}{\partial n} - \Psi \frac{\partial \varphi}{\partial n} \right) d\sigma = \iiint_{\tau} (\nabla^2 \Psi - \Psi \nabla^2 \varphi) d\tau \quad (\text{II-1})$$

n = outside normal to the integration volume τ and substitute for the field Ψ a solution of the homogeneous equation

$$\nabla^2 g + k^2 g = 0 \quad (\text{II-2})$$

that is finite in the whole space of integration. The right hand side of Eq. (II-1) then is zero. To obtain the field at a particular point $r = 0$, we must distinguish this point from all other points; this is done by identifying g with the Green's function $\frac{1}{r} e^{-jkr}$ for a point source.

The region near $r = 0$ must now be excluded because at $r = 0$, $g(r)$ is singular, and $\nabla^2 g(r)$ is undeterminate. We exclude this point by enclosing it in a little sphere. Hence we have

$$\begin{aligned} 0 &= \int_{\sigma} d\sigma \text{ (surface)} + \int \text{(little sphere)} d\sigma \\ &= \int_{\sigma} \left(\varphi \frac{\partial g}{\partial n} - g \frac{\partial \varphi}{\partial n} \right) d\sigma + \left\{ \varphi \left[\left(-\frac{1}{r^2} - \frac{jk}{r} \right) e^{-jkr} \right]_{r \rightarrow 0} 4\pi r^2 \right\}_{r \rightarrow 0} \frac{\partial r}{\partial n} \\ &\quad + \left[\frac{e^{-jkr}}{r} \cdot \frac{\partial \varphi}{\partial n} 4\pi r^2 \right]_{r=0} = \int_{\sigma} \left(\varphi \frac{\partial g}{\partial n} - g \frac{\partial \varphi}{\partial n} \right) d\sigma - 4\pi \varphi(r=0) \cdot (-1) \quad (\text{II-3}) \end{aligned}$$

because $\frac{\partial}{\partial n} = -\frac{\partial}{\partial r}$ and $r \rightarrow 0$.

Hence we have

$$\varphi(0) = \frac{1}{4\pi} \int (g \frac{\partial \varphi}{\partial n} - \varphi \frac{\partial g}{\partial n}) d\sigma \quad (\text{II-4})$$

To obtain this integral, the field point $r = 0$ had to be enclosed by the surface of integration. If the field point is outside this surface, then the last integral is zero. If both the field point and a source are located inside the surface of integration,

$$\varphi = \varphi_1(x,y,z) + \frac{A e^{-jk |\vec{r} - \vec{r}_2|}}{|\vec{r} - \vec{r}_2|} \quad (\text{II-5})$$

We then have to exclude also a small sphere around $\vec{r}_2 = 0$ from the space of integration, and obtain also a term $-4\pi A e^{-jkr_2}$ in addition to the term $4\pi \Phi(0)$ that resulted through the integration around $r = 0$. The sign of this source term is negative because it results from the first term of the integrand (which has a sign that is opposite to that of the second term). We thus obtain, as would be expected

$$\varphi(0) = \frac{A e^{-jkr_2}}{r_2} + \frac{1}{4\pi} \int_{\sigma} (g \frac{\partial \varphi}{\partial n} - \varphi \frac{\partial g}{\partial n}) d\sigma \quad (\text{II-6})$$

where r_2 is the distance of the source from the field point.

The above result can also be derived purely and formally with the aid of the spherical $\delta(r)$ function defined by

$$\int_0^\epsilon \delta(r) 4\pi r dr = 4\pi, \quad \int_\epsilon^0 \delta(r) 4\pi r dr = 0, \quad (\text{II-7})$$

The function g then satisfies an equation

$$\nabla^2 g + k^2 g = \delta(r), \quad (\text{II-8})$$

Recalling that φ satisfies the homogeneous equation $\nabla^2 \varphi + k^2 \varphi = 0$, then on the right hand side the integral becomes (after substituting for $\nabla^2 g = -k^2 g + \delta(\underline{r})$)

$$\iiint [\varphi(\delta(\underline{r}) - k^2 g) - g \nabla^2 \varphi] d\tau = \iiint [\varphi \delta(r) - g(\nabla^2 \varphi + k^2 \varphi)] d\tau = \iint (\varphi \delta(r) d\tau = 4\pi \varphi(0) \quad (\text{II-9})$$

If both source and field point are inside surface of integration, then

$$\begin{aligned} \nabla^2 g + k^2 g &= \delta(r) \\ \nabla^2 \varphi + k^2 \varphi &= \delta(r_2) \end{aligned} \quad (\text{II-10})$$

- 96 -

$$\begin{aligned}
 \iiint_{\epsilon} (g \nabla^2 \varphi - \varphi \nabla^2 g) d\tau &= \int g[\delta(r_2) - k^2 \varphi] - \varphi[\delta(r) - k^2 g] d\tau \\
 &= \int^{\tau} [g\delta(r_2) - \varphi\delta(r)] d\tau \\
 &= 4\pi [g(r_2) - \varphi(0)] \quad (II-11)
 \end{aligned}$$

$$\varphi(0) = g(r_2) + \frac{1}{4\pi} \iint_{\sigma} \left(g \frac{\partial \varphi}{\partial n} - \varphi \frac{\partial g}{\partial n} \right) d\sigma \quad (II-12)$$

APPENDIX III

Fermat's Principle

In geometrical optics the light rays are defined as the orthogonal trajectories to the wave-fronts $\varphi(x,y,z) = \text{const.}$ by

$$\underline{n} \frac{d\vec{r}}{ds} = \text{grad } \varphi \quad (\text{III-1})$$

where s is the distance along the light ray and \underline{n} is the index of refraction of the medium in which the ray travels.

The "ray vector" $\underline{n}\vec{s}_0 = \underline{n}d\vec{r}/ds$ where \vec{s}_0 is its unit integral vector and satisfies the relation

$$\text{curl } \underline{n}\vec{s}_0 = \text{curl } \left(\underline{n} \frac{d\vec{r}}{ds} \right) = \text{curl } (\text{grad } \varphi) = 0 \quad (\text{III-2})$$

and by integration this relation over an area $\vec{\sigma}$ bounded by a closed curve, we obtain the Lagrange relation:

$$\oint \text{curl } \underline{n}\vec{s}_0 \cdot d\vec{\sigma} = \oint \underline{n}\vec{s}_0 \cdot d\vec{r} = 0 \quad (\text{III-3})$$

This means that the Lagrange integral,

$$\int_{P_1}^{P_2} \underline{n}\vec{s}_0 \cdot d\vec{r} \quad (\text{III-4})$$

is independent of the path of integration. By comparing the Lagrange relation over an element of the actual path with that over an arbitrary curve of the same end points we finally arrive at Fermat's principle

$$\int_{\substack{\text{actual} \\ \text{path}}} nds \leq \int_{\substack{\text{arbitrary} \\ \text{path}}} nds \quad (\text{III-5})$$

(Reference: M. Borne and E. Wolf, Principles of Optics, Pergamon Press, New York, 1965).

To prove Fermat's principle, we take a pencil of rays and compare a segment P_1P_2 of a ray \bar{C} with an arbitrary curve C joining P_1 and P_2 (Fig. 46). Let two neighboring orthogonal trajectories (wave-fronts) of the pencil intersect C in Q_1 and Q_2 and \bar{C} in \bar{Q}_1 and \bar{Q}_2 . Further let Q'_2 be the point of intersection of the trajectory $Q_2Q'_2$ with the ray \bar{C}' which passes through Q_1 .

Applying Lagrange's integral relation to the small triangle $Q_1Q_2Q'_2$, we have

$$(\vec{ns} \cdot d\vec{r})_{Q_1Q_2} + (\vec{ns} \cdot d\vec{r})_{Q_2Q'_2} - (nds)_{Q_1Q'_2} = 0 \quad (\text{III-6})$$

Now from the definition of the scalar product

$$(\vec{ns} \cdot d\vec{r})_{Q_1Q_2} \leq (nds)_{Q_1Q_2} \quad .$$

Further, s is orthogonal to dr on the wave-front, so that

$$(\vec{ns} \cdot d\vec{r})_{Q_2Q'_2} = 0 \quad .$$

Also, since Q_1, Q'_2 and \bar{Q}_1, \bar{Q}_2 are corresponding points on the two wave-fronts,

- 99 -

$$(nds)_{Q_1 Q_2} = (nds)_{\bar{Q}_1 \bar{Q}_2} .$$

On substituting from the last three relations into (IV-6) we find that

$$(nds)_{\bar{Q}_1 \bar{Q}_2} \leq (nds)_{Q_1 Q_2} \quad (III-7)$$

whence, on integration

$$\int_{\bar{C}} nds \leq \int_C nds . \quad (III-8)$$

APPENDIX IV

Derivation of the Rubinowicz Integral

The surface integral Φ_d , Equation (20) in the text, can be transformed from a surface integral over the face of the aperture into a line integral over its edge. For this transformation, we divide the surface of the radiation cone, shown in Figure (47), into triangular areas with one corner at the apex of the cone and two sides through the end points of the edge element $d\vec{s}$ of the aperture. The element $d\vec{s}$ is drawn parallel to $d\vec{s}$, and has a direction such that the vector-cross product

$$d\vec{\sigma} = d\vec{\rho} \times d\vec{s}' = d\sigma \vec{n} \quad (\text{IV-1})$$

represents a unit area vector of the shadow boundary that points into the shadow region. Furthermore, we have (because of similar triangles) the relationship:

$$\frac{ds'}{ds} = \frac{\rho}{\rho_s}, \quad (\text{IV-2})$$

and therefore,

$$d\vec{\sigma} = d\vec{\rho} \times d\vec{s}' = (d\vec{\rho} \times \frac{\rho}{\rho_s} d\vec{s}). \quad (\text{IV-3})$$

To evaluate Equation (20), we still need the distance \vec{r} from the field point Q to a point on the shadow boundary P. This distance is given by (see Figure 47)

$$\vec{PQ} = \vec{r} = \vec{r}_s + (\vec{\rho} - \vec{\rho}_s), \quad (\text{IV-4})$$

- 101 -

and because $d\rho = \frac{\rho_s}{\rho_s} d\rho$,

$$\begin{aligned}\vec{r} \cdot d\vec{\sigma} &= r \cos(\vec{n}, \vec{r}) d\sigma = \frac{\rho_s \vec{r}_s}{\rho_s} \cdot (d\vec{\rho} \times d\vec{s}) \\ &= \frac{\rho}{\rho_s} \vec{r}_s \cdot (\vec{\rho}_s \times d\vec{s}) d\rho.\end{aligned}\quad (\text{IV-5})$$

The diffraction integral, Equation (20) of the text, thus becomes

$$\begin{aligned}\Phi_d &= \frac{1}{4\pi} \int_{\text{edge}} \frac{1}{\rho_s} \vec{r}_s \cdot (\vec{\rho}_s \times d\vec{s}) \int_{\rho_s}^{\infty} e^{-jk(\rho+r)} \\ &\quad \left(\frac{-jk}{r^2} - \frac{1}{r^3} \right) d\rho.\end{aligned}\quad (\text{IV-6})$$

where the integration extends from ρ_s to ∞ , and the element $d\vec{s}$ runs over the edge s of the aperture.

The ρ integration can be performed explicitly. It is expedient to introduce the vector $\vec{LP} = 2\vec{a}$:

$$\vec{LP} = 2\vec{a} = \vec{LQ} - \vec{PQ} = \vec{\rho} - \vec{r}.\quad (\text{IV-7})$$

If we square this equation and add $2\vec{r} \cdot \vec{\rho}$ to both sides, we obtain

$$r\rho + \vec{r} \cdot \vec{\rho} = 1/2 [(r + \rho)^2 - 4a^2];\quad (\text{IV-8})$$

which when differentiated with respect to $d\rho$ becomes:

$$dr/d\rho = \cos(\vec{r}, \vec{\rho}) = \vec{r} \cdot \vec{\rho}/r\rho.\quad (\text{IV-9})$$

With the aid of the last two equations, we easily verify the relation

$$\begin{aligned} \frac{d}{d\rho} \left[\frac{\rho}{r} \frac{e^{-jk(r+\rho)}}{\rho + \vec{r} \cdot \vec{\rho}} \right] &= \frac{d}{d\rho} \left[\frac{2\rho}{r} \frac{e^{-jk(r+\rho)}}{(r + \rho)^2 - 4a^2} \right] \\ &= e^{-jk(r+\rho)} \left(\frac{-jk}{r^2} - \frac{1}{r^3} \right). \end{aligned} \quad (IV-10)$$

At the edge of the aperture, $\rho = \rho_s$, $r = r_s$, and integration of Equation (IV-10) leads to the relation

$$\int_{\rho_s}^{\infty} e^{-jk(r+\rho)} \left(\frac{-jk}{r^2} - \frac{1}{r^3} \right) d\rho = -\rho_s \frac{e^{-jk(r_s + \rho_s)}}{r_s(\rho_s + \vec{r}_s \cdot \vec{\rho}_s)}. \quad (IV-11)$$

Hence we have [see Equations (20) and (IV-6)]:

$$\begin{aligned} \Phi &= \alpha \Phi_g - \frac{1}{4\pi} \int_{\text{edge}} \frac{e^{-jk\rho}}{\rho} \frac{e^{-jkr}}{r} \frac{\vec{r} \cdot (\vec{\rho} \times d\vec{s})}{\rho + \vec{r} \cdot \vec{\rho}} \\ &= \alpha \Phi_g - \frac{1}{4\pi} \int_{\text{edge}} \frac{e^{-jk\rho}}{\rho} \frac{e^{-jkr}}{r} \frac{\cos(\vec{r}, \vec{n})}{1 + \cos(\vec{r}, \vec{\rho})} \sin(\vec{\rho}, d\vec{s}) ds, \end{aligned} \quad (IV-12)$$

where we have dropped the subscripts s ; and where $\alpha = 1$ inside the cone of radiation, while $\alpha = 0$ outside the cone, i.e. in the geometric shadow region.

The integration is performed around the contour of the aperture in a clockwise sense, when looking at the light source. Note that \vec{n} is the external normal to the cone through the shadow boundary (pointing into the shadow region) at the point of the element $d\vec{s}$, and $\angle(\vec{r}, \vec{\rho})$ is the angle between the light ray from the source and the radius vector from the field point to $d\vec{s}$, as shown in Figure (7).

APPENDIX V

Frenet Formulae

Differentiation of position vectors locating points on curved edges are known as Frenet formulae. Let \vec{r} be the position vector to a curved edge, s be the coordinate system for the edge curve, see Figures 7 and 9. Letting $\vec{r} = \vec{r}(s)$, $r^2 = \vec{r} \cdot \vec{r}$, then

$$\vec{t} = \frac{d\vec{r}}{ds} \quad (V-1)$$

where \vec{t} is the unit tangent vector to the edge. Likewise,

$$\frac{dr}{ds} = \cos(\vec{r}, d\vec{s}) = \frac{\vec{r} \cdot \vec{t}}{r} \quad (V-2)$$

$$\frac{d\vec{t}}{ds} = \frac{\vec{h}}{R_k} \quad (\text{see Figure 9}) \quad (V-3)$$

where \vec{h} is the unit vector pointing towards the center of curvature of the edge at s and R_k is the radius of curvature at s . It can therefore be seen that

$$\vec{t} \cdot \vec{t} = 1 \quad \vec{t} \cdot \frac{d\vec{t}}{ds} = \vec{t} \cdot \frac{\vec{h}}{R_k} = 0 \quad (V-4)$$

Thus, differentiating again yields the relation

$$\begin{aligned} \frac{d^2r}{ds^2} &= -\frac{1}{r^2} (\vec{r} \cdot \vec{t}) \frac{dr}{ds} + \frac{1}{r} \left(\frac{d\vec{r}}{ds} \cdot \vec{t} \right) + \frac{1}{r} \left(\vec{r} \cdot \frac{d\vec{t}}{ds} \right) \\ &= -\frac{1}{r^3} (\vec{r} \cdot \vec{t})^2 + \frac{1}{r} + \frac{1}{rR_k} (\vec{r} \cdot \vec{h}) \\ &= -\frac{1}{r} \cos^2(\vec{r}, d\vec{s}) + \frac{1}{r} + \frac{1}{R_k} \cos(\vec{r}, \vec{h}) \\ &= \frac{1}{r} \sin^2(\vec{r}, d\vec{s}) + \frac{1}{R_k} \cos(\vec{r}, \vec{h}) \end{aligned} \quad (V-5)$$

Differentiating the unit vector \vec{h} , results in

$$\frac{d\vec{h}}{ds} = \frac{\vec{B}}{T}, \quad (V-6)$$

where \vec{B} is the unit vector along the binormal and T is the torsion. Thus,

$$\begin{aligned} \frac{d^3\vec{r}}{ds^3} &= \frac{3}{r^4} (\vec{r} \cdot \vec{t})^2 \frac{d\vec{r}}{ds} - \frac{2}{r^3} (\vec{r} \cdot \vec{t}) \left(\frac{d\vec{r}}{ds} \cdot \vec{t} \right) \\ &\quad - \frac{2}{r^3} (\vec{r} \cdot \vec{t}) \left(\vec{r} \cdot \frac{d\vec{t}}{ds} \right) - \frac{1}{r^2} \frac{d\vec{r}}{ds} - \frac{1}{r^2 R_k} \frac{d\vec{r}}{ds} (\vec{r} \cdot \vec{h}) \\ &\quad + \frac{1}{r R_k} \left(\frac{d\vec{r}}{ds} \cdot \vec{h} \right) + \frac{1}{r R_k} \left(\vec{r} \cdot \frac{d\vec{h}}{ds} \right) - \frac{1}{r R_k^2} \frac{dR_k}{ds} (\vec{r} \cdot \vec{h}) \\ &= \frac{3}{r^2} \cos^3 (\vec{r}, d\vec{s}) - \frac{2}{r^2} \cos (\vec{r}, d\vec{s}) - \frac{2}{r R_k} \cos (\vec{r}, d\vec{s}) \\ &\quad \cos (\vec{r}, \vec{h}) - \frac{1}{r^2} \cos (\vec{r}, d\vec{s}) - \frac{1}{r R_k} \cos (\vec{r}, d\vec{s}) \cos (\vec{r}, \vec{h}) \\ &\quad + \frac{1}{r R_k} \cos (\vec{r}, \vec{B}) - \frac{1}{R_k^2} \frac{dR_k}{ds} \cos (\vec{r}, \vec{h}) \end{aligned} \quad (V-7)$$

Rewriting the terms in (V-7), one can show that

$$\begin{aligned} \frac{d^3\vec{r}}{ds^3} &= - \frac{3}{r^2} \sin^2 (\vec{r}, d\vec{s}) \cos (\vec{r}, d\vec{s}) - \frac{3}{r R_k} \cos (\vec{r}, d\vec{s}) \\ &\quad \cos (\vec{r}, \vec{h}) + \frac{1}{r R_k} \cos (\vec{r}, \vec{B}) - \frac{1}{R_k^2} \frac{dR_k}{ds} \cos (\vec{r}, \vec{h}). \end{aligned} \quad (V-8)$$

- 105 -

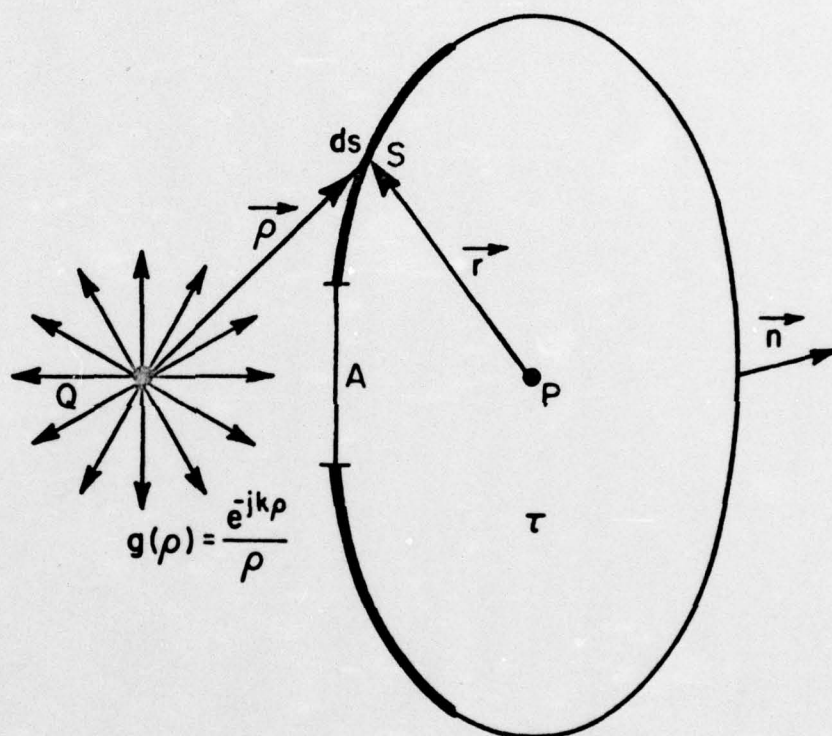


Figure 1- Surfaces of Integration in the Helmholtz-Huyghens Integral

- 106 -

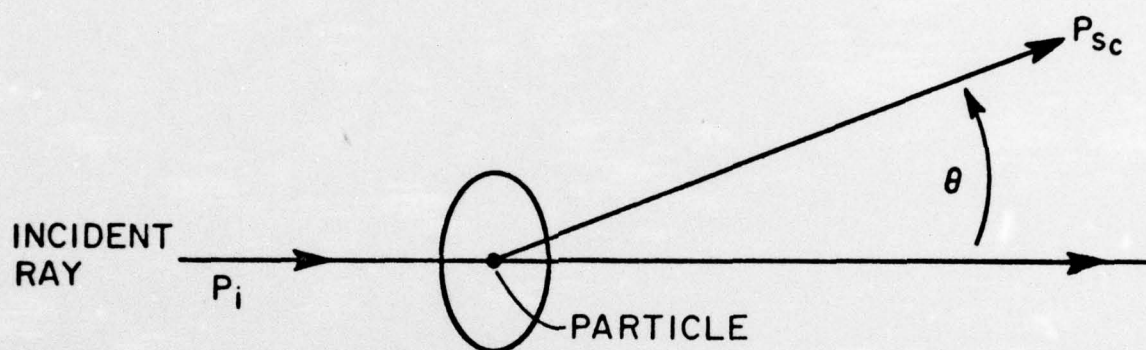


Figure 2- Angle dependence of the scattered field from a particle

- 107 -

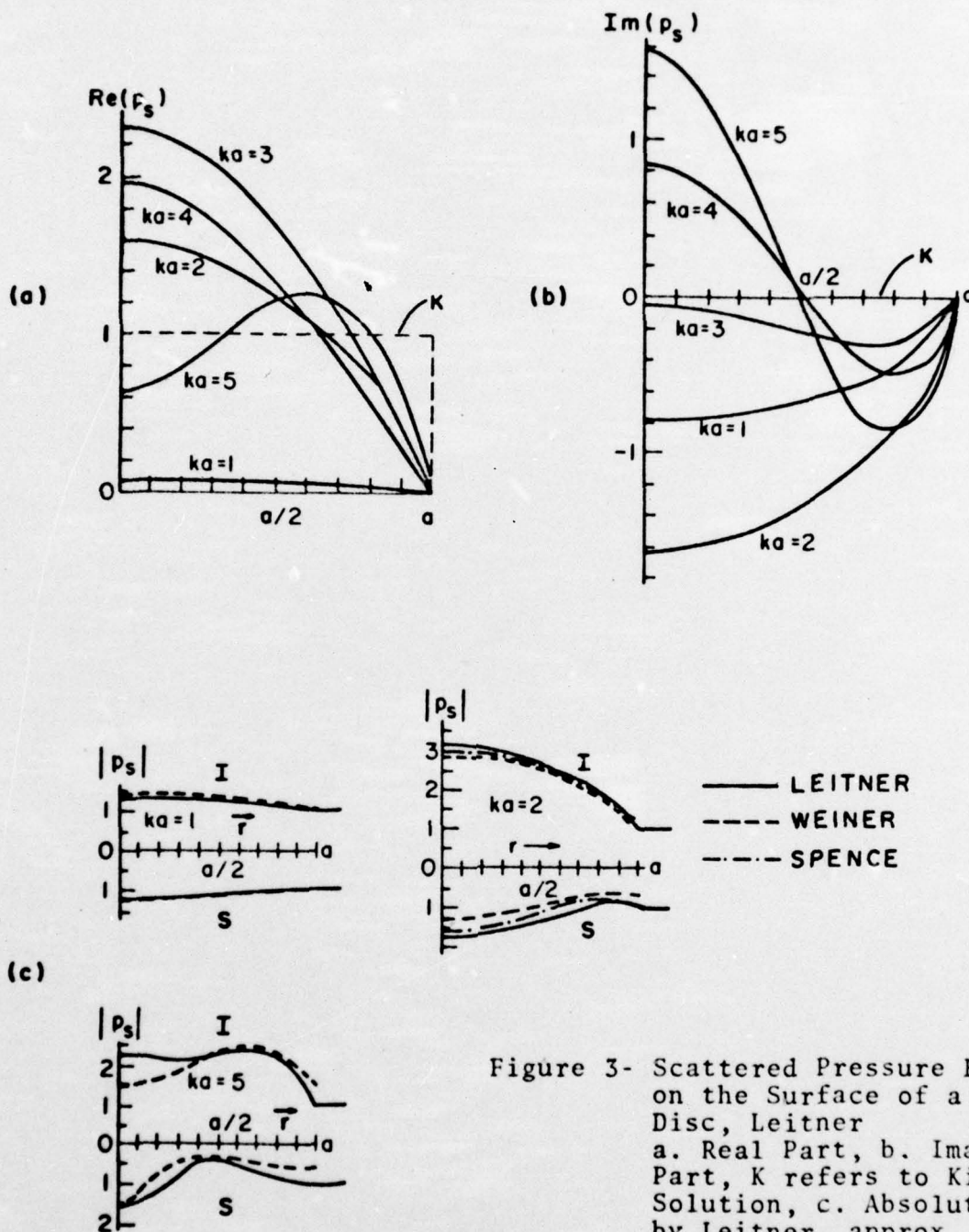
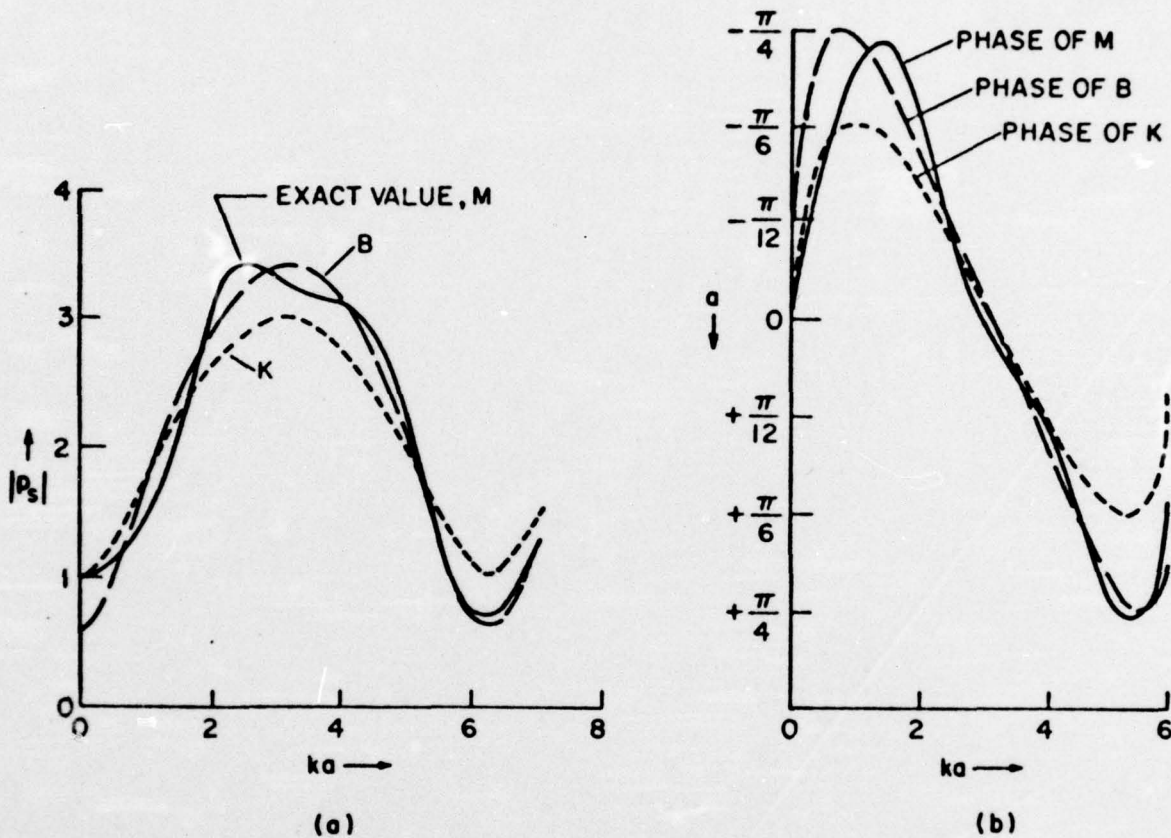
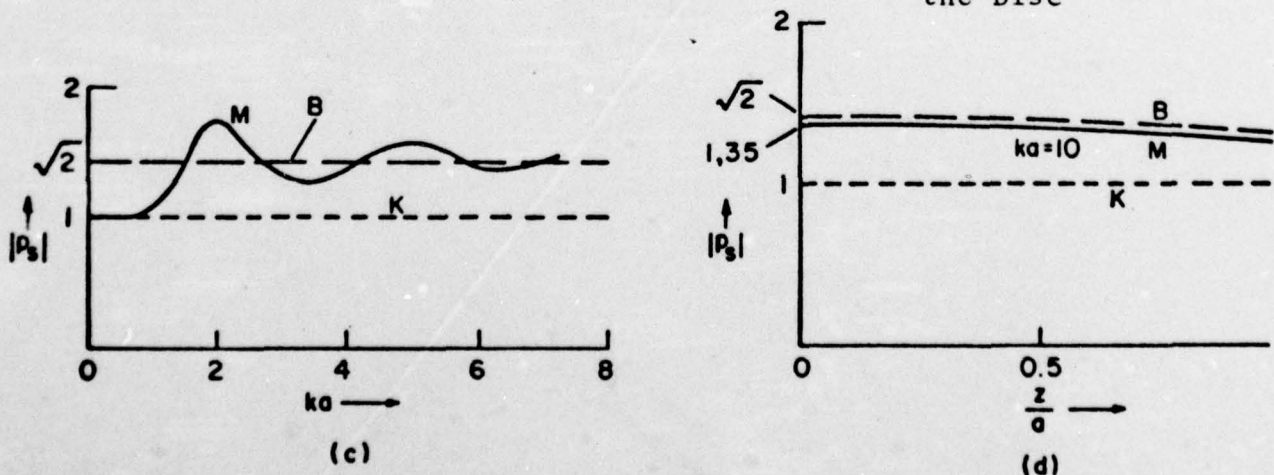


Figure 3- Scattered Pressure Field on the Surface of a Rigid Disc, Leitner
 a. Real Part, b. Imaginary Part, K refers to Kirchhoff Solution, c. Absolute Value by Leitner, approx. by Spence, experimental Data by Weiner. I and S Refer to the Illuminated and Shadow Sides of the Disc.



(a) Amplitude at Center of Illuminated Side of the Disc

(b) Phase at the Center of the Illuminated Side of the Disc



(c) Amplitude at the Center of the Disc, Shadow Side

(d) Amplitude Along Axis of the Disc, Shadow Side

Figure 4- Comparison of the Exact Solution of Meixner (M) with Approximation of Kirchoff (K) and Braunbeck (B)

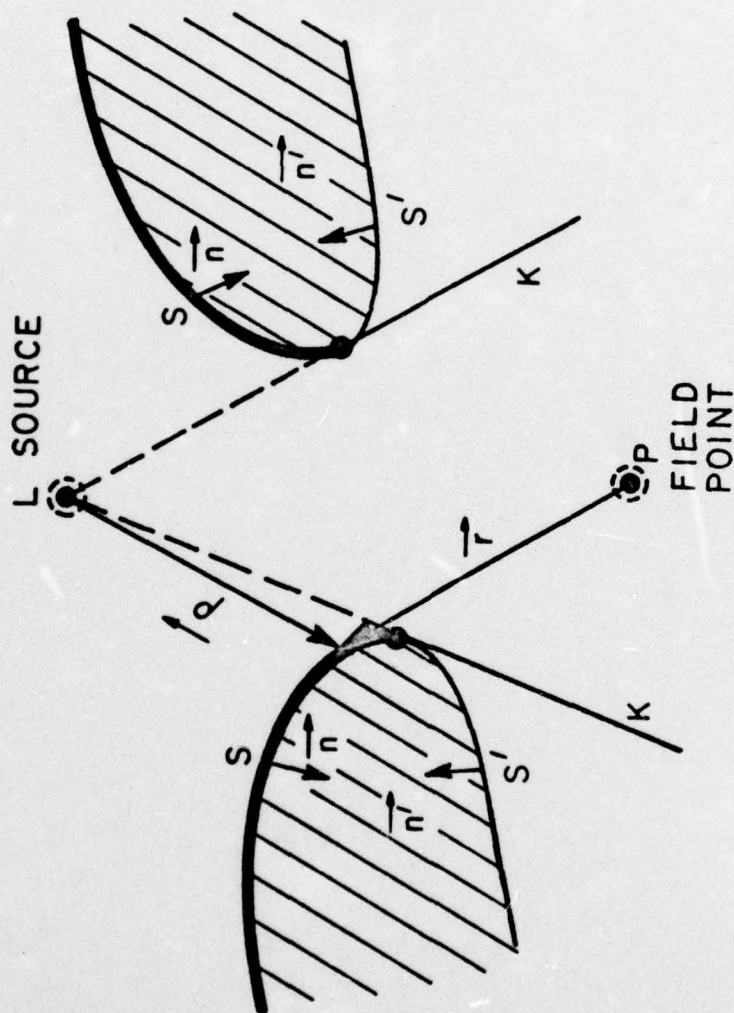


Figure 5- Diffracting Contour and the Shadow Boundary
of an Aperture

- 110 -

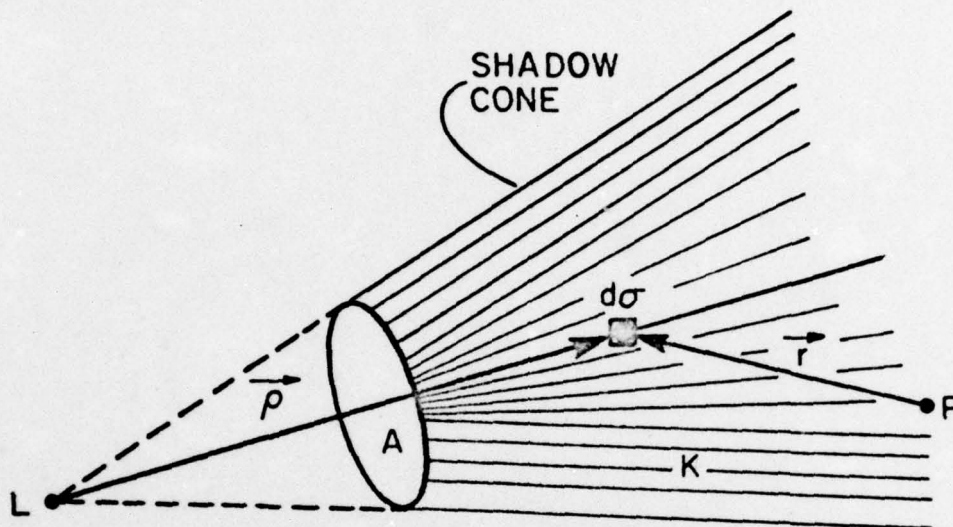


Figure 6- Integration Surface on the Shadow Cone

- 111 -

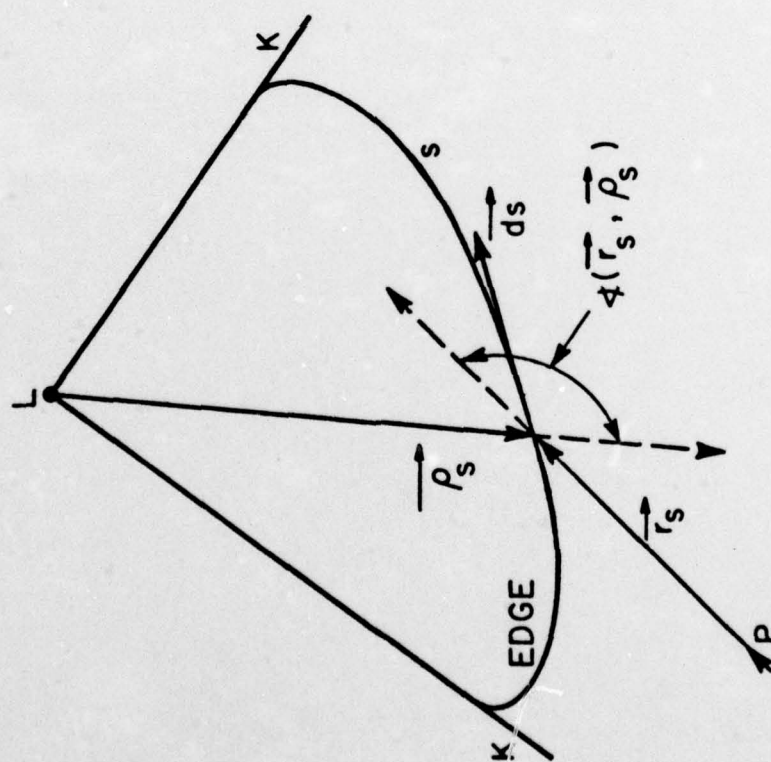
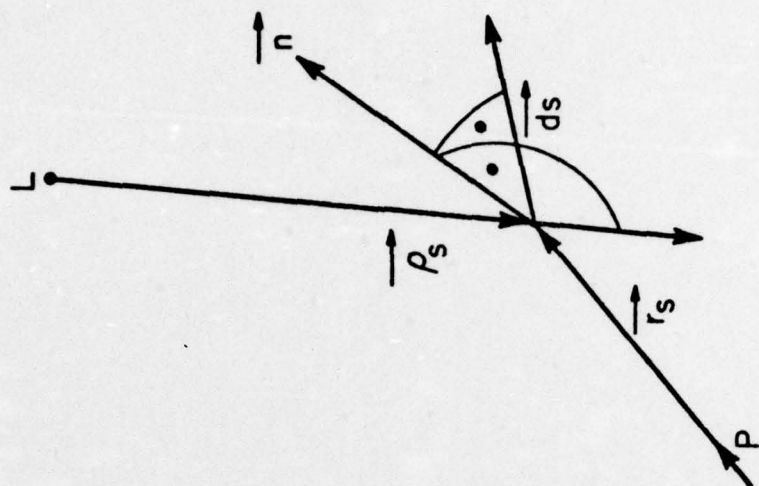


Figure 7- Coordinate System and Angles for the Rubinowicz Integral

May 14, 1973
EJS:SIH:ADS:1ms

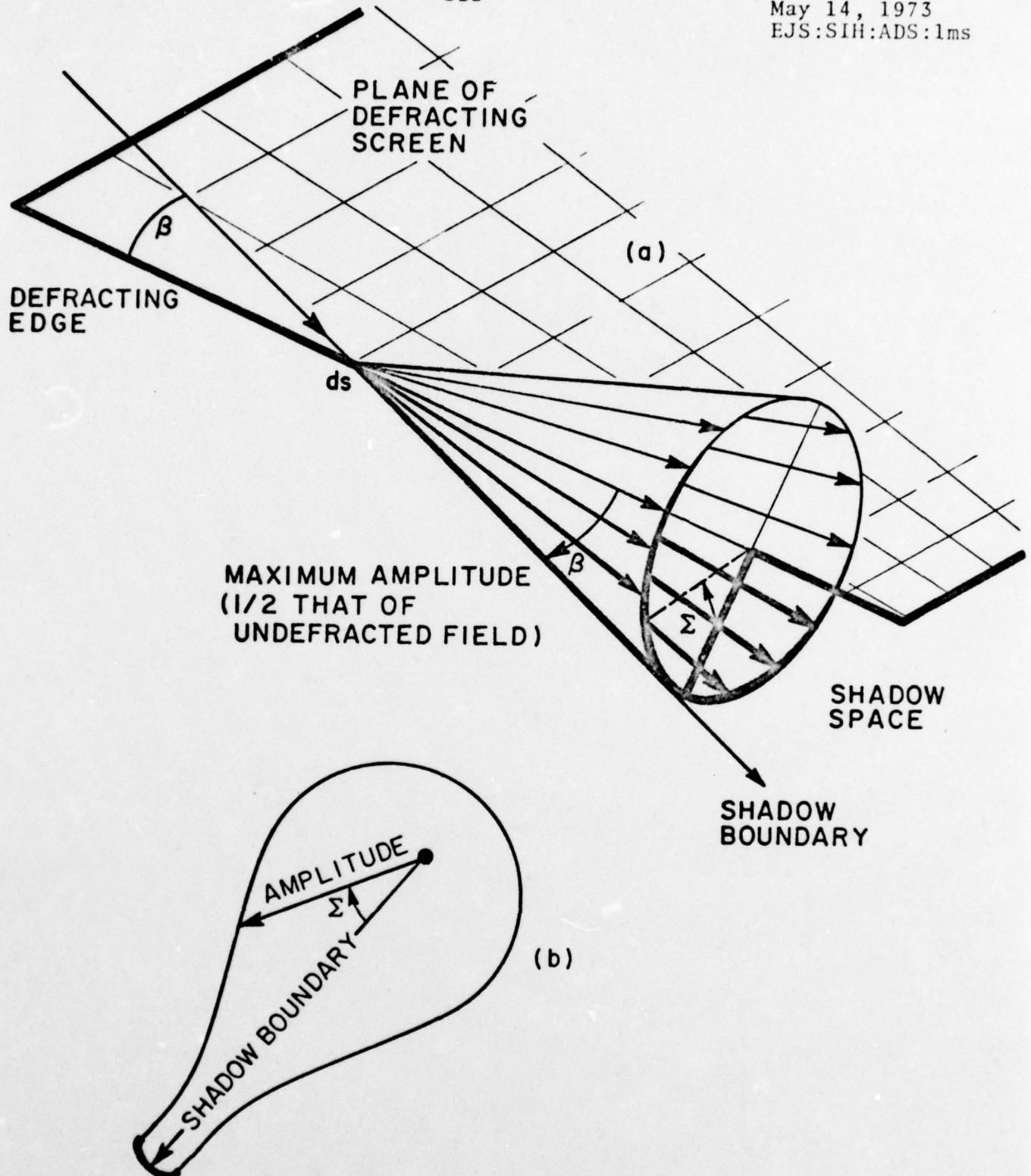


Figure 8- (a) Section through diffraction cone containing incident ray and shadow boundary. The great intensity of the diffracted amplitude near the shadow boundary is indicated by a thickening of the ellipse on the drawing.

(b) Amplitude of diffracted rays as a function of angle from shadow region.

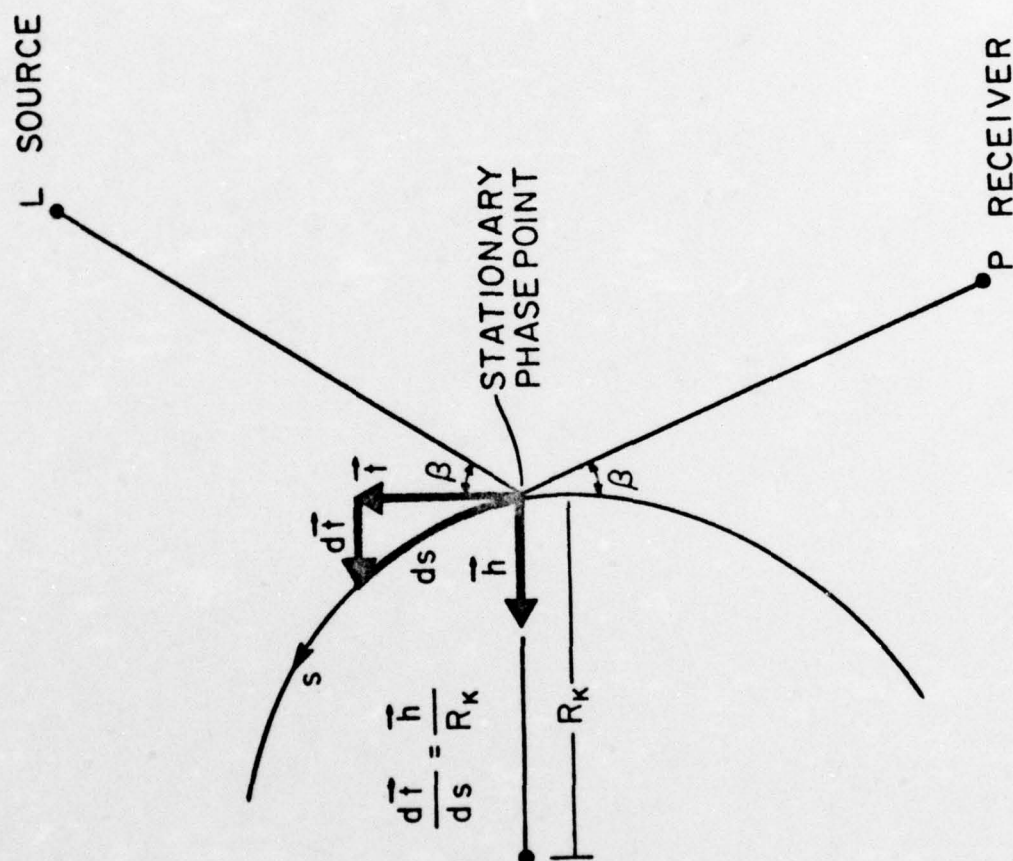


Figure 9- Unit Vectors and Angles in the Rubinowicz Solution, Equation (32)

- 114 -

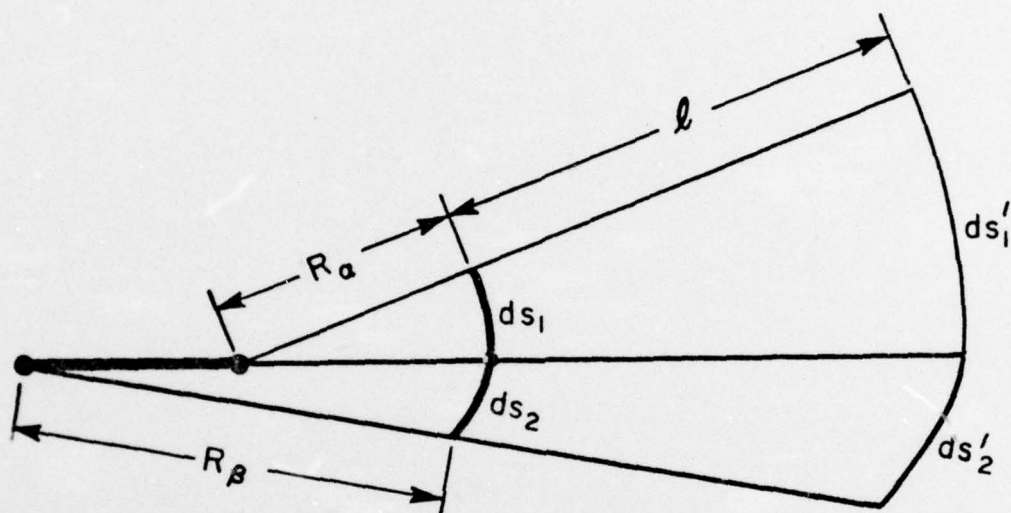


Figure 10- Cross Section of a Diffracted Bundle of Rays

- 115 -

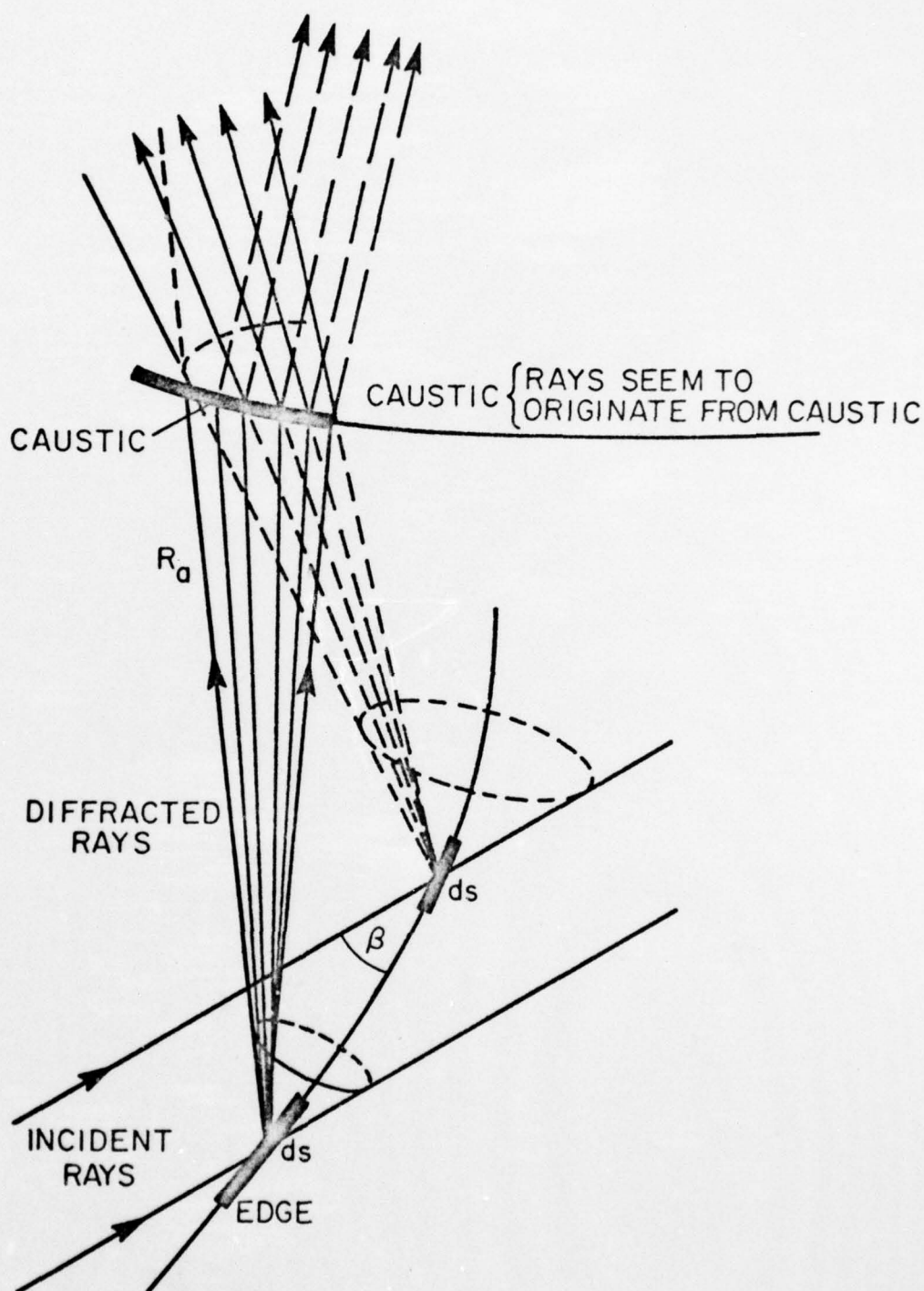


Figure 11- A pair of neighboring rays incident on a curved edge of a flat screen, and resulting diffracted cones. The two cones of diffracted rays intersect at the caustic, which is at the distance R_d from the edge along one of the diffracted rays.

- 116 -

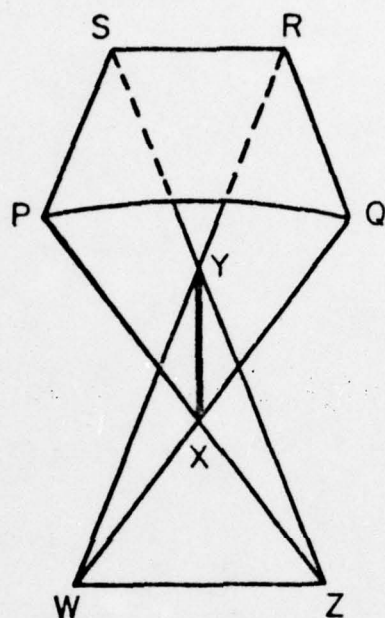


Figure 12- The focal lines of a pencil. A portion of the axis of rotation and a surface of revolution whose meridian section is the evolute of the meridian section of the wavefront. (D. S. Jones, The Theory of Electromagnetism, Page 375).

- 117 -

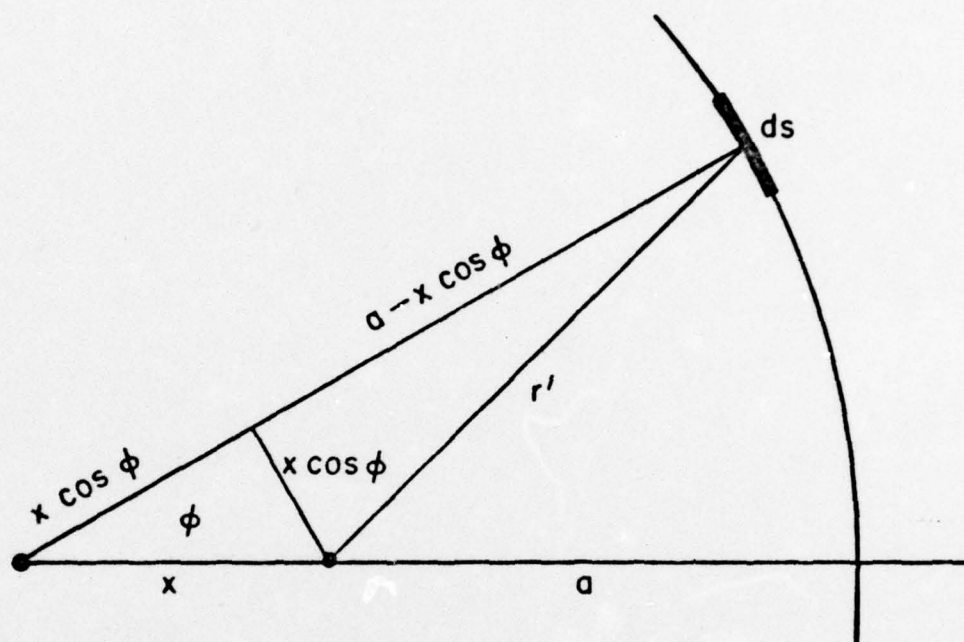
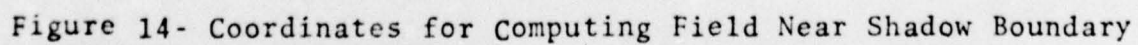


Figure 13- Coordinates for the Diffraction from the Arc of a Circular Edge of Radius a



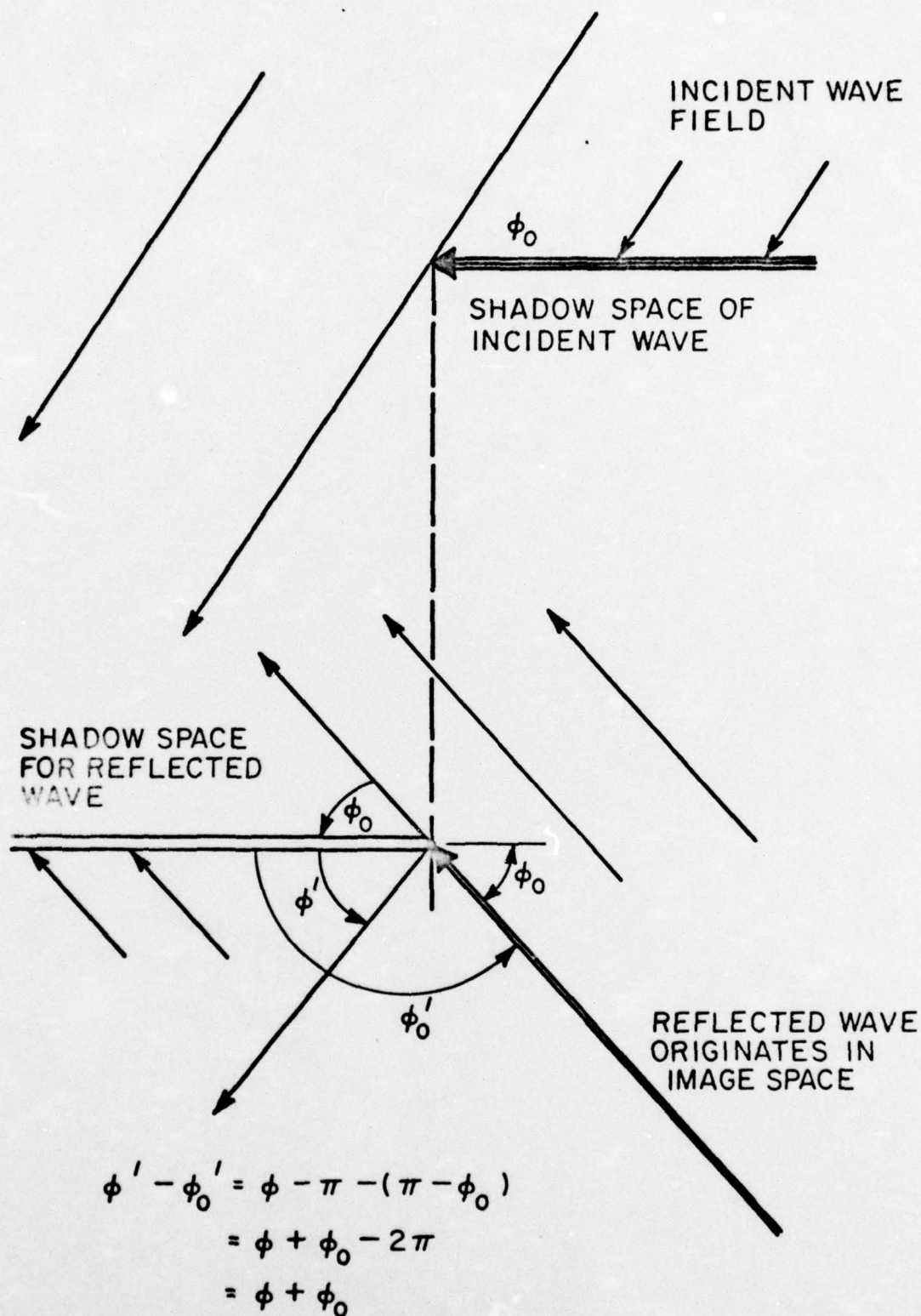


Figure 15- Shadow Boundaries of Incident and Reflected (Image Space) Waves

- 120 -

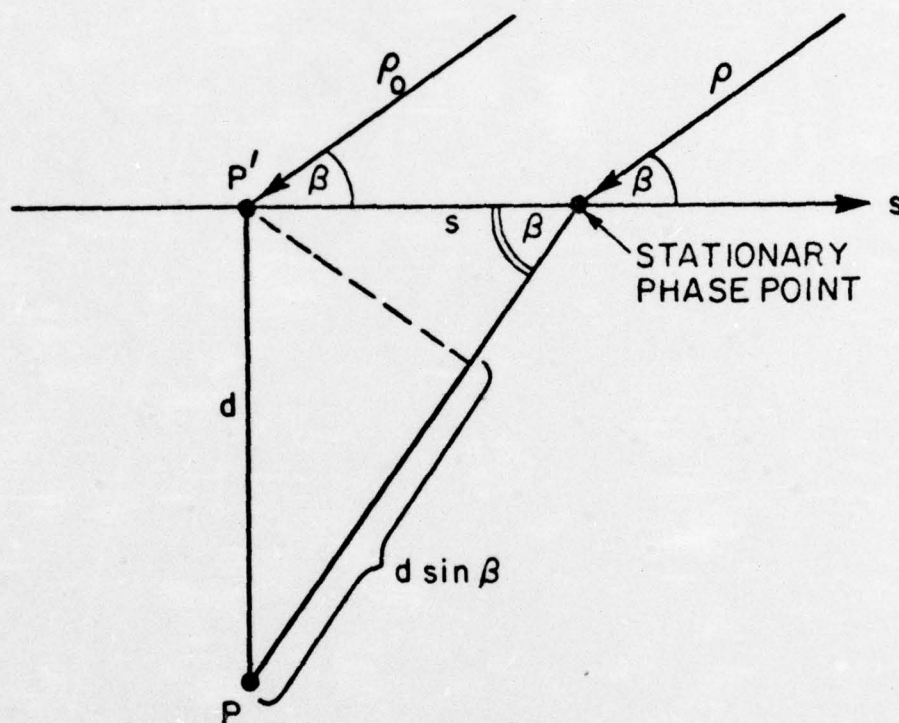


Figure 16- Coordinates used for Determining Stationary Phase Point
for a Plane Wave Incident on a Straight Edge

May 14, 1973
 EJS:SIH:ADS:ims

- 121 -

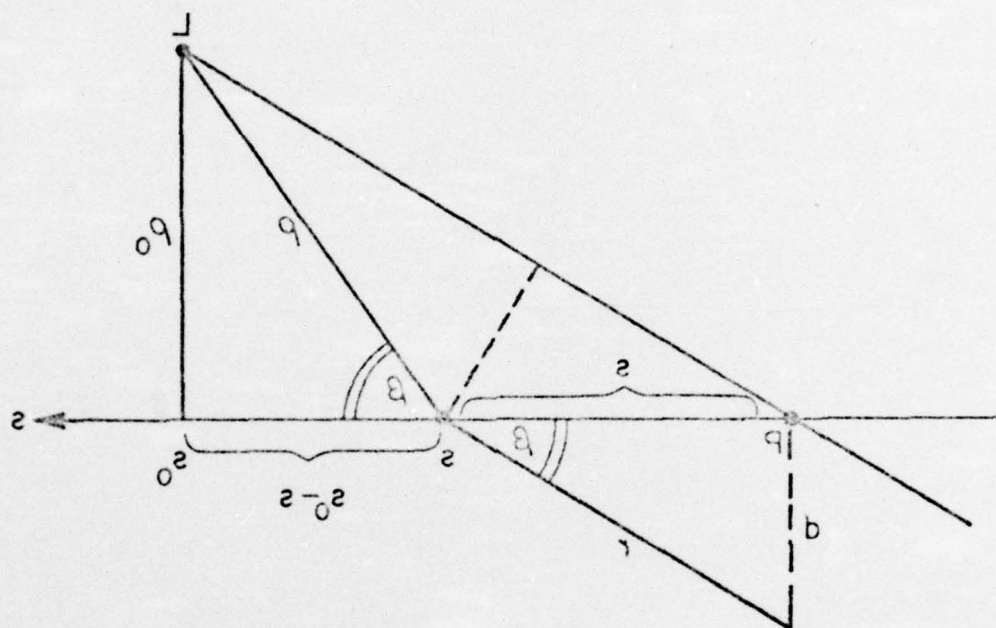


Figure 17- Coordinates used for Determining Stationary Phase Point
 for a Spherical Wave Incident on a Straight Edge

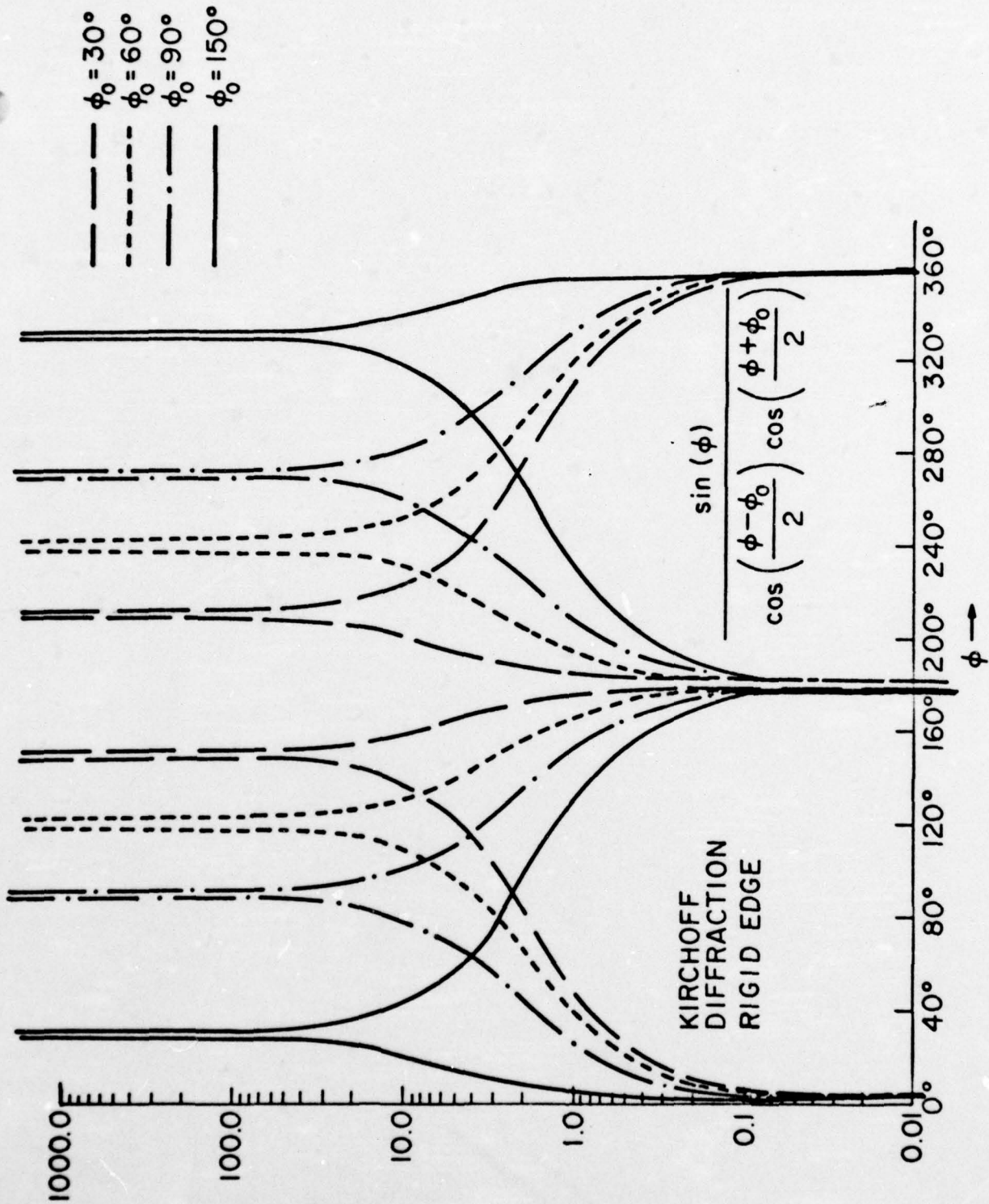


Figure 18- Kirchhoff Solution for the Diffraction from a Rigid Edge, for Various Angles of Incidence ϕ_0

- 123 -

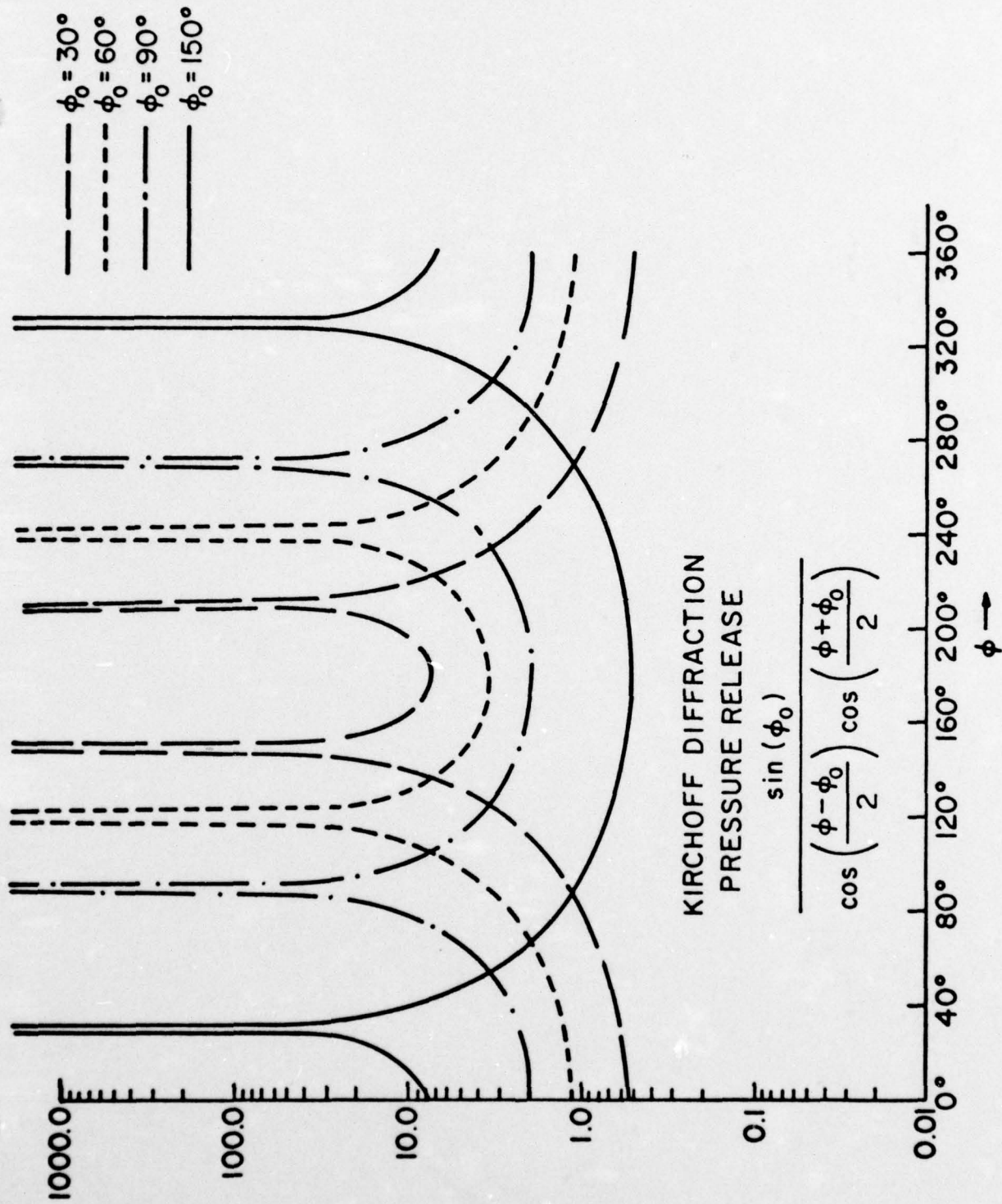


Figure 19- Kirchhoff Solution for the Diffraction from a Pressure Release Edge, for Various Angles of Incidence ϕ_0

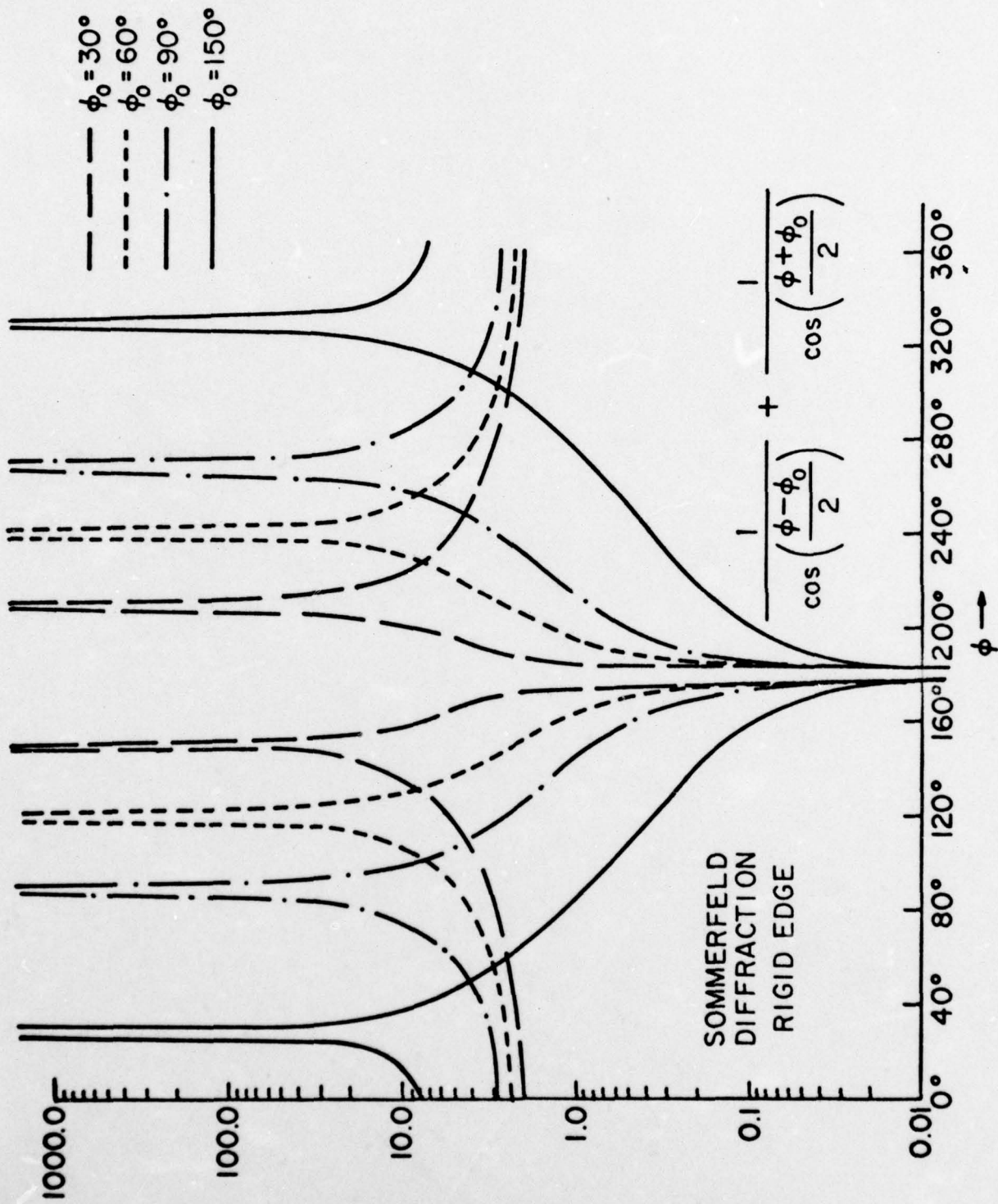


Figure 20- Sommerfeld (Exact) Solution for the Diffraction from Rigid Edge, for Various Angles of Incidence ϕ_0

- 125 -

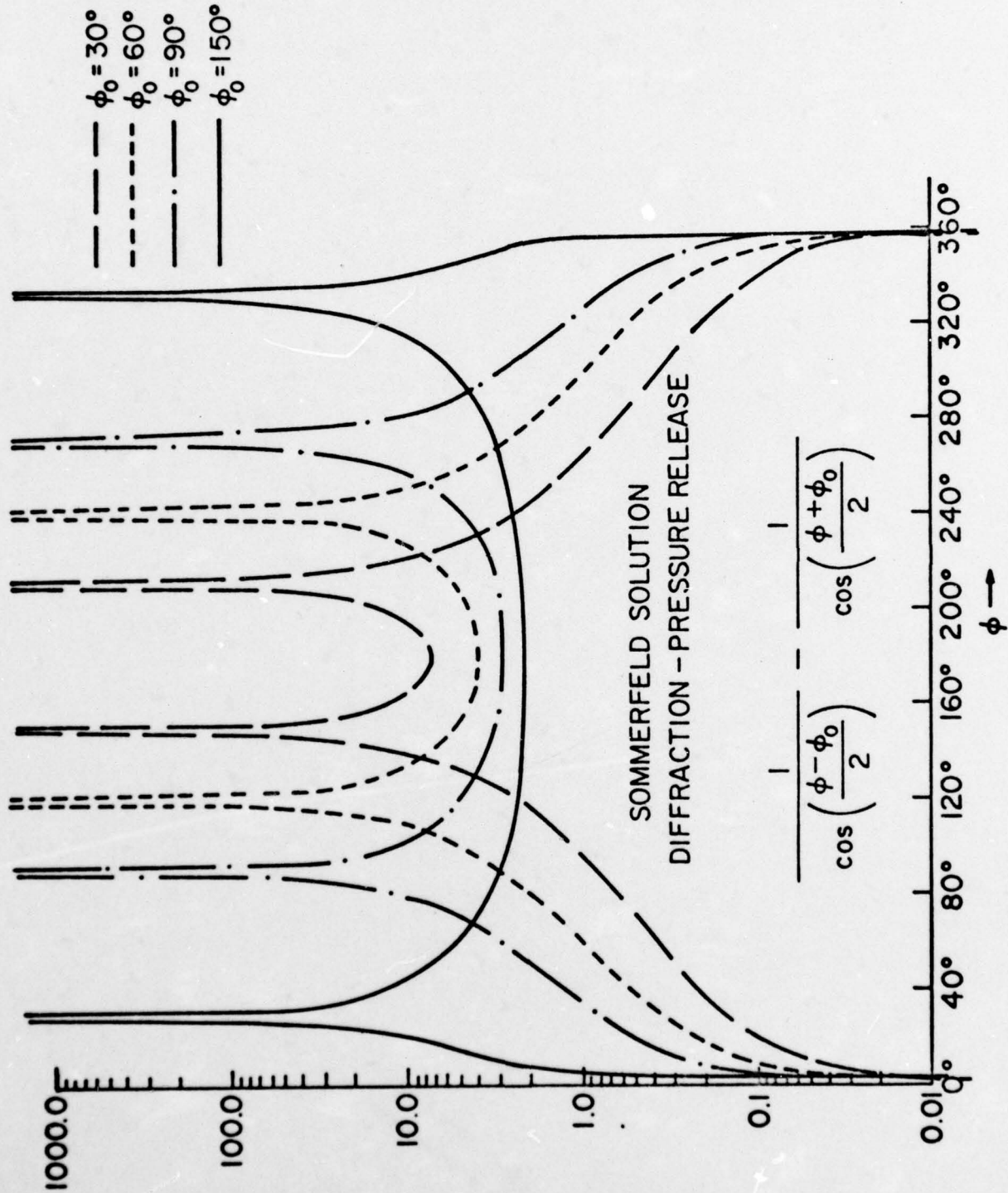


Figure 21- Sommerfeld (Exact) Solution for the Diffraction from a Pressure Release Edge, for Various Angles of Incidence ϕ_0

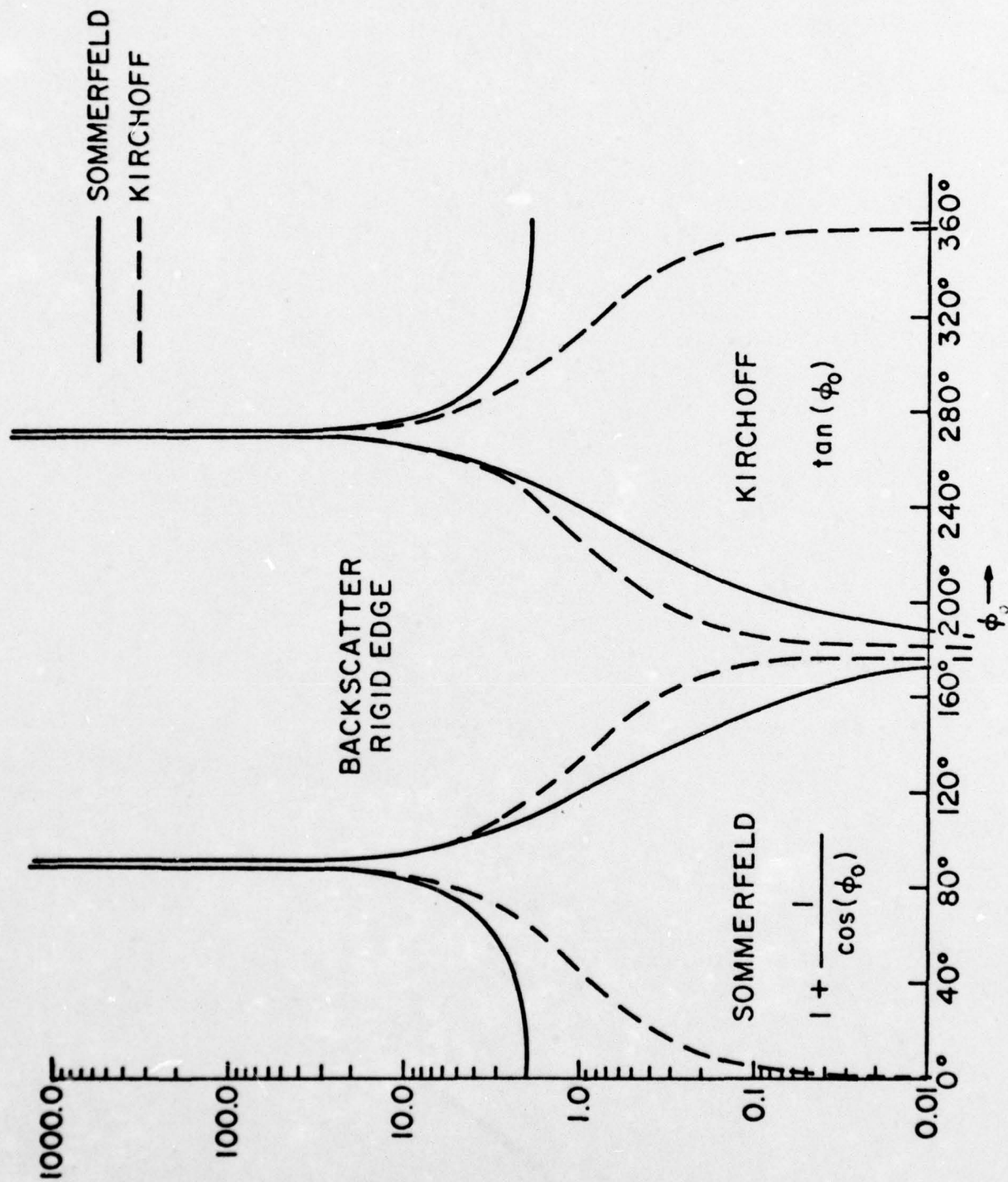


Figure 22- Backscattered Field of Rigid Edge, Sommerfeld and Kirchhoff Solutions

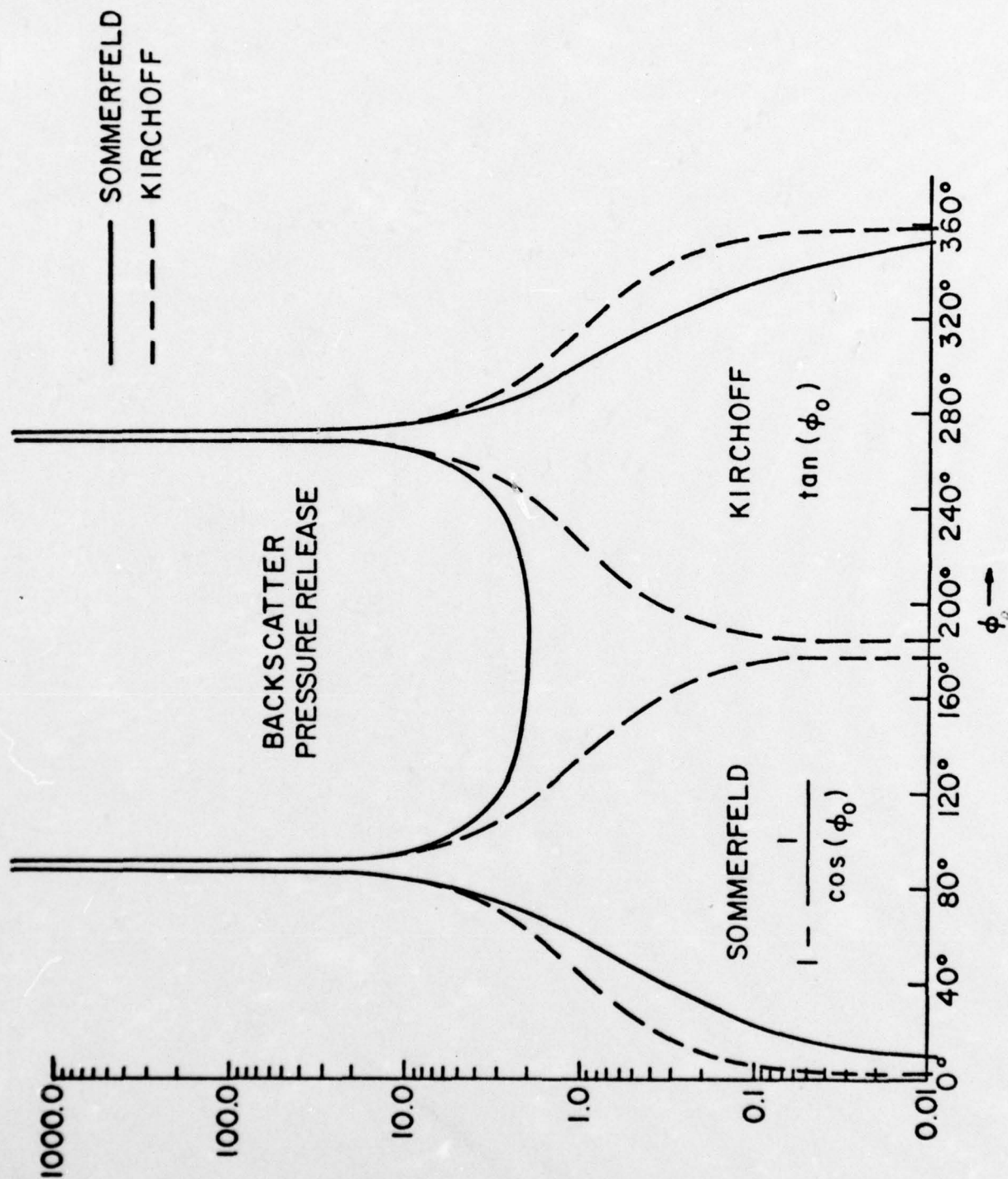


Figure 23- Backscattered Field of a Pressure Release Edge, Sommerfeld and Kirchhoff Solutions

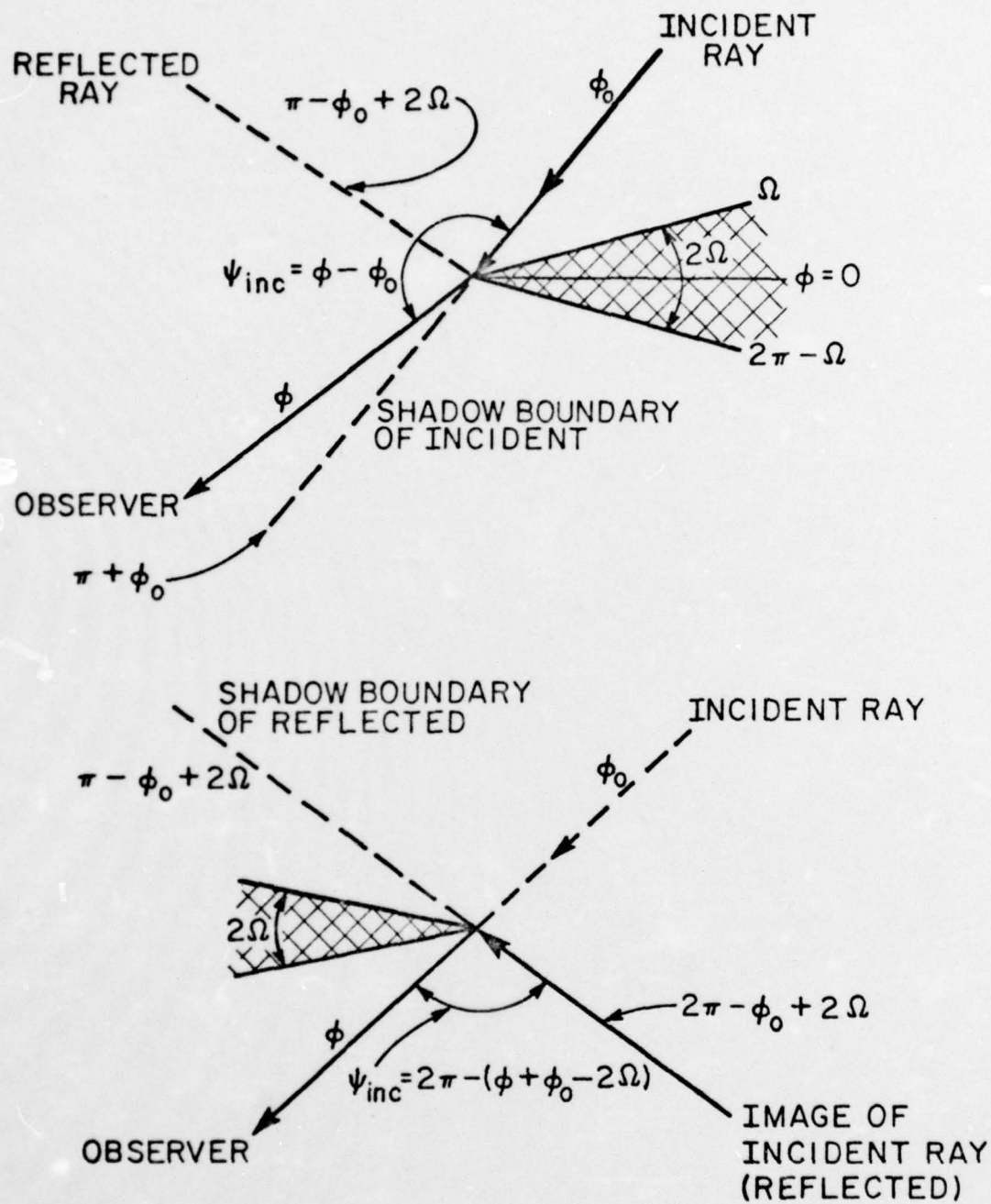


Figure 24- Shadow Boundaries of Incident and Reflected (Image Space) Waves for a Wedge Angle 2Ω

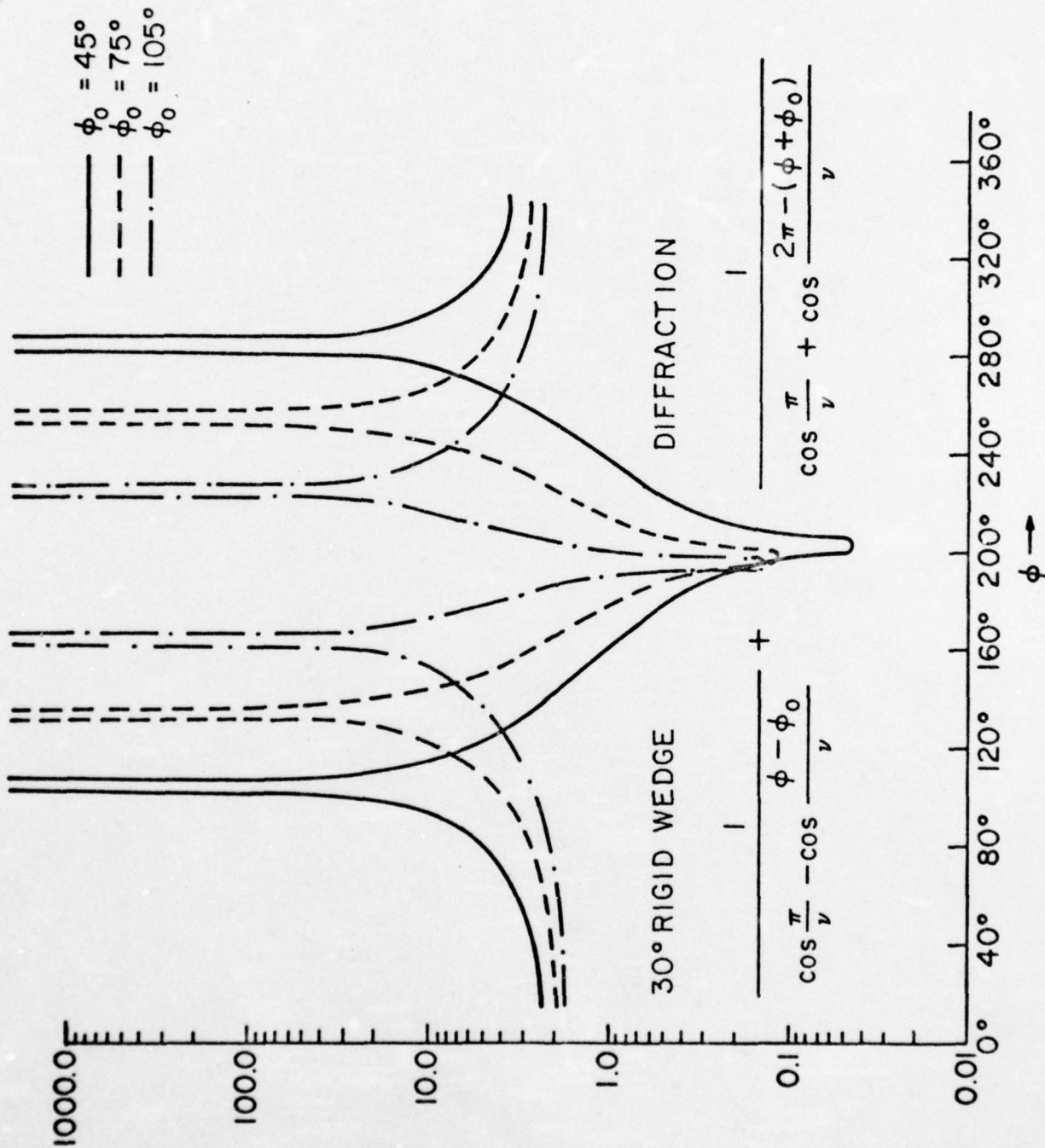


Figure 25- Diffraction from a 30° Rigid Wedge for Various Angles of Incidence ϕ_0

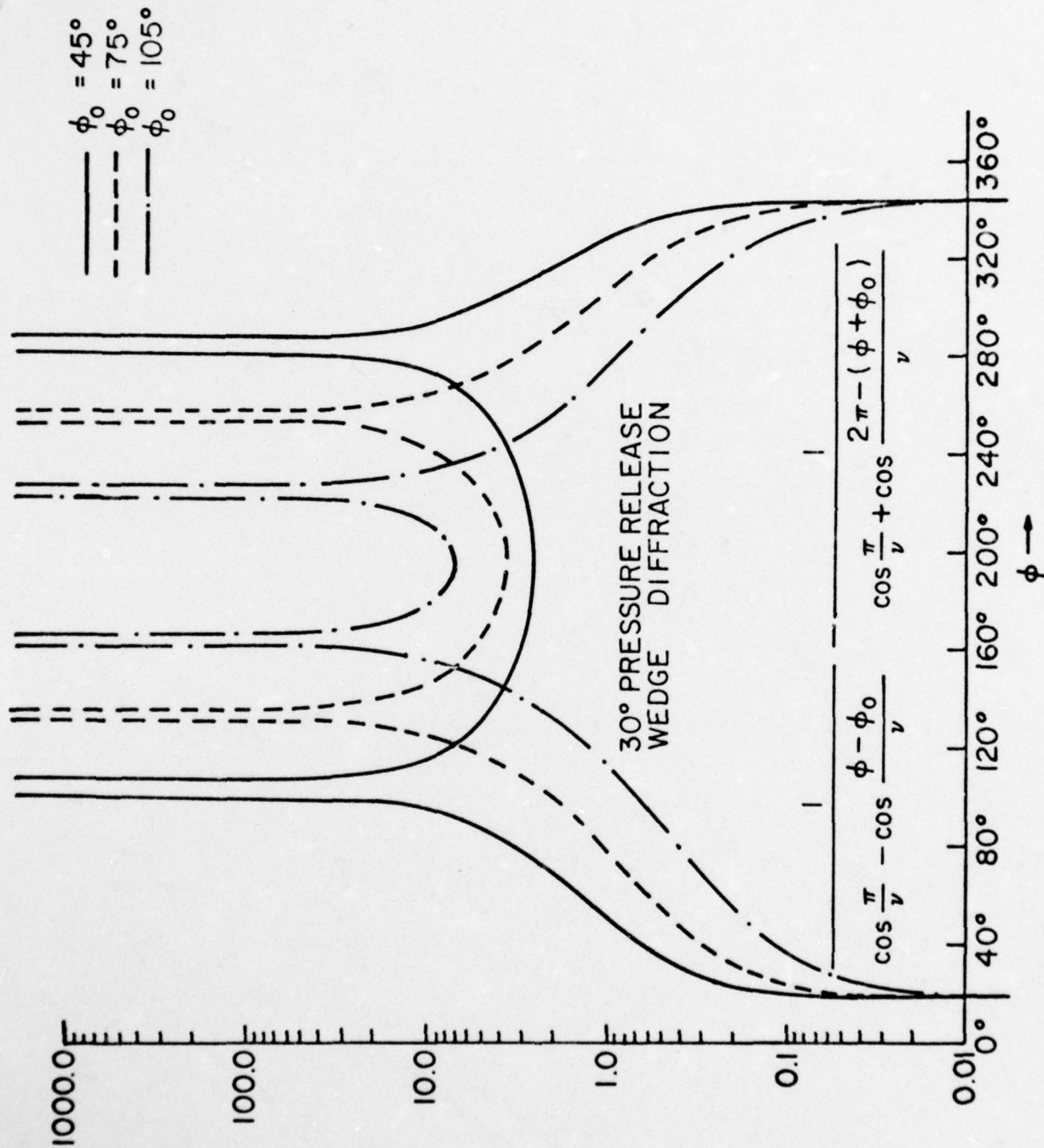


Figure 26- Diffraction from a 30° Pressure Release Wedge, for Various Angles of Incidence ϕ_0

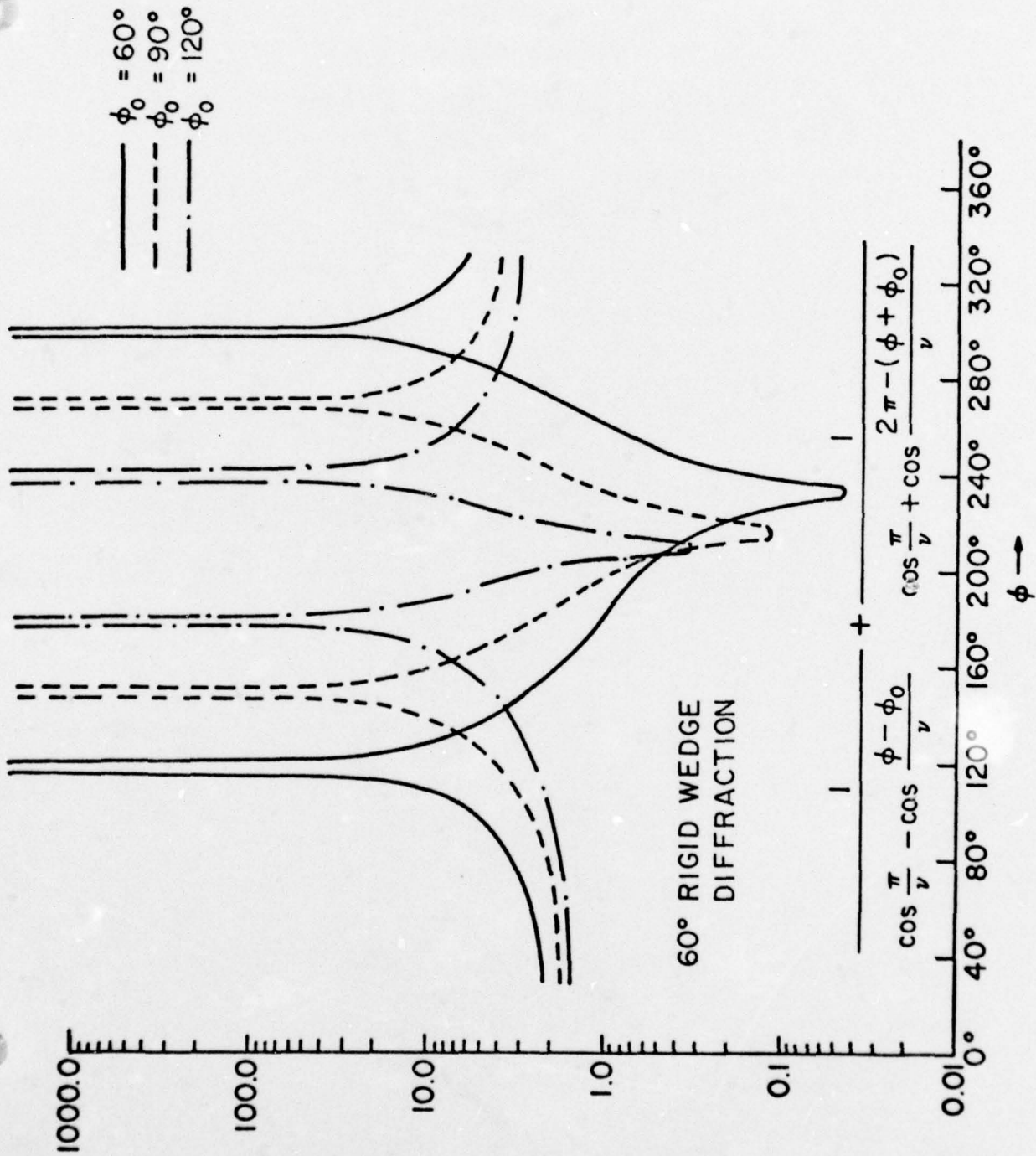


Figure 27- Diffraction from a 60° Rigid Wedge for Various Angles of Incidence ϕ_0

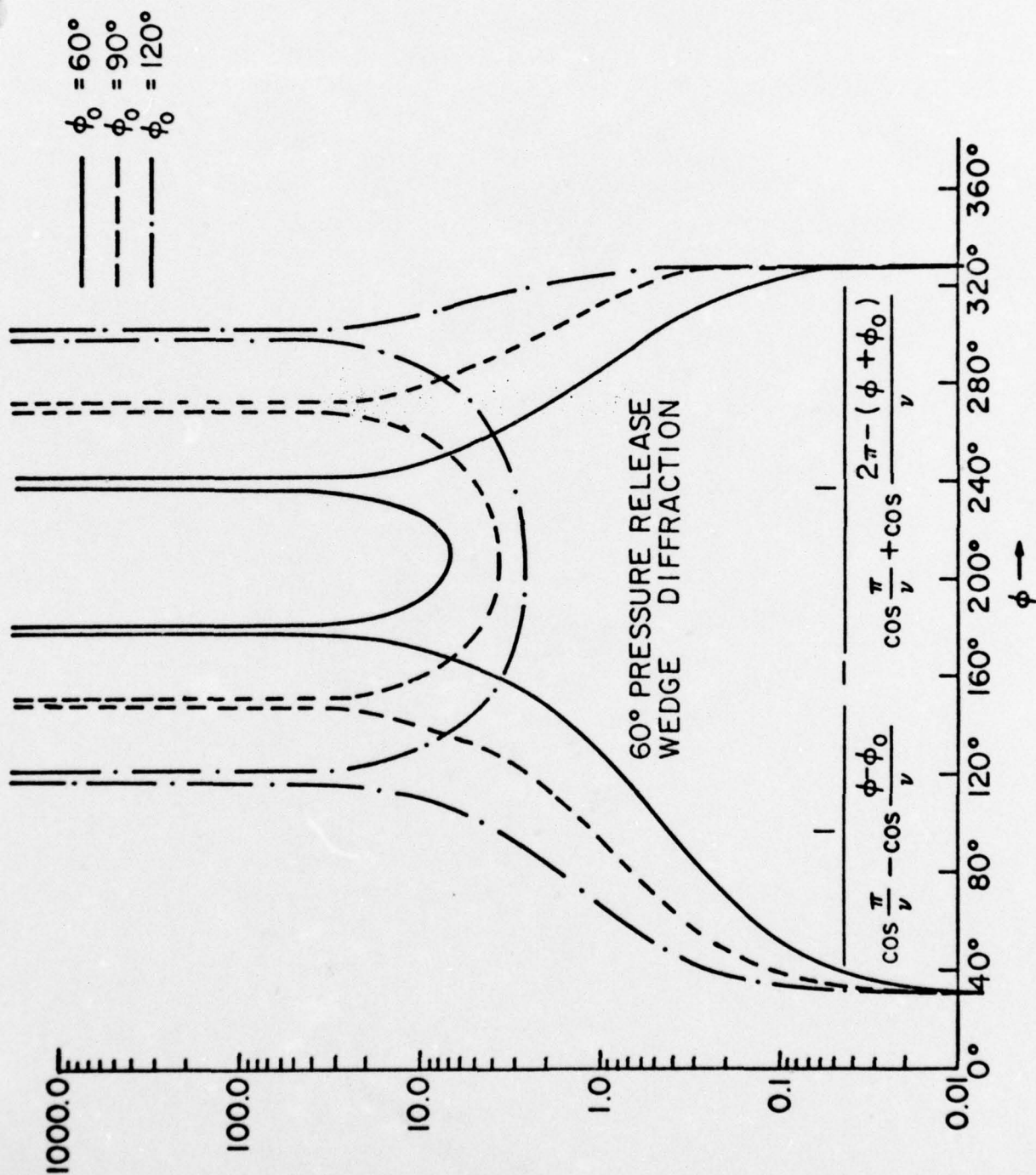


Figure 28- Diffraction from a 60° Pressure Release Wedge, for Various Angles of Incidence ϕ_0

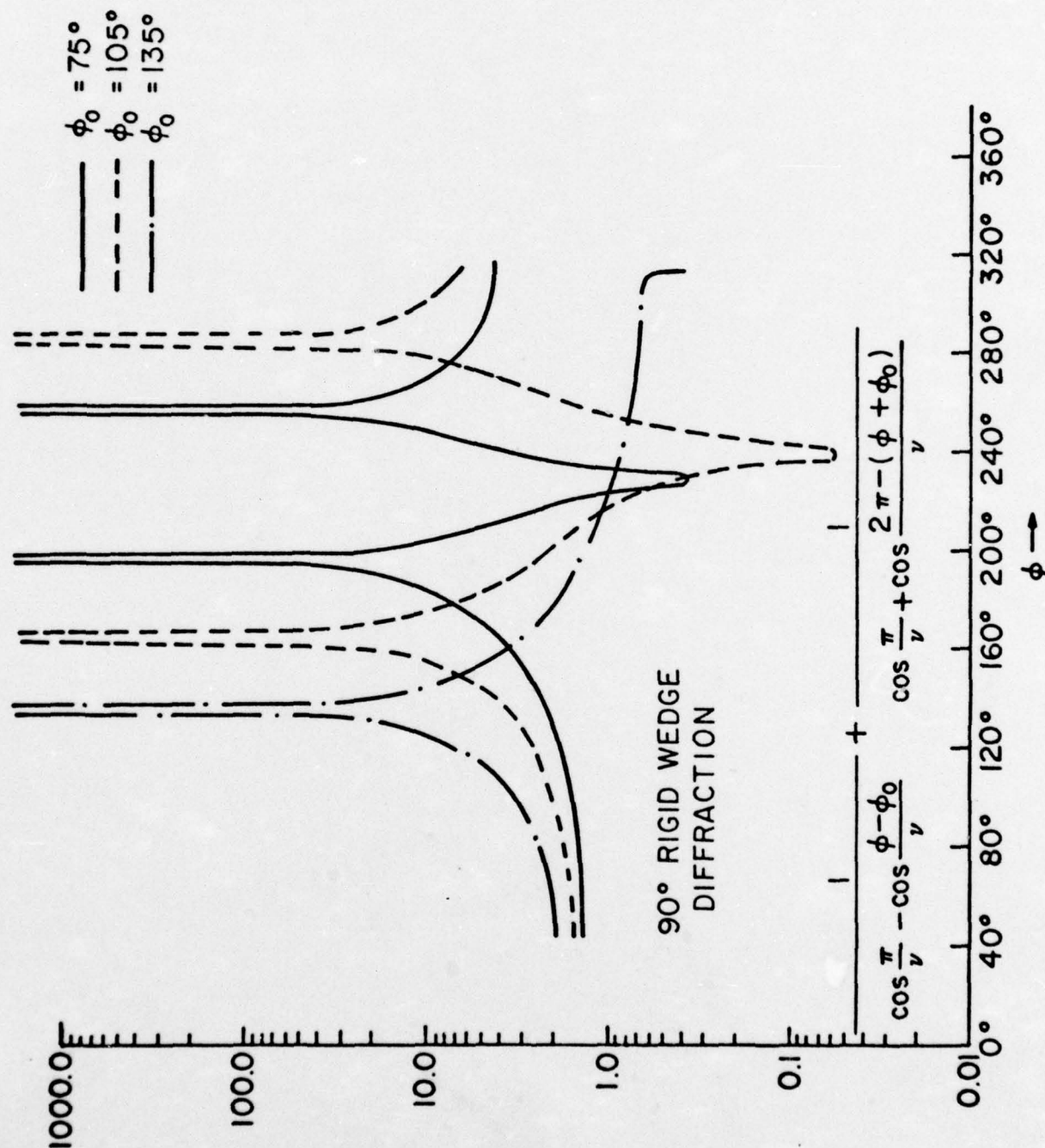


Figure 29- Diffraction from a 90° Rigid Wedge for Various Angles of Incidence ϕ_0

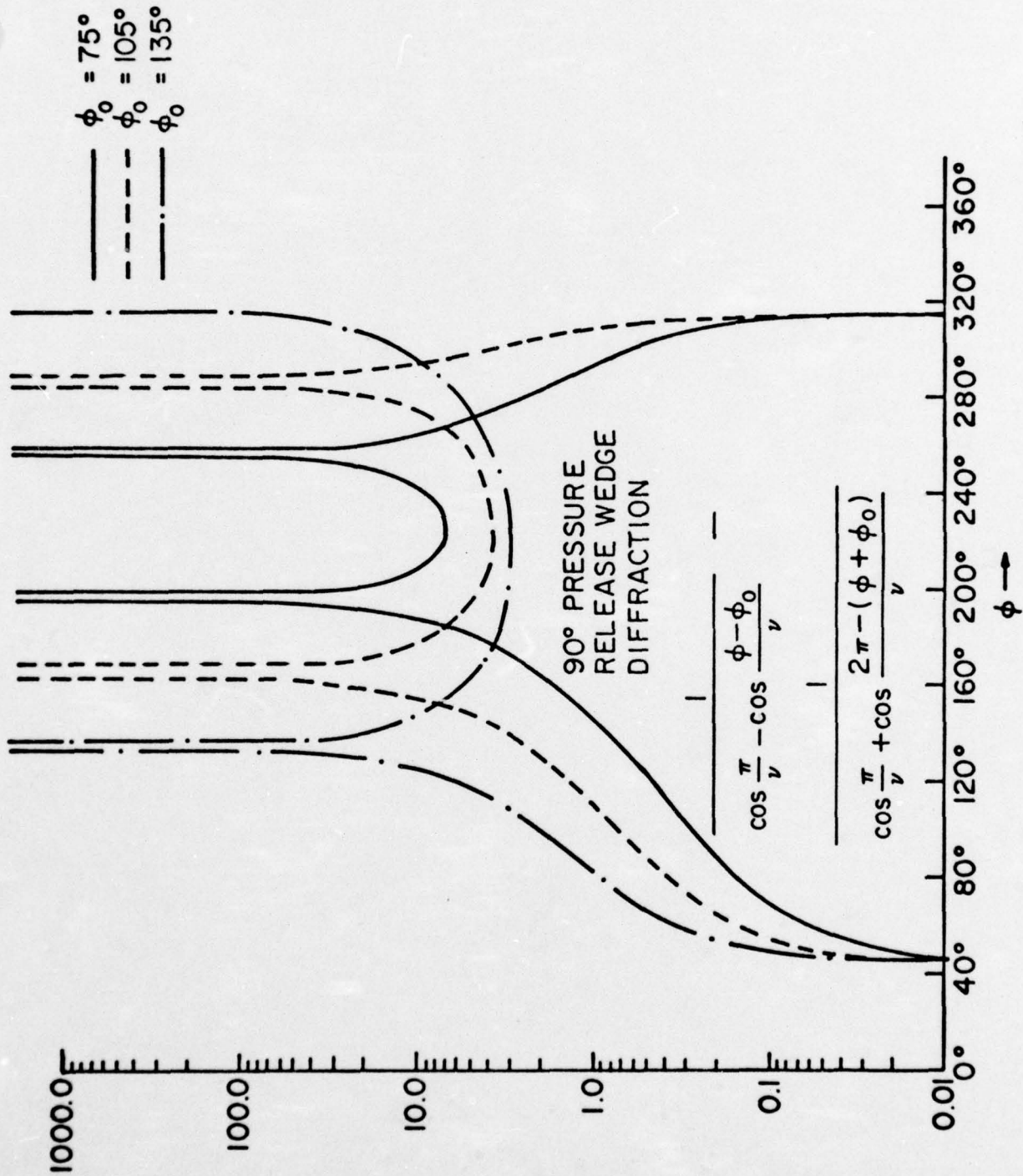


Figure 30- Diffraction from a 90° Pressure Release Wedge, for Various Angles of Incidence ϕ_0

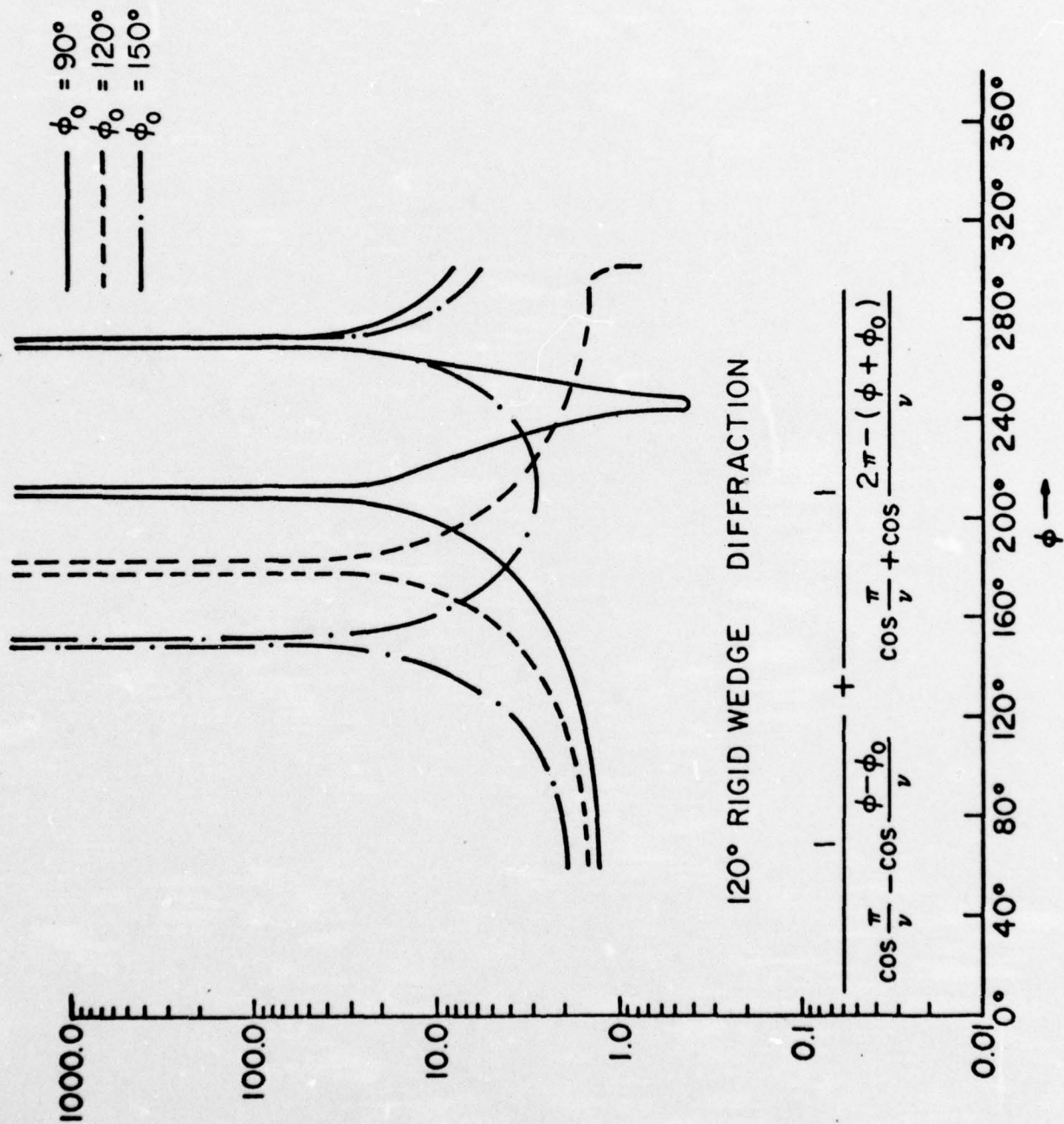


Figure 31- Diffraction from a 120° Rigid Wedge for various Angles of Incidence ϕ_0

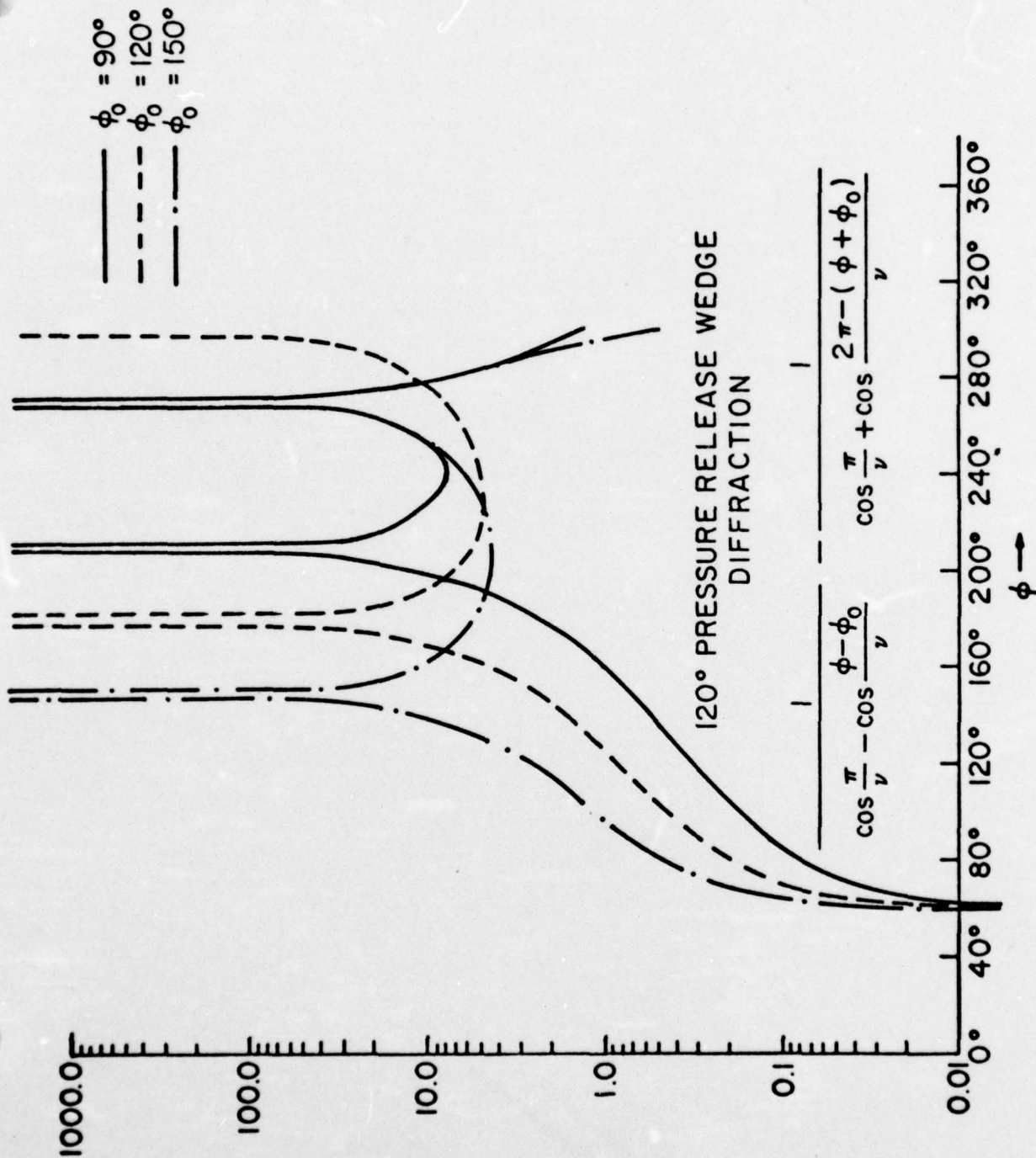


Figure 32- Diffraction from a 120° Pressure Release Wedge, for Various Angles of Incidence ϕ_0

- 137 -

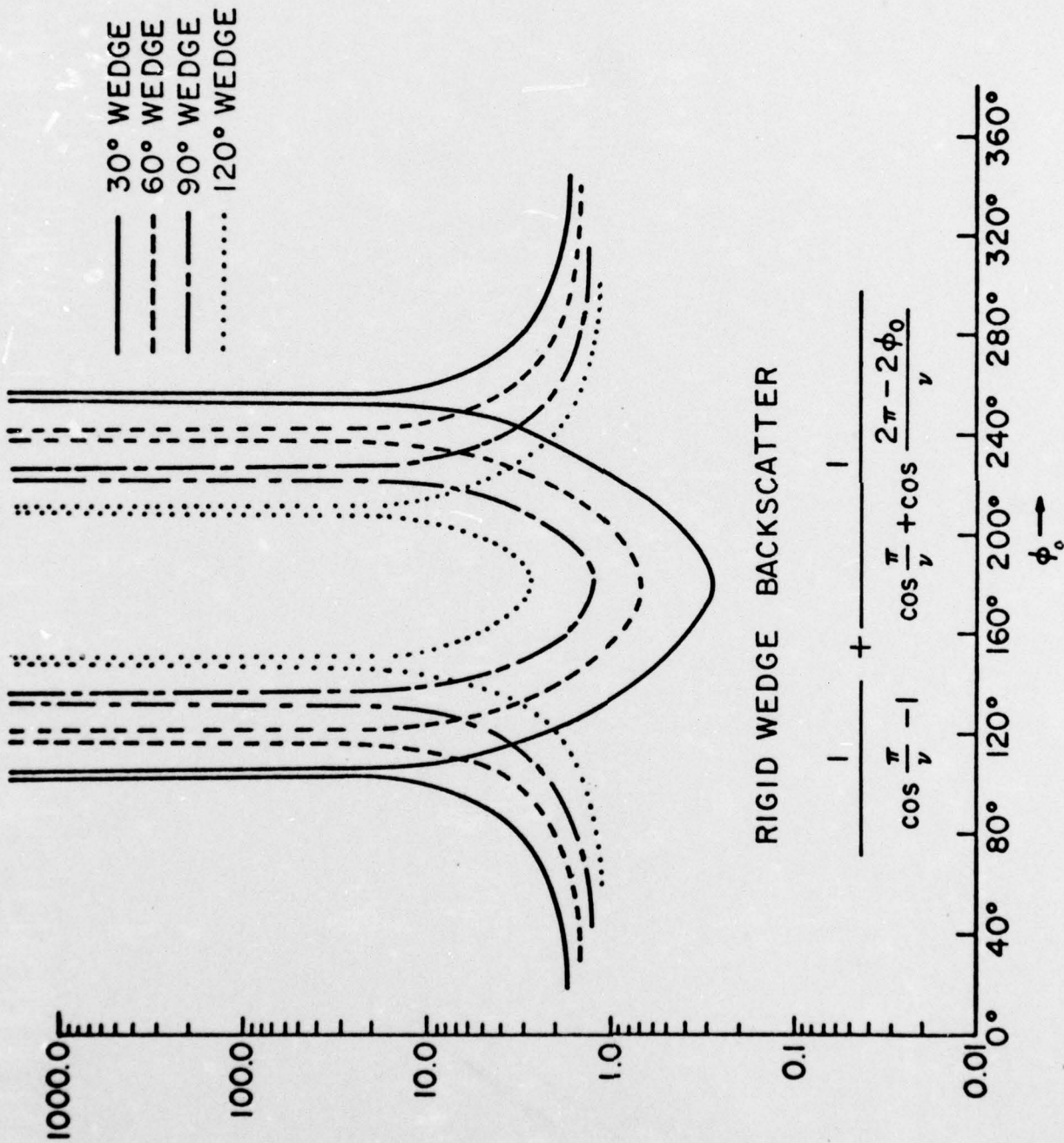


Figure 33- Backscattering from Rigid Wedges, Wedge Angles $2\Omega = 30^\circ, 60^\circ, 90^\circ$ and 120°

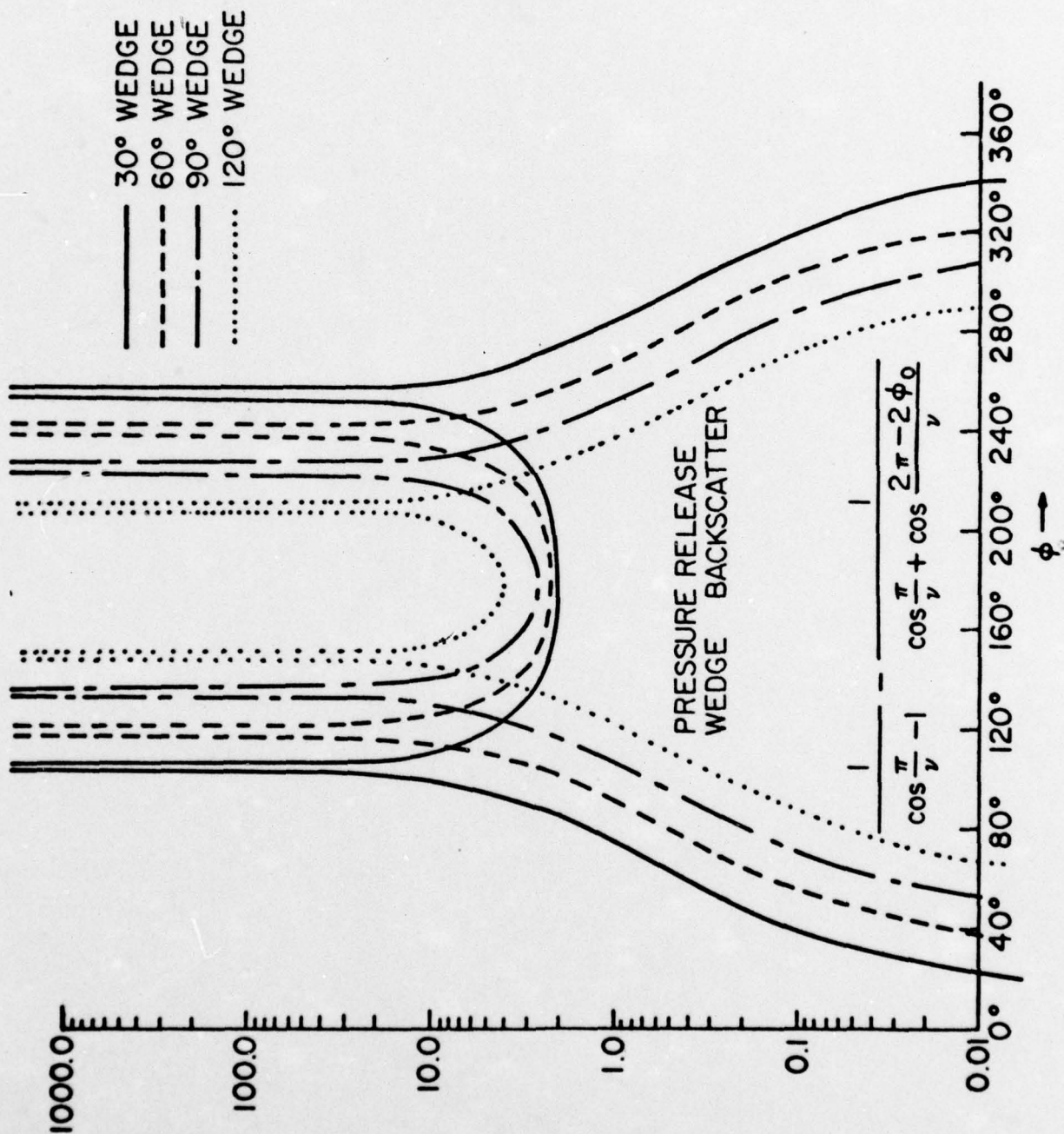


Figure 34- Backscattering from Pressure Release Wedges, Wedge Angles $2\Omega = 30^\circ, 60^\circ, 90^\circ$ and 120°

May 14, 1973
EJS:SIH:ADS:1ms

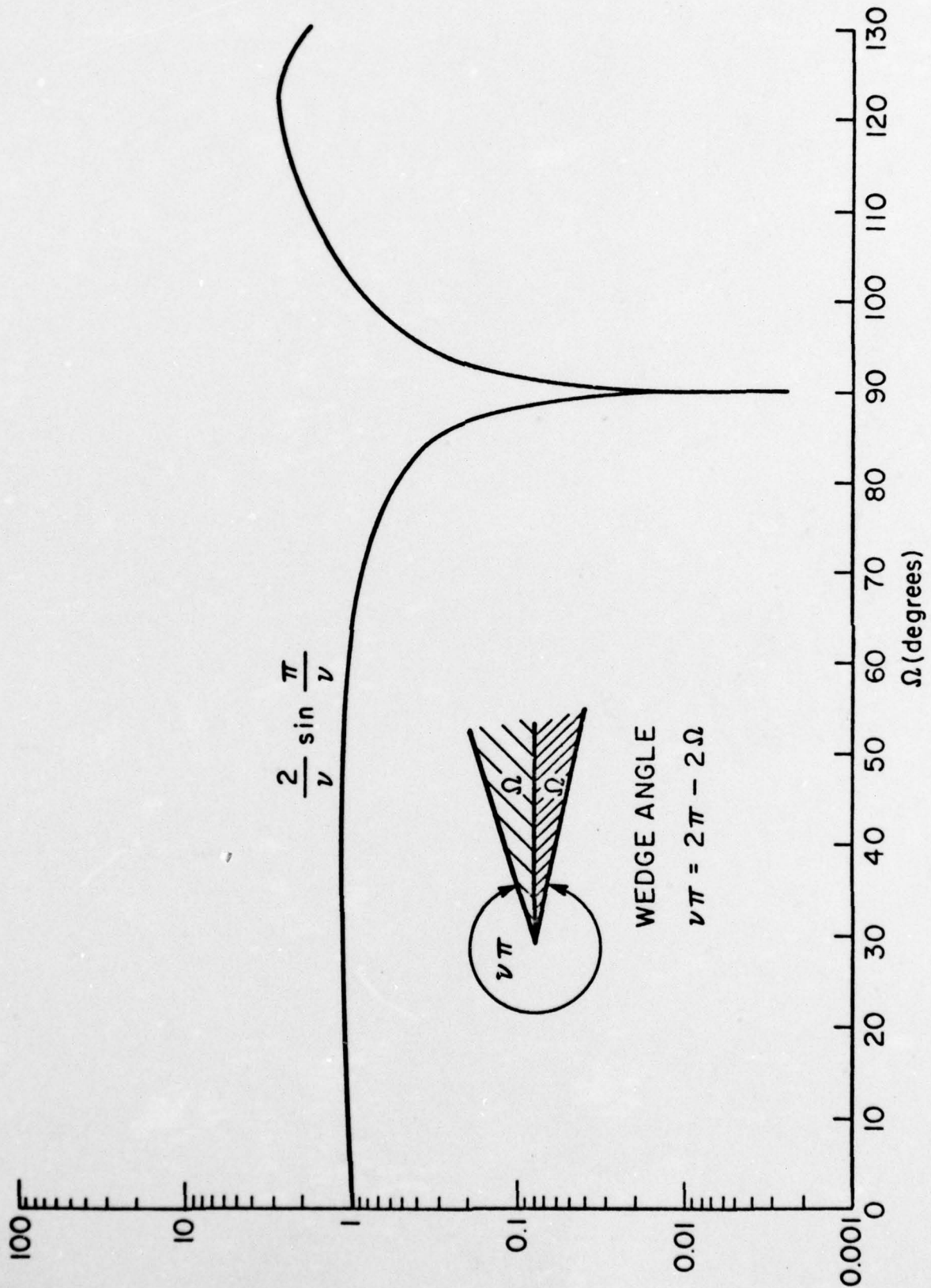


Figure 35- Discontinuity Factor for Wedge

- 140 -

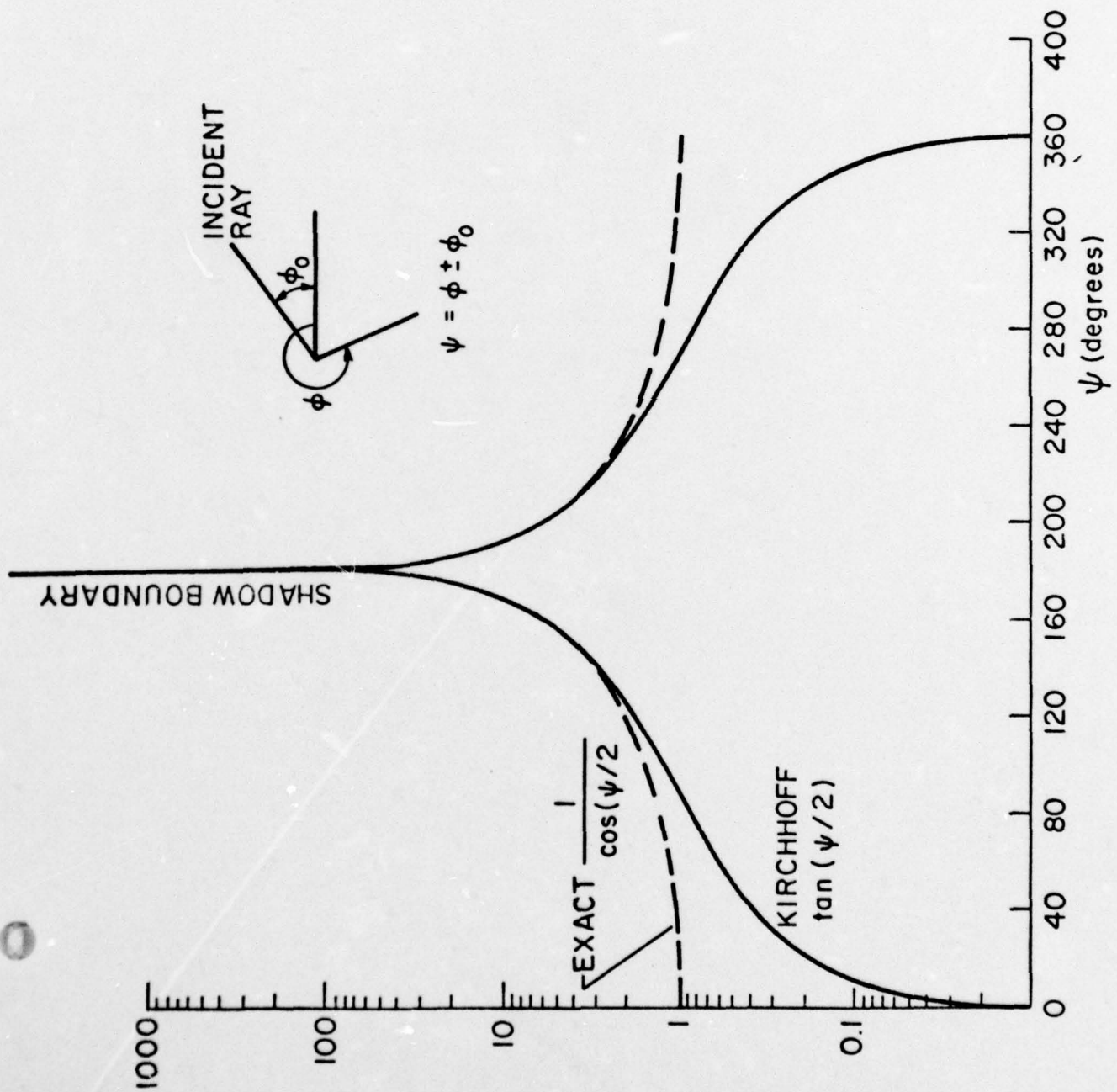


Figure 36- Comparison of the Kirchhoff and Sommerfeld Solutions of the Diffraction from a Straight Edge for an Incident Wave Only.

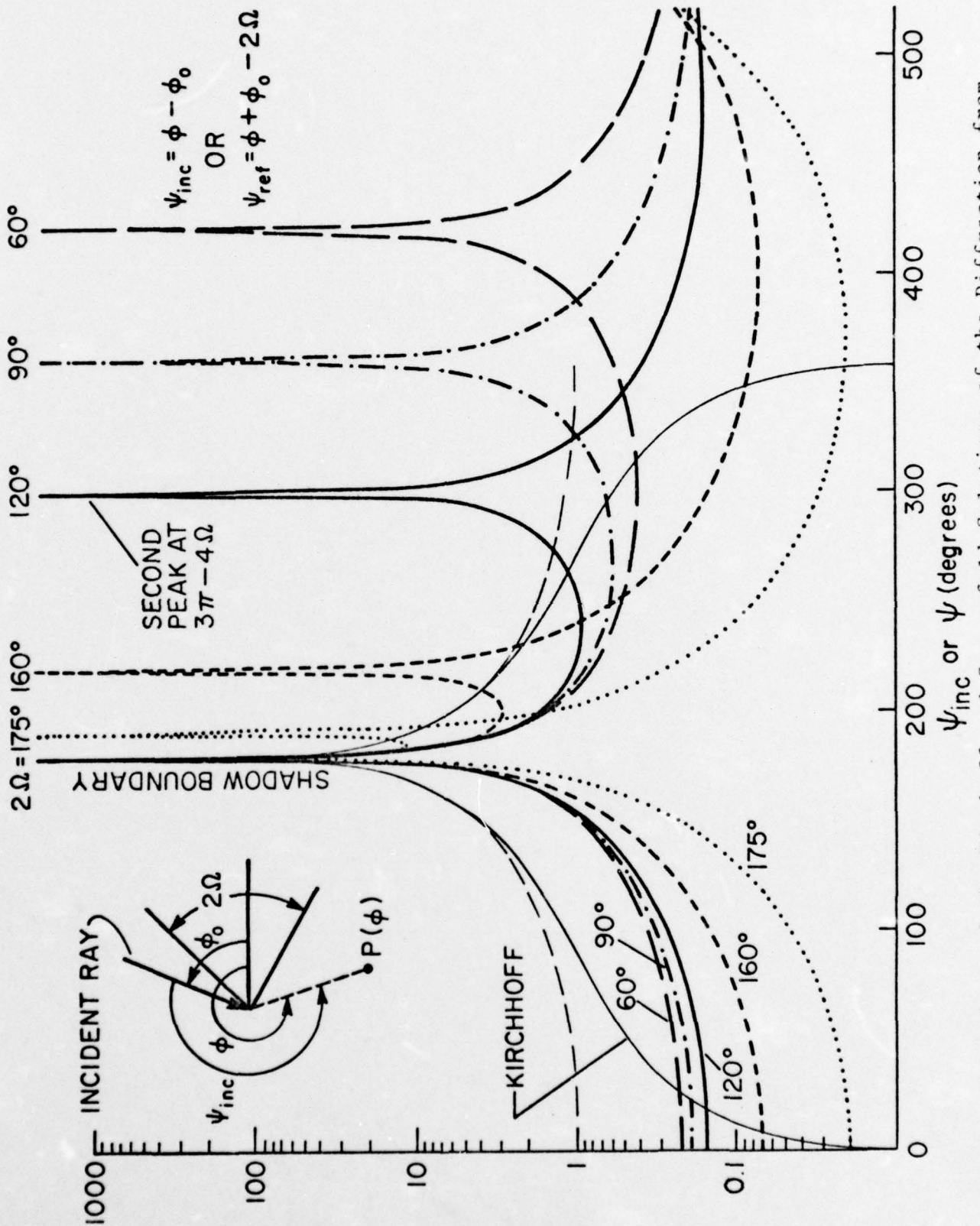


Figure 37- Comparison of the Kirchhoff and Sommerfeld Solutions of the Diffraction from Wedges of Various Wedge-Angles 2Ω for Incident Wave Only

- 142 -

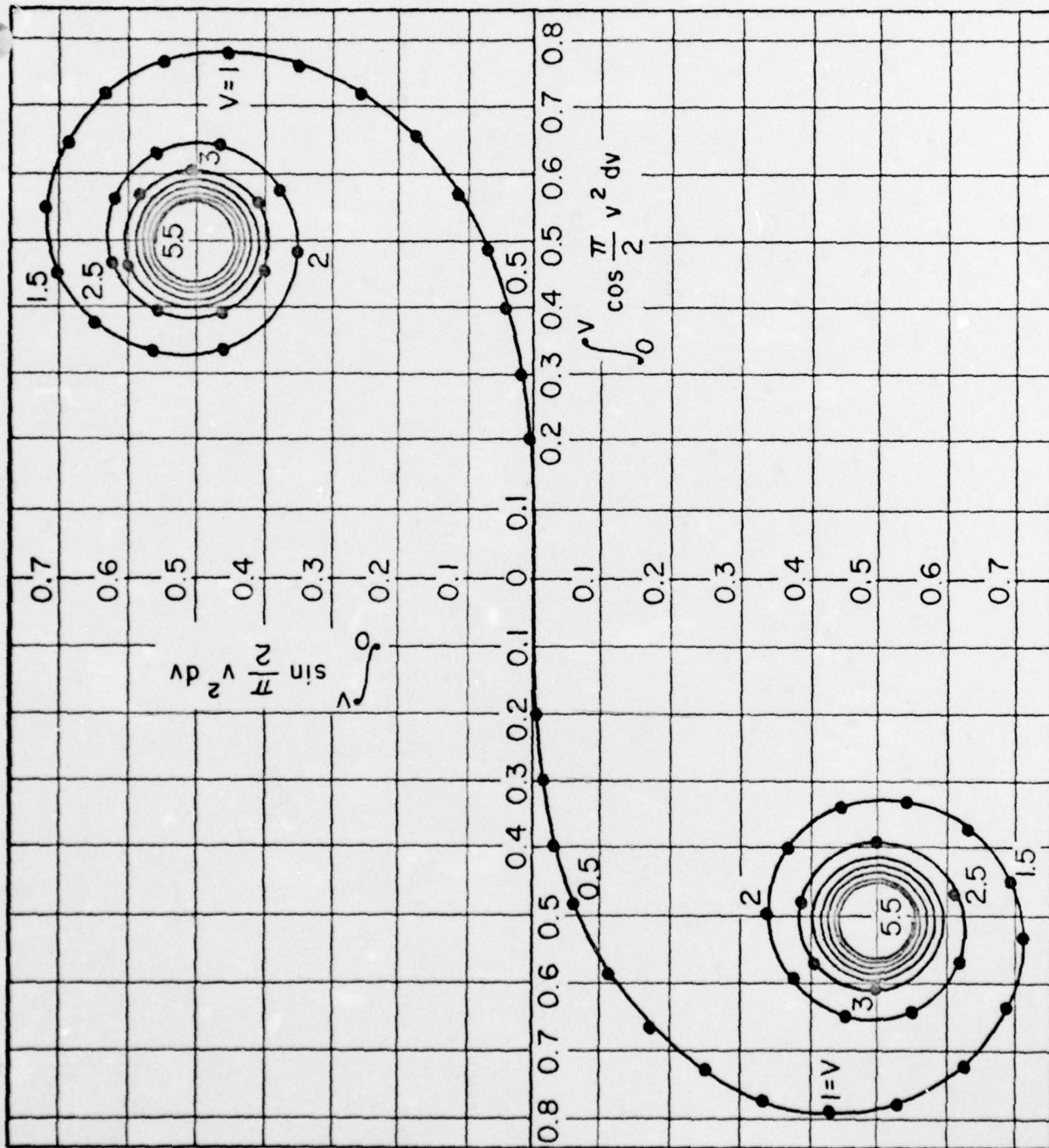


Figure 38- Cornu Spiral Curve

- 143 -

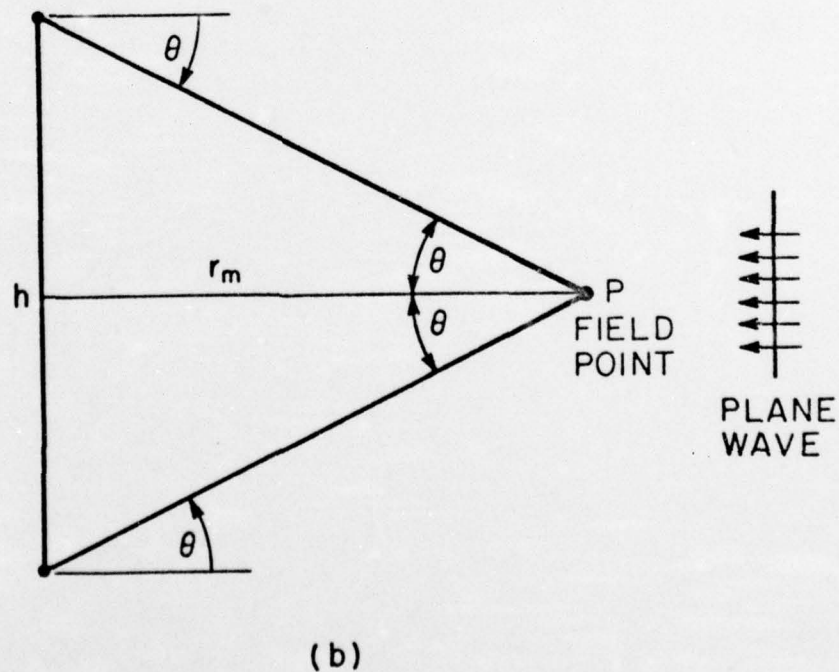
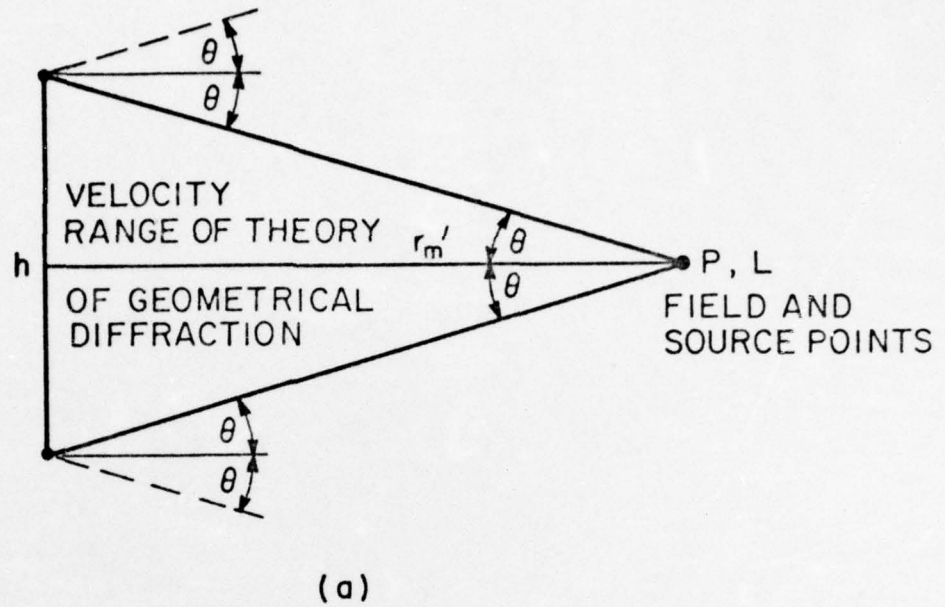


Figure 39- Limit Range and Angles of the Geometrical Theory of Diffraction from a Square Scatterer for (a) Point Source and (b) Plane Wave Incidence

- 144 -

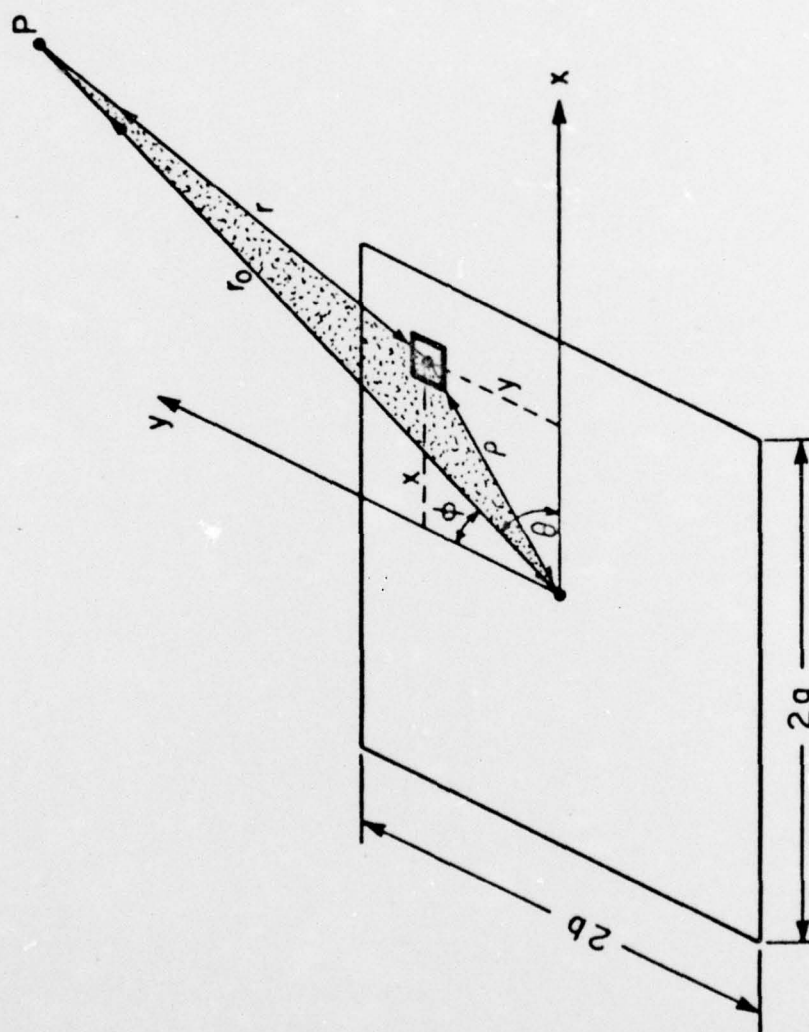


Figure 40- Coordinate System for the Diffracted Field of Plane Scatterers

May 14, 1973
EJS:SIH:ADS:1ms

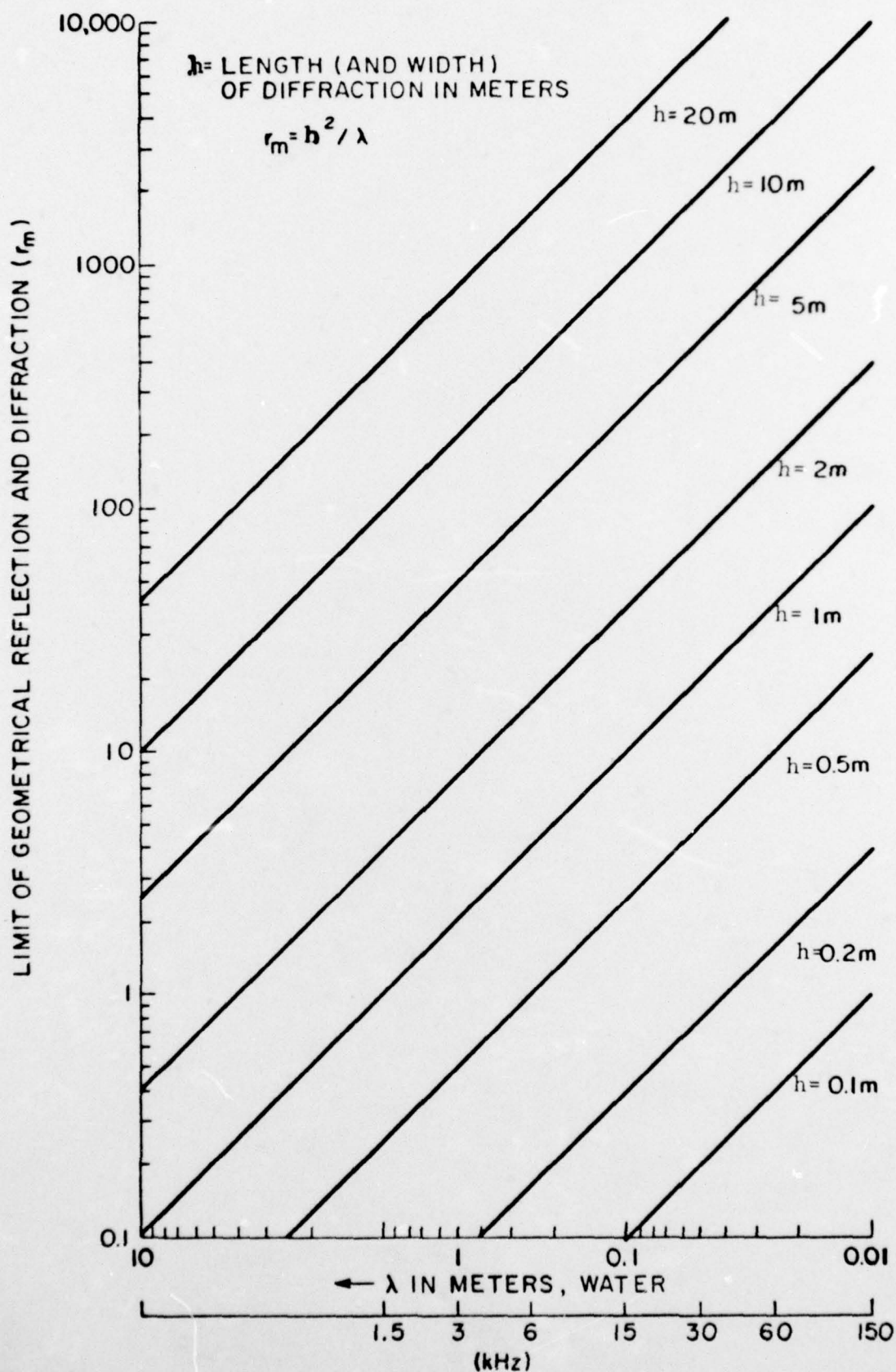


Figure 41- Limiting Range r_m for geometric optical propagation as a function of wavelength in water (or frequency) v.s. the linear dimension of diffractor h for plane wave incidence

May 14, 1973
EJS:SIH:ADS:lms

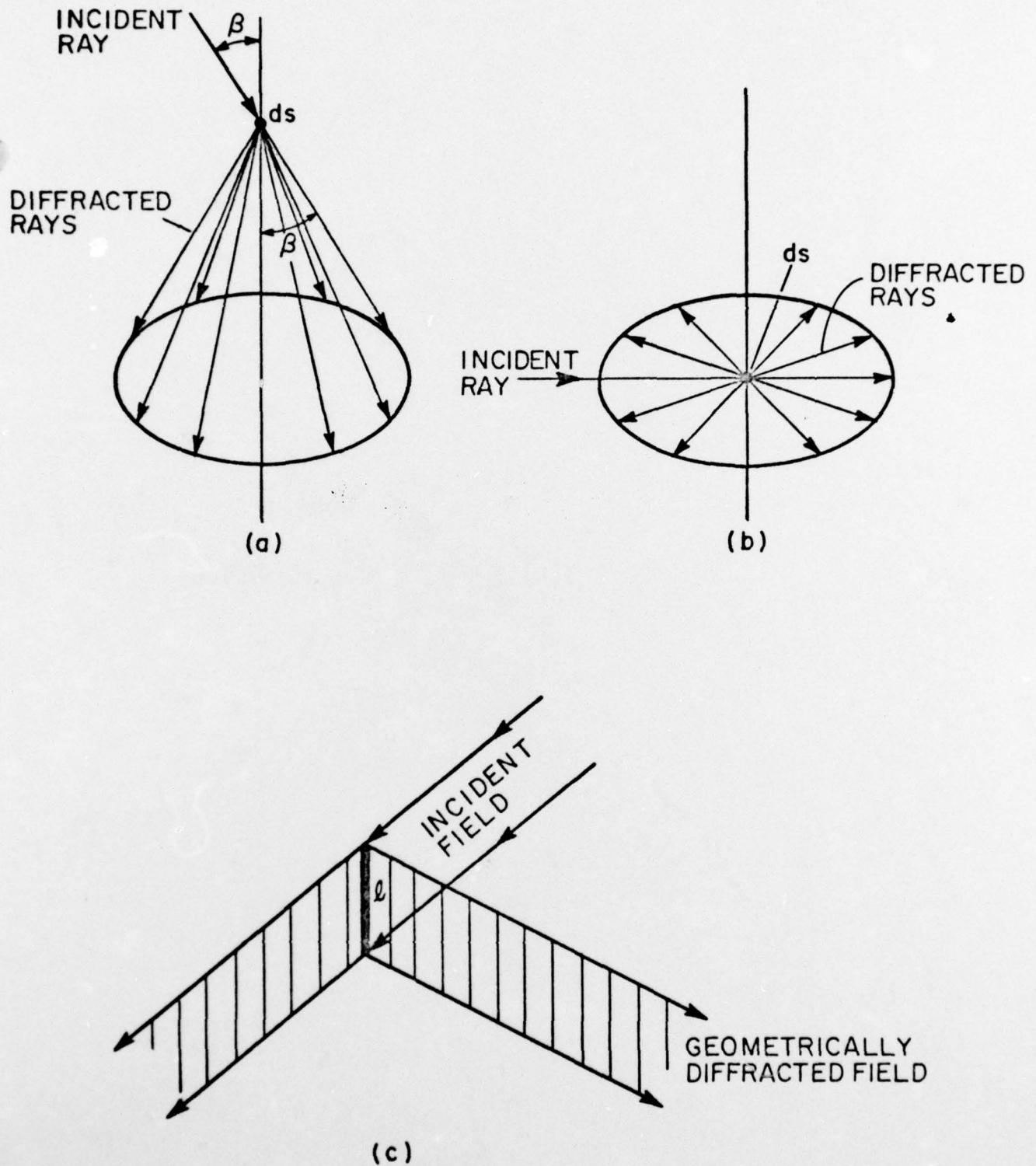


Figure 42- (a) Scattering Cone for an Infinite Edge at Oblique Incidence (b) Scattering Plane for an Infinite Edge at Normal Incidence (c) Scattering Conical Shell for a Finite Edge

- 147 -

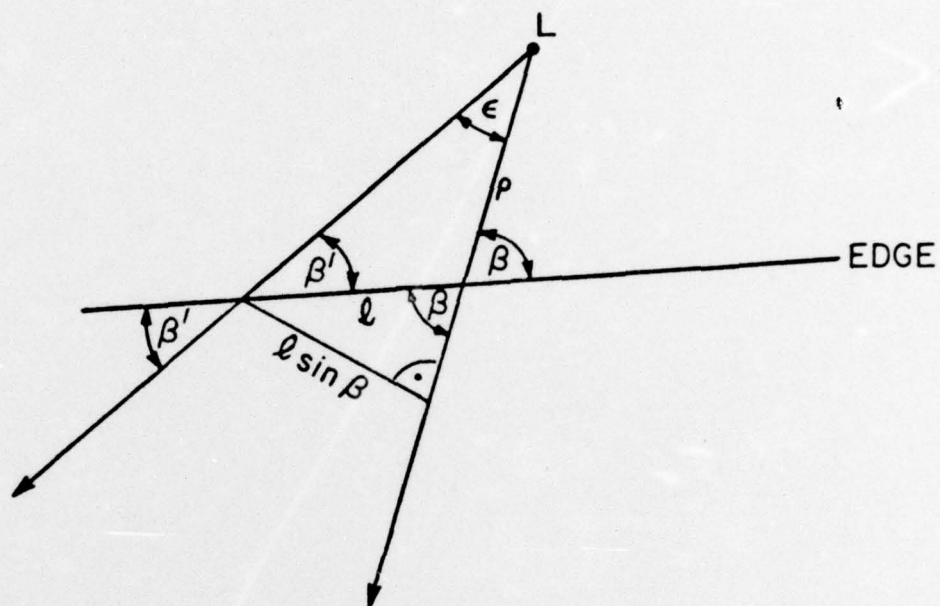


Figure 43- Scattering by a Finite Edge of Length l
of an Incident Point Source Field

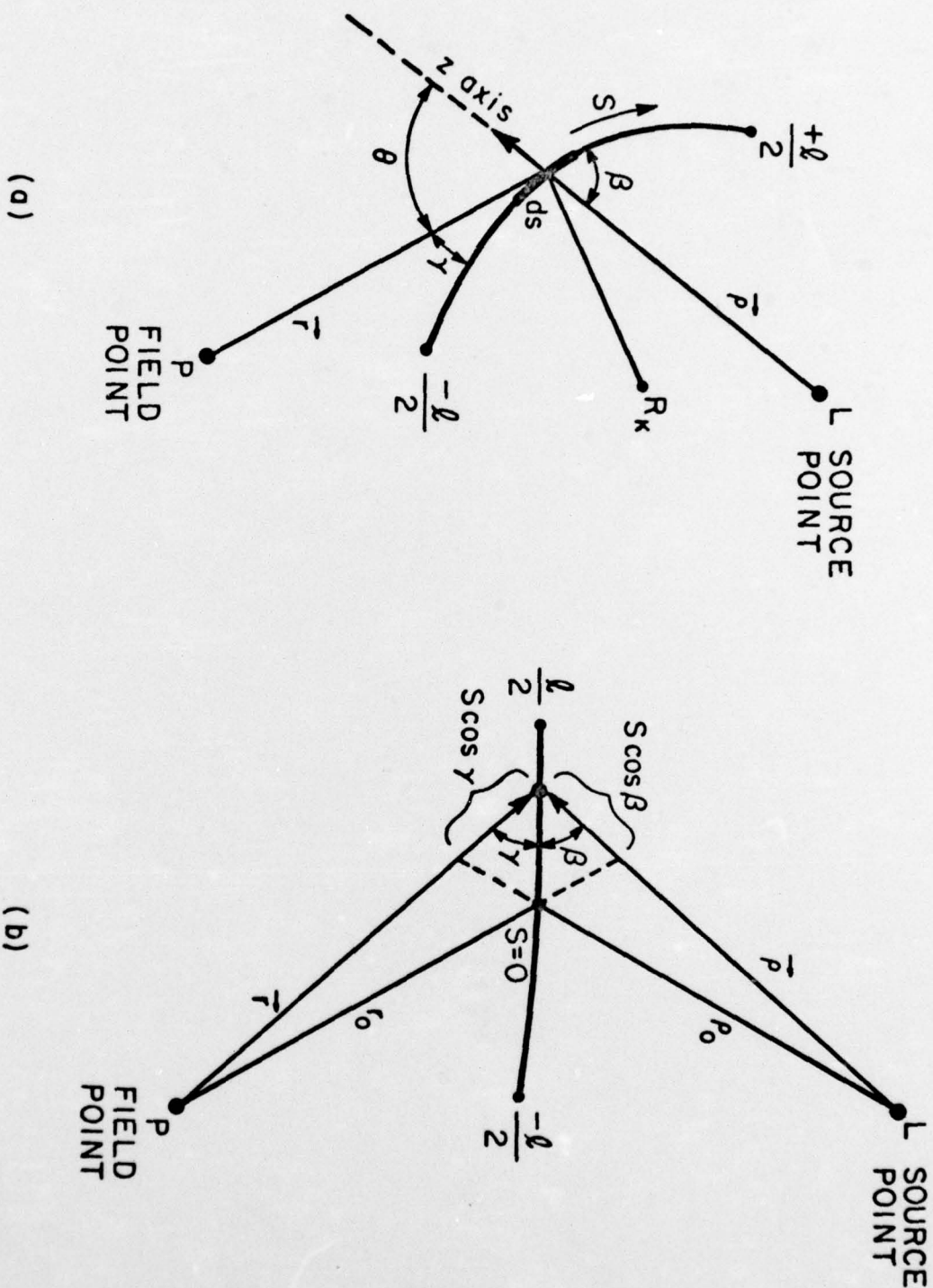


Figure 44- Coordinate System for Curved and Straight Finite Edges

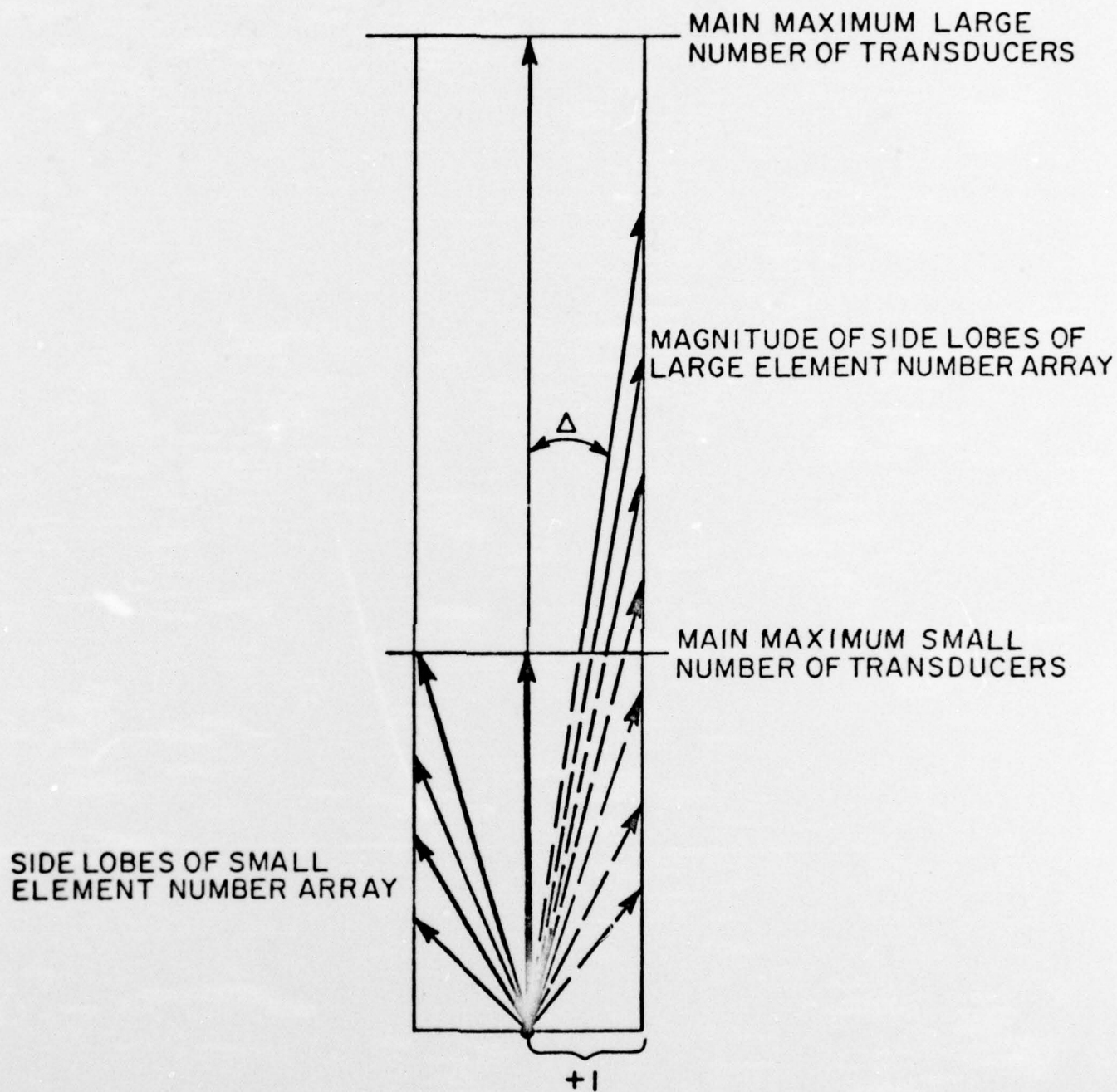


Figure 45- Radiation from a Finite Linear Array. The Off-Axis Radiation is Independent of the Number of Elements in the Array.

- 150 -

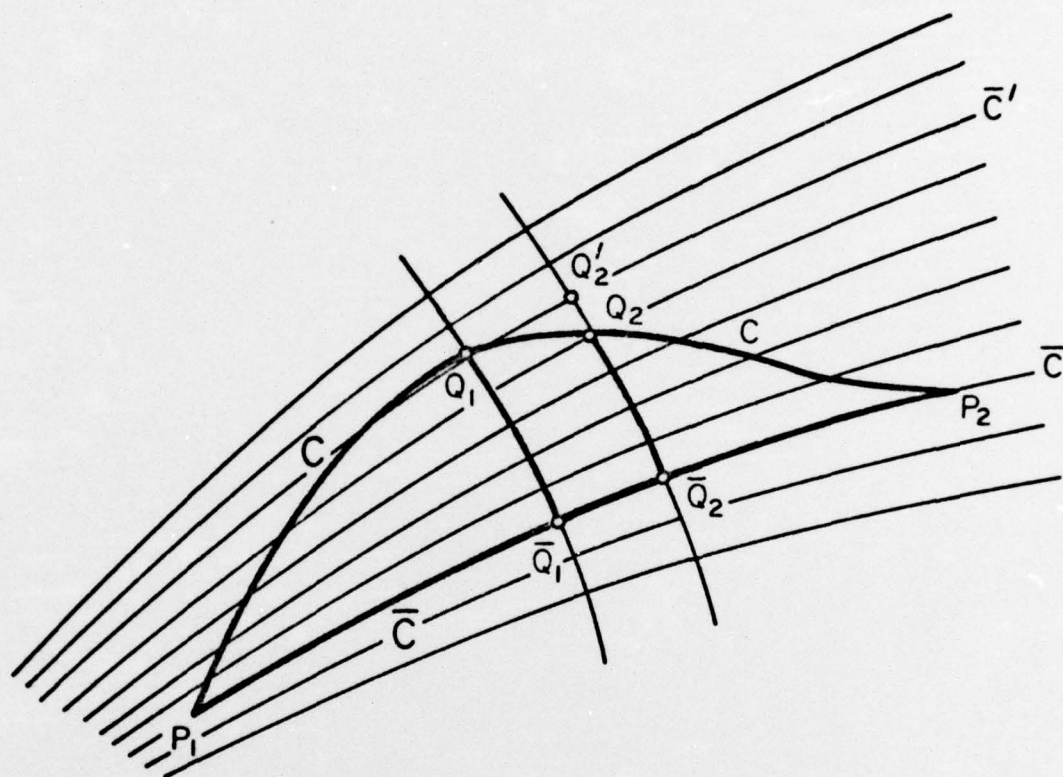


Figure 46- Diagram for Proof of Fermat's Principle

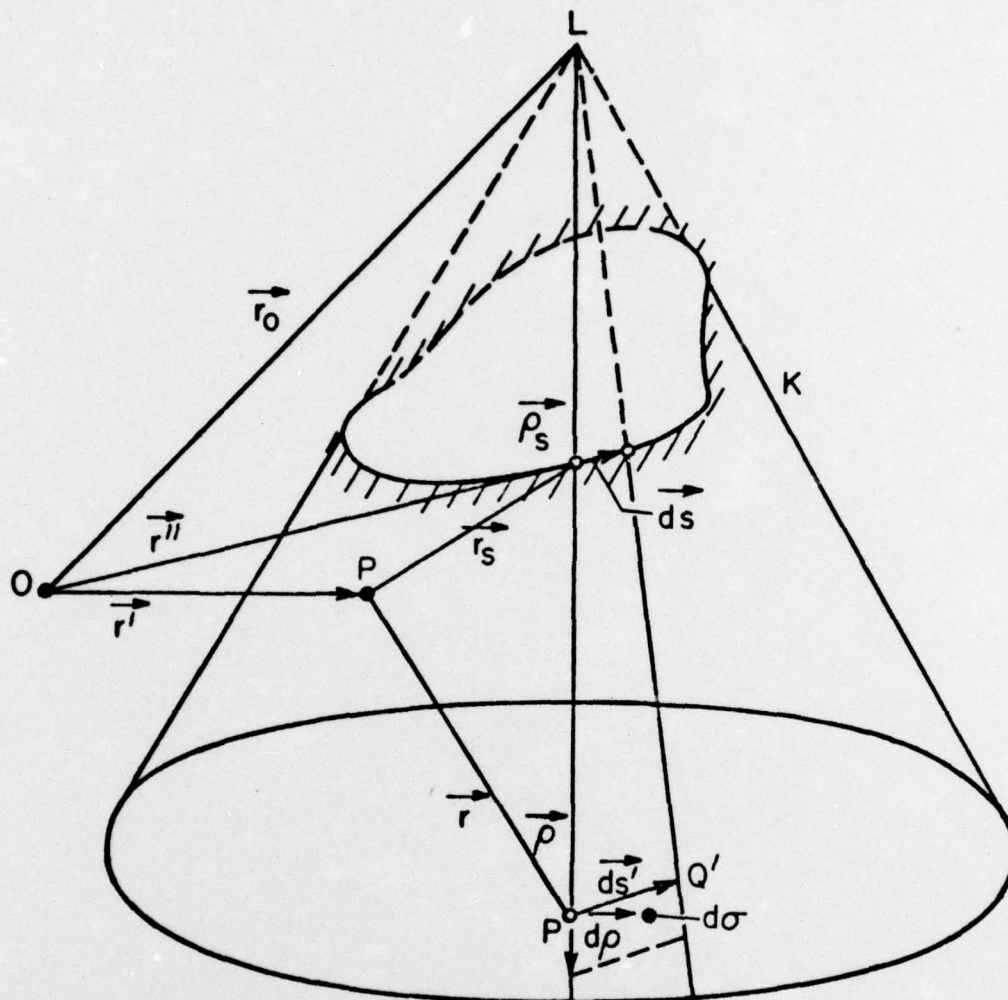


Figure 47- Transformation of the Kirchoff Surface Integral to a Line (Edge) Integral.

Security Classification

DOCUMENT CONTROL DATA - R & D

(Security classification of title, body of abstract and indexing annotation must be entered when the overall report is classified)

1. ORIGINATING ACTIVITY (Corporate author) Applied Research Laboratory, P. O. Box 30, State College, Pa. 16828		2a. REPORT SECURITY CLASSIFICATION UNCLASSIFIED	
		2b. GROUP	
3. REPORT TITLE "ACOUSTIC DIFFRACTION PART I - PLANE DIFFRACTORS AND WEDGES			
4. DESCRIPTIVE NOTES (Type of report and inclusive dates) Technical Memorandum			
5. AUTHOR(S) (First name, middle initial, last name) Eugene J. Skudrzyk, Sabih I. Hayek, Alan D. Stuart			
6. REPORT DATE May 9, 1973		7a. TOTAL NO. OF PAGES 157	7b. NO. OF REFS 15
8a. CONTRACT OR GRANT NO. N00017-70-C-1407		9a. ORIGINATOR'S REPORT NUMBER(S) TM 73-109	
b. PROJECT NO.		9b. OTHER REPORT NO(S) (Any other numbers that may be assigned this report)	
c.			
d.			
10. DISTRIBUTION STATEMENT APPROVED FOR PUBLIC RELEASE DISTRIBUTION UNLIMITED Per NAVORD Aug. 16, 1973			
11. SUPPLEMENTARY NOTES		12. SPONSORING MILITARY ACTIVITY NOSC	
13. ABSTRACT This memorandum documents the theoretical investigations in the Acoustic Diffraction Program. This report discusses the acoustic diffraction and backscattering phenomena for plane and wedge scatterers which are insonified by plane or point sources. The theories of diffraction used in this report are those of the approximate integral representations of Kirchoff-Rubinowicz. Those were compared with the geometrical theory of diffraction (GTD) which is developed by J. B. Keller, and is based on the ray theory. It was found that the integral representation agrees well with the GTD at high frequencies for infinite edges and long curved edges only. The agreement was worse when the scatterer size or edge length is finite. New expressions for diffraction from finite scatterers and edges were derived and the deviation of the GTD from these solutions were estimated.			

14 KEY WORDS	LINK A		LINK B		LINK C	
	ROLE	WT	ROLE	WT	ROLE	WT
Acoustic Diffraction	8					
Approximate Integral	8					
Backscattering	8					
Finite Scatterers	8					
Geometrical Theory	8					
KIRCHOFF-RUBINOWICZ	8					
Plane Diffraction	8					
Ray Theory	8					
Wedges	8					

DISTIRBUTION LIST FOR TECHNICAL MEMORANDUM NO. TM 73-109

Commander
Naval Ordnance Systems Command
Department of the Navy
Washington, D. C. 20360
Attention: Library, ORD-632
Copy No. 1 and 2

Commander
Naval Ordnance Systems Command
Department of the Navy
Washington, D. C. 20360
Attention: Stanly Marcus, Code 03A
Copy No. 3

Commander
Naval Ordnance Systems Command
Department of the Navy
Washington, D. C. 20360
Attention: Edward Liszka, Code 034A1
Copy No. 4

Commander
Naval Ordnance Systems Command
Department of the Navy
Washington, D. C. 20360
Attention: Edward McKinney, Code 034B
Copy No. 5

Commander
Naval Ordnance Systems Command
Department of the Navy
Washington, D. C. 20360
Attention: William August, Code 0541A
Copy No. 6

Commander
Naval Undersea Center
Pasadena Laboratory
3202 E. Foothill Blvd.
Pasadena, California 91107
Attention: Douglas Chabries
Copy No. 7

Commander
Naval Undersea Center
Pasadena Laboratory
3202 E. Foothill Blvd.
Pasadena, California 91107
Attention: Carl Johansen
Copy No. 8

DISTRIBUTION LIST FOR TECHNICAL MEMORANDUM NO. TM 73-109 - Continued

Commander
Naval Undersea Center
Pasadena Laboratory
3202 E. Foothill Blvd.
Pasadena, Calif. 91107
Attention: Joel Young
Copy No. 9

Commander
Naval Undersea Center
Pasadena Laboratory
3202 E. Foothill Blvd.
Pasadena, Calif. 91107
Attention: Jon Reeves
Copy No. 10

Commander
Naval Ordnance Laboratory
White Oak
Silver Spring, Maryland 20910
Attention: Guillermo C. Gaunard
Copy No. 11

Commander
Naval Ordnance Laboratory
White Oak
Silver Spring, Maryland 20910
Attention: Walter Madigosky
Copy No. 12

Commander
Naval Underwater Systems Center
Newport Laboratory
Newport, Rhode Island 02840
Attention: Fred Cancilliere
Copy No. 13

Commander
Naval Underwater Systems Center
Newport Laboratory
Newport, Rhode Island 02840
Attention: Dwain Hartge
Copy No. 14

Commander
Naval Underwater Systems Center
Newport Laboratory, Bldg. 679
Newport, Rhode Island 02840
Attention: Edward Barile
Copy No. 15

DISTRIBUTION LIST FOR TECHNICAL MEMORANDUM NO. TM 73-109 - Continued

Commander
Naval Underwater Systems Center
New London Laboratory
New London, Connecticut 06321
Attention: Jan Holland
Copy No. 16

Commander
Naval Coastal Systems Laboratory
Panama City, Florida 32401
Attention: Bruce Nolte, Code 762
Copy No. 17

Commander
Naval Ship Research & Development Center
Washington, D. C.
Attention: Maurice Sevik, Code 900
Copy No. 18

Defense Documentation Center
Camron Station
Alexander, Virginia 22314
Copy No. 19-30

Via: Commander (ORD-632)
Naval Ordnance Systems Command
Department of the Navy
Washington, D. C. 20360